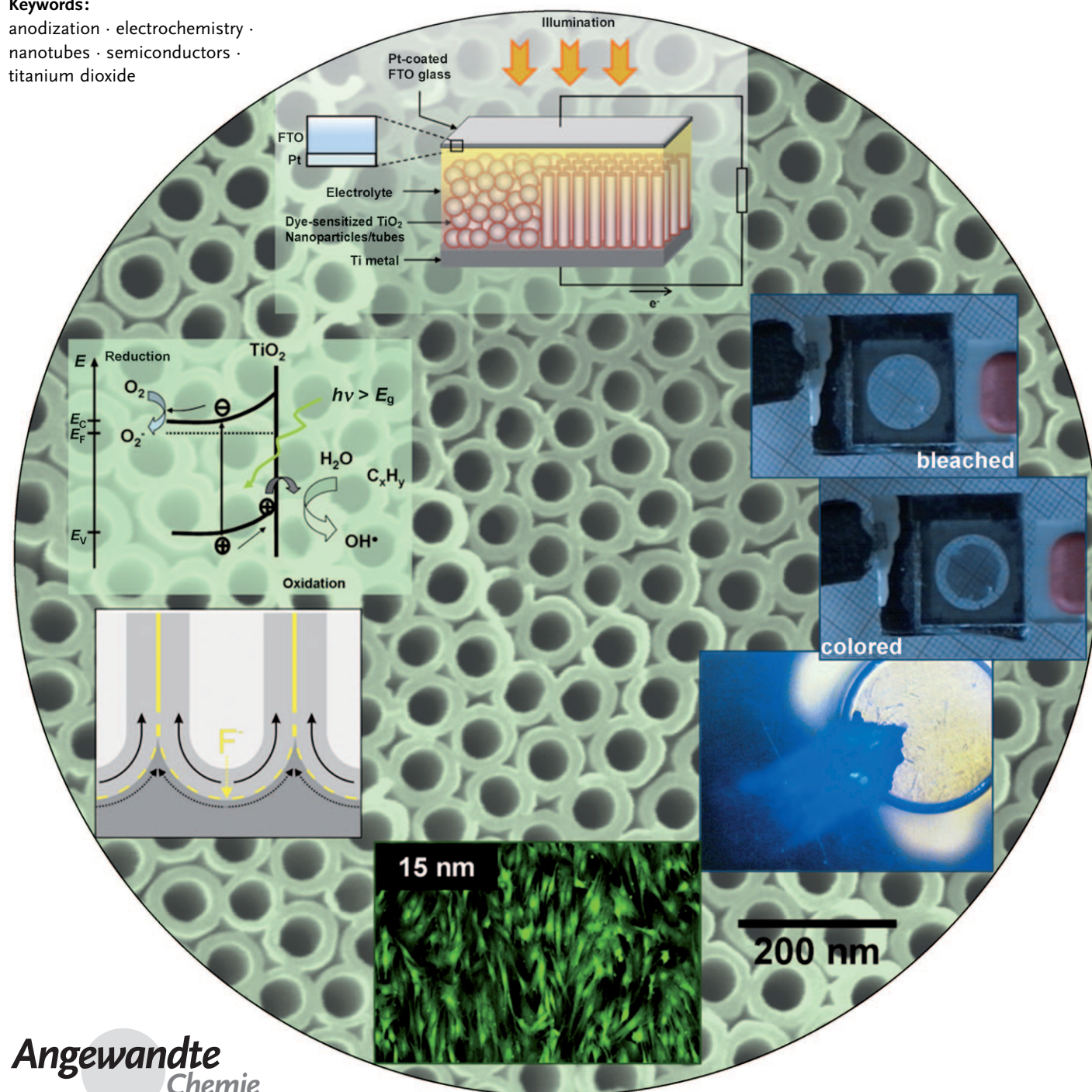


TiO₂ Nanotubes: Synthesis and Applications

Poulomi Roy, Steffen Berger, and Patrik Schmuki*

Keywords:

anodization · electrochemistry ·
nanotubes · semiconductors ·
titanium dioxide



TiO₂ is one of the most studied compounds in materials science. Owing to some outstanding properties it is used for instance in photocatalysis, dye-sensitized solar cells, and biomedical devices. In 1999, first reports showed the feasibility to grow highly ordered arrays of TiO₂ nanotubes by a simple but optimized electrochemical anodization of a titanium metal sheet. This finding stimulated intense research activities that focused on growth, modification, properties, and applications of these one-dimensional nanostructures. This review attempts to cover all these aspects, including underlying principles and key functional features of TiO₂, in a comprehensive way and also indicates potential future directions of the field.

1.1. Introduction

1.1. Why TiO₂ Nanotubes?

Ever since Iijima discovered carbon nanotubes,^[1] this combination of extreme molecular geometry and exciting properties has not only inspired the field of nanotechnology but also triggered enormous efforts in physics, chemistry, and materials science. These one-dimensional (1D) nanostructures provide unique electronic properties, such as high electron mobility or quantum confinement effects, a very high specific surface area, and even show a very high mechanical strength.^[2–4] Although carbon is still the most explored nanotube material, a considerable range of other materials, which are mainly transition metal oxides and sulfides, have been synthesized in a 1D or virtually 1D geometry (nanowires, nanorods, nanofibers, or nanotubes) and have also shown fascinating new properties and features.^[2,5–8]

While carbon nanotubes are mainly explored for their use in microelectronic technology, inorganic nanotubes (especially metal sulfides or oxides) are mostly fabricated to exploit other material-specific properties, and the focus of interest is on biomedical, photochemical, electrical, and environmental applications.^[5–18] Among all transition-metal oxides, TiO₂ is the most extensively studied material (with more than 40 000 publications over the past 10 years), which makes TiO₂ to one of the most investigated compounds in materials science. Bulk TiO₂ is known to be a very useful non-toxic, environmentally friendly, corrosion-resistant material: it is frequently used in paint, white pigments, and sun-blockers. The key functional features are, however, exceptional biocompatibility (use in medicine) and even more the almost unique ionic and electronic properties of this oxide. TiO₂ in all its crystal forms is a wide-bandgap semiconductor ($E_g \approx 3$ eV) with suitable band-edge positions that enable its use in solar cells and for photocatalytic reactions. Photogenerated electron–hole pairs can be used for splitting water into oxygen and hydrogen (potentially the fuel of the future), or can be used for the remediation of hazardous wastes, such as contaminated ground waters, or the control of toxic air contaminants.^[19–21] Historically, some milestones were certainly the reports by Fujishima and Honda in 1972 on water splitting on a TiO₂ electrode,^[22] and the works by Gerischer and

Tributsch,^[23] Dare-Edwards et al.,^[24] and Grätzel and O'Regan^[25] that introduced the use of the material for solar energy conversion in the 80s and 90s.^[26] Over the past 20 years, the palette of potential applications has been widened towards devices with increasingly sophisticated photovoltaic, electrochromic, antifogging, or self-cleaning properties, biomedical coatings, sensors, or smart-surface coatings.^[27–39]

For many of these applications, it is crucial to maximize the specific surface area (which is, for example, obvious for any catalytic reaction) to achieve a maximum overall efficiency, and therefore nanoparticulated forms of TiO₂ are widely used. However, other nanosize geometries, and in particular nanotubes or nanorods, may allow for a much higher control of the chemical or physical behavior. By diminishing dimensions to the nanoscale, not only the specific surface area increases significantly but also the electronic properties may change considerably (owing for example to quantum size effects, strong contribution of surface reconstruction, or surface curvature). These effects may also contribute to drastically improve the reaction/interaction between a device and the surrounding media, thereby making the system more effective (kinetics),^[40–43] or even allow for entirely novel reaction pathways.

Synthesis of 1D TiO₂ nanostructures may be achieved by various routes including sol–gel methods, template-assisted methods, hydro/solvothermal approaches, and by electrochemical means.^[8,10,14,15,36,37,44–58] A brief overview of various synthesis techniques is given in Section 1.2.

The present review will, however, focus on perhaps the most spectacular and surprising 1D structure: self-organized TiO₂ nanotube layers. These layers can be formed by a simple

From the Contents

1. Introduction	2905
2. Electrochemical Anodization and Self-Organization	2907
3. Properties of TiO₂ and TiO₂ Nanotubes	2917
4. Modification of Tube Properties	2920
5. Oxide Nanotube Layers on Other Transition Metals and Alloys	2926
6. Applications	2927

[*] P. Roy, S. Berger, P. Schmuki
 Department of Materials Science, WW4-LKO
 University of Erlangen-Nuremberg
 Martensstrasse 7, 91058 Erlangen (Germany)
 Fax: (+49) 9131-852-7582
 E-mail: schmuki@ww.uni-erlangen.de

electrochemical oxidation reaction of a metallic titanium substrate under a specific set of environmental conditions (Figure 1a). This type of self-aligned oxide nanotube layers has attracted considerable interest over the past 10 years. Currently, the publication rate shows an almost exponential trend, with more than 1000 papers being published over the last 3 years. This rate can be ascribed to the fact that these structures represent a unique combination of the highly functional features of TiO_2 with a regular and controllable nanoscale geometry (length, tube diameter, and self-ordering can be adjusted over large length scales). The synthesis is carried out by a low-cost parallel process: conventional electrochemical anodization. It is furthermore remarkable that the self-ordering anodization approach is not limited to titanium but can be applied to a large range of other transition metals or alloys to form highly aligned oxide nanotube or pore structures, which will be addressed more extensively in Section 5.

In the following sections we will discuss the synthesis of these nanotubes and means to influence the degree of self-organization, tube length, diameter, and crystal structure of the tubes. We will introduce specific nanoscale morphologies that can be achieved (free-standing membranes, nanobamboo, tube stacks, tube-to-pore transitions), show methods to influence electronic and ionic properties (bandgap engineering, doping), and also biointerface properties. Finally, we give examples of using these nanotube structures in various devices and applications.

1.2. Electrochemical Synthesis versus Other Approaches

This review will focus exclusively on electrochemical formation of self-organized TiO_2 nanotubes in later sections,

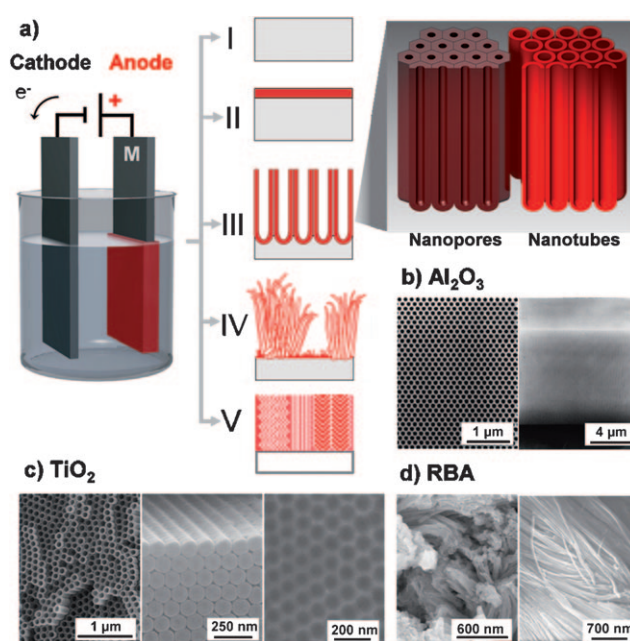


Figure 1. The electrochemical anodization process and possible anodic morphologies: a) I) metal electropolishing, II) formation of compact anodic oxides, III) self-ordered oxides (nanotubes or nanopores), IV) rapid (disorganized) oxide nanotube formation, V) ordered nanoporous layers. Examples of morphologies of obtained structures: b) Classical highly organized nanoporous alumina (taken with permission from Ref. [116]), c) highly ordered TiO_2 nanotubes (in top and side view) with dimpled structure (right) on metal surface when tubes are removed, d) disordered TiO_2 nanotubes growing in bundles. RBA = rapid-breakdown anodization.



Poulomi Roy studied chemistry at Vidyasaagar University, India, and obtained her PhD on Inorganic Nanomaterials from the Indian Institute of Technology, Kharagpur in 2007. She joined the group of Prof. Patrik Schmuki at University of Erlangen-Nuremberg, Germany in 2008 as a postdoctoral fellow. Her research interests include the synthesis of semiconductor nanomaterials and their application in various energy-related and biomedical fields.



Steffen Berger studied materials science at the Friedrich Alexander University Erlangen-Nuremberg, Germany, and obtained his Diplom in 2005. He completed his PhD in 2009 in the group of Prof. Patrik Schmuki at the Chair for Surface Science and Corrosion, where he is continuing his research as a postdoctoral fellow. His research interests include the synthesis of self-organized nanomaterials by electrochemical methods with the direction of application in energy conversion and storage devices.



Patrik Schmuki studied physical chemistry at the University of Basel and obtained his PhD from the ETH Zurich in 1992. From 1994 to 1997 he worked at Brookhaven National Laboratory, USA, and the Institute for Microstructural Sciences of the National Research Council of Canada. From 1997 until 2000 he was an Associate Professor for Microstructuring Materials at EPFL, Switzerland, and since 2000 he has been Full Professor and Head of the Institute for Surface Science at the Materials Science Department of the University of Erlangen-Nuremberg. His current research interests cover electrochemistry and materials science at the nanoscale, with a particular focus on functional materials and the control of self-assembly processes.

but it should be noted that prior and parallel to the anodization approach, other methods were/are studied to synthesize TiO₂ nanotubes. The first targeted effort to produce titania nanotubes was probably the work by Hoyer,^[10] who used an electrochemical deposition method into an ordered alumina template. Later methods mainly involved other template-assisted methods, sol–gel techniques, and hydro/solvothermal methods with or without templates^[14, 44, 47–50, 52, 56–59] and atomic layer deposition (ALD) into the template.^[60–63] Many of the processes are acid-catalysed hydrolysis reactions of titanium alkoxide precursors followed by condensation reactions (that is, a gel-type polymeric Ti–O–Ti chain is developed, which then hydrolyzes and thus results in TiO₂ precipitates). For example, TiO₂ sol was sucked into the pores of the alumina template, then a heat treatment was applied, and afterwards the alumina template was selectively dissolved out.^[52] TiO₂ nanoparticles or nanorods are also prepared by using micelle templates of appropriate surfactants above their critical micelle concentration (the surfactant molecules aggregate and disperse in a liquid to give so-called spherical or rod-like micelles, which are used as template for TiO₂ preparation). In this approach, nanotube formation is mostly carried out using water containing reverse micelles with a cylindrical exterior surface. The titanium precursor can then react at the micelle surface, and after removal of the surfactant (burn-off), a nanotube structure is obtained.^[8] Usually TiCl₄ or any other titanium alkoxide solutions are employed as the titanium precursor. Using certain H₂O:micelle ratios^[45, 46] allows the crystallite size to be varied.

Another well-established solution-based method to synthesize 1D TiO₂ nanostructures is the hydro/solvothermal method, which was first reported by Kasuga et al.^[14, 47] In this method, bulk TiO₂ powder is treated with NaOH solution in a Teflon-lined autoclave at 100–150 °C for several hours, followed by an acid treatment in HCl.^[14, 47, 48] The general formation of the tube geometry is based on exfoliation of TiO₂ crystal planes in the alkali environment and stabilization as Ti–O–Na⁺. This step is followed by a rolling of the nanolayer sheets into tubes during cooling or in the HCl treatment. Some debate exists in literature on the exact cause for the rolling-up, and several experimental factors are crucial to indeed obtain a tubular material. Such tubular structures consist of multishells, with an inner shell diameter of about 5 nm, a shell spacing of less than 1 nm, and an average tube diameter of about 10 nm. The amount of synthesized nanotubes and also their length (typically several tens to hundred nanometers) and size distribution depend on the specific reaction conditions.^[48]

In ALD, surfaces of templates (such as porous alumina) can be coated conformably one atomic layer after the other by using alternating cycles of exposure to a titania precursor (such as TiCl₄ or Ti(OiPr)₄) followed by purging and hydrolysis.^[60–63] While alumina-template approaches allow nanotubular or rod structures to be formed that are vertically aligned to the substrate, they involve a sometimes critical template-removal step.

For other transition-metal oxides, such as WO₃, ZnO, ZrO₂, V₂O₅, Nb₂O₅, Ta₂O₅, MnO, and CuO, nanorod or

nanotubular structures can also be fabricated using precursor and template techniques.^[64] Applications target such areas as catalytic, optical, electrical, and mechanical devices and sensors. For example, CuO, V₂O₅, and MnO are very often used as intercalation compounds in lithium ion batteries;^[65] in several cases nanotubes show enhanced electrochemical properties with both better lithium intercalation capacity and extraction rate than bulk or powdered materials. WO₃ and Nb₂O₅ are the commonly used oxides in electrochromic devices, and gas sensors.^[66–72]

All these titanium precursor solution/template-based processes result in single tubes or loose agglomerates of tubes or bundles that are dispersed in a solution, and often a wide distribution of tube lengths is obtained. To make use of the structures in electrically contacted devices, the tubes are usually compacted into layers on an electrode surface. However, this process leads to an arbitrary orientation of the nanotubes on the electrode, which unfortunately eliminates many advantages of the one-dimensional directionality (for example providing a 1D electron path to the electrode). In contrast, the electrochemical anodization approach discussed herein is self-organizing: it leads to an array of oxide nanotubes aligned perpendicular to the substrate surface (such as in Figure 1) and to a well-defined (and controllable) tube length. The tubes are attached to the metal surface and are thus already electrically connected and easy to handle. The use of an electrochemical anodization method allows virtually any shape of titanium (and other metal) surfaces to be coated with a dense and defined nanotube layer and is thus an extremely versatile parallel (and thus easy to scale up) structuring process.

Regarding anodic treatments, photoelectrochemical etch channels were also reported^[56–58] and the growth of less-organized (usually non-substrate-adherent) TiO₂ nanotube bundles has been introduced by Masuda et al.^[73] Later this process was referred to as rapid-breakdown anodization (RBA)^[74] and extended to other electrolytes^[73–75] and metals^[74, 76] or metal alloys.^[77] Solar-cell applications were usually targeted.^[75, 78, 79] The main advantage of the technique is that comparably long nanotubes (several 100 μm)^[76] can be grown within very short times (some seconds to minutes; an example is shown in Figure 1d). The main disadvantage is that the tubes are not well-defined regarding length distribution, not well-organized over larger surface areas, and they are hardly connected to the substrate.

The anodic formation of several 10 μm thick ordered nanoporous TiO₂ layers (structure V in Figure 1a) with channels several nanometers to several tens of nanometers in diameter has been recently reported.^[80–83] These nanoscopic morphologies adhere well to the substrate, but to date they have not been explored extensively in view of achievable geometries or applications.

2. Electrochemical Anodization and Self-Organization

Self-organized oxide tube arrays or pore arrays can be obtained by an anodization process of a suitable metal. When

metals are exposed to a sufficiently anodic voltage in an electrochemical configuration (as in Figure 1), an oxidation reaction $M \rightarrow M^{n+} + n e^-$ will be initiated. Depending mainly on the electrolyte and the particular anodization parameters, essentially three possibilities for reactions exist (Figure 1): I) The M^{n+} ions are solvated in the electrolyte; that is, the metal is continuously dissolved (and corrosion, or electro-polishing of the metal, is observed); II) the M^{n+} ions formed react with O^{2-} (provided by H_2O in the electrolyte) and form a compact oxide (MO) layer if MO is not soluble in the electrolyte; III) under some electrochemical conditions, competition between solvation and oxide formation is established (leading to porous MO). Under even more specific experimental conditions, a situation is established where self-organization during the growth of porous oxide takes place; furthermore, under some specific conditions, disorganized rapid growth of TiO_2 nanotube bundles (IV in Figure 1 a, and Figure 1 d) or formation of thick self-organized mesoporous layers (V in Figure 1 a) can be observed.

The best investigated system, in which almost perfect self-organization of pores in oxide can be established, is the anodic growth of porous Al_2O_3 on aluminum. Over 50 years ago,^[84] it was realized that upon anodic treatment of aluminum in neutral to alkaline electrolytes, a flat, compact oxide would grow, but when anodized in acidic electrolytes relatively regular porous oxide structures could be grown to considerable thicknesses ($> 100 \mu m$).

Such thick robust porous oxide layers on aluminum were used for many years in corrosion protection and coloration of aluminium surfaces.^[85,86] Around 1990, the first reports by Uosaki et al.^[87] and later by Martin^[88] appeared that explored the use of porous alumina as a template for the synthesis of functional nanomaterials. In 1995, in a ground-breaking paper, Masuda and Fukuda^[89] reported that under specific experimental conditions, pore growth that shows a very high degree of self-organization can be achieved (see Figure 1 b). This finding triggered hundreds of papers dealing with the modification and use of porous alumina either directly (such as in filters or for photonic crystals) or indirectly (as a template for nanorod, nanowire, and nanotube synthesis by deposition of metal, semiconductor, or polymer materials.^[88,90-93]

Models that try to provide a mechanistic reasoning for the occurrence of self-organization of porous alumina growth ascribe the origin to: 1) stress at the metal-oxide interface (volume expansion/electrostriction),^[94,95] 2) repulsion of electric fields,^[96] or 3) establishing maximum current-flow conditions.^[97,98]

As we will describe in the following chapters, many of the principles and mechanisms for self-organized porous alumina can be transferred to the formation of self-organized tubes or pores on other metals, taking into account some specific differences in the chemical character of the different metal oxides.

In the light of recent findings we will also show that the distinction between porous or tubular morphology (as differentiated in Figure 1) is mechanistically not really justified. It should also be noted that the terminology pores or tubes was

used in some early work interchangeably; that is, it represents pure semantics.

2.1. Self-Organized TiO_2 Nanotube Arrays

The first self-organized anodic oxides on titanium were reported for anodization in chromic acid electrolytes containing hydrofluoric acid by Zwilling and co-workers in 1999.^[99,100] This work showed that organized nanotube layers (although the author called the structure porous) of up to about 500 nm in thickness. The tube structure was not highly organized and the tubes showed considerable sidewall inhomogeneity. It was however recognized that small additions of fluoride ions to an electrolyte are the key to form these self-organized oxide structures. It is also noteworthy that in 1979, Kelly et al.^[101] explored the influence of fluorides on the passivity of titanium and concluded that porous oxide layers formed for low fluoride concentrations, but they did not perform electron microscopy at a sufficiently high resolution to resolve the (likely) presence of self-organized TiO_2 nanotube layers.

After 1999, several approaches^[102,103] that used acidic fluoride-containing electrolytes essentially confirmed Zwilling's findings (although the original Zwilling work was not always properly referenced). This early work established that the as-formed material is amorphous but may contain some crystallites,^[103] that sidewall inhomogeneity is associated with current fluctuations,^[103] and the limited thickness of the tube layers was ascribed to a oxide-growth/chemical-dissolution equilibrium (steady-state).

Most crucial improvements to the geometry of the tubes were established by Macak et al.^[104-106] First, it was demonstrated that the pH plays a crucial role in improving the tube layer thickness; that is, at neutral pH values, much longer tubes could be grown^[104,105] (other reports^[107] turned out to be incorrect owing to false scale bars in SEM images). Second, it was demonstrated that in non-aqueous electrolytes, smooth tubes without sidewall inhomogeneity (ripples) can be grown to much higher aspect ratios and show a strongly improved ordering.^[106]

Using organic electrolyte systems, such as ethylene glycol, almost ideal hexagonally arranged tube layers can be grown to a thickness of several hundreds of micrometers.^[108] Furthermore, an optimized two-step anodization treatment, similar to the one reported for porous anodic alumina,^[109] can lead to virtually perfect hexagonally ordered arrays of TiO_2 nanotubes.^[110] Several other type of solvent systems, such as ionic liquids^[111] or other protic solvents (CH_3COOH), were explored,^[112] but apart from the fact that in the latter approach comparably narrow tube diameters were observed, no further significant enhancement could be achieved. Regarding nanotubes, self-ordered surface dimples may also be encountered^[113-115] (Figure 1 c). These dimples are in fact metallic surfaces from which the tube layers have been removed; that is, owing to the rounded oxide tube bottoms drilling into the metallic substrate, a scalloped interface results that becomes visible when oxide layers are lifted off by

voltage pulses, mechanical breakaway, or selective oxide dissolution.^[116]

2.2. Stages and Factors in TiO₂ Nanotube Growth

Anodization to form tube layers is usually carried out by applying a potential step (or ramp) at a constant voltage between 1–30 V in aqueous electrolyte or 5–150 V in non-aqueous electrolytes containing approximately 0.05 M–0.5 M (0.1–1 wt%) fluoride ions (and usually some background ion species). The growth of the oxide can then be monitored by recording the current–time characteristics (Figure 2a). In

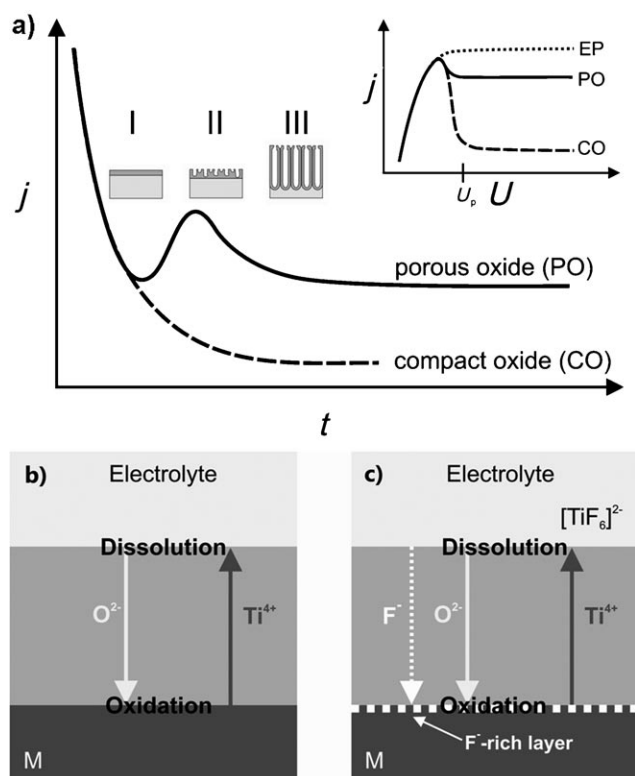
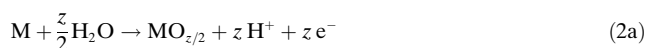


Figure 2. a) Typical current–time (j – t) characteristics after a voltage step in the absence (----) and presence (—) of fluoride ions in the electrolyte. Either compact oxide (fluoride free) or porous/tubular metal oxide formation (containing fluoride) forms by different morphological stages (I–III). The inset shows typical linear sweep voltammograms (j – U curves) for different fluoride concentrations resulting in either electropolished metal (high fluoride concentration), compact oxide (very low fluoride concentration), or tube formation (intermediate fluoride concentration). b, c) Schematic drawing showing field-aided transport of mobile ions through the oxide layers in the absence and presence of fluoride ions: rapid fluoride migration leads to accumulation at the metal–oxide interface.

absence of fluoride ions, a compact oxide layer forms on the TiO₂ surface according to Equations (1)–(3):



Simultaneously, the counter reaction, which is hydrogen evolution, takes place at the cathode [Equation (4)]:



This is the classical anodization scheme, involving ion formation [Ti⁴⁺; Eq. (1)], reaction with O²⁻ [created by (field-aided) deprotonation of H₂O or OH⁻; Eq. (2), (3)] and high-field ion migration of Ti⁴⁺ and O²⁻ through the oxide (Figure 2b).

After initiation, the growth of an anodic oxide layer is determined by the field-aided transport of mobile ions through the oxide (Figure 2b). Depending on the migration rate of the involved ionic species (Ti⁴⁺, O²⁻), the growth of new oxide either proceeds at the interface between metal and oxide or at the interface between oxide and electrolyte (compact anodic TiO₂ layers may in principle grow at either interfaces, but under most experimental conditions oxide grows at the metal–oxide interface). Under a constant voltage U , the field $F = U/d$ drops constantly, thus lowering the driving force (for solid-state ion migration) with increasing film thickness d . The result is an (exponential) drop in the anodic current with time (Figure 2a) until the field effect is lost (that is, is on the order of kT). At this point, a (practically) finite thickness is reached that mainly depends on the anodization voltage. For many transition metals (so-called valve metals), this final thickness is given by $d = fU$, where f is the so-called growth factor of the oxide (typically in the range of 2–4 nm V⁻¹). Typically, the layer which is grown at the oxide/electrolyte interface consists of less-dense oxide containing oxyhydroxides,^[117,118] while the layer at the metal–oxide interface consists of dense and stable TiO₂.

Often, electrochemical reactions, such as anodization processes, are characterized by current–voltage curves (Figure 2a, inset). From these curves, threshold voltages U_p for oxide formation, or the rates of electrochemical processes (for example ion-migration rates) may be determined. For oxide formation in absence of fluorides, a typical active–passive behavior can frequently be observed (Figure 2a, inset).

The presence of fluorides in the electrolyte strongly affects the anodization process, as fluorides form water-soluble [TiF₆]²⁻ species. On one hand, complexation occurs with Ti⁴⁺ ions that are ejected at the oxide–electrolyte interface [after migration through the oxide film; Equation (5)] and on the other hand by chemical attack of the formed TiO₂ [Equation (6)]:



Depending on the fluoride concentration, three very different electrochemical characteristics can be obtained^[103] (Figure 2a, inset). If the fluoride content is very low

(≤ 0.05 wt %), a characteristics as in the fluoride-ion-free case is observed; that is, after anodizing the material to a voltage above U_p , a stable compact oxide layer is formed. If the fluoride concentration is high (ca. 1 wt %), no oxide formation can be observed, as all the Ti^{4+} formed immediately reacts with the abundant fluoride to form soluble $[TiF_6]^{2-}$ (the reaction may then be controlled by diffusion of $[TiF_6]^{2-}$ from the surface, and electropolishing of the sample occurs).^[103]

For intermediate fluoride concentrations, a competition between oxide formation and Ti^{4+} solvation takes place and porous oxide or nanotube formation can be observed. A typical $I-t$ curve for conditions that lead to nanotube formation is shown in Figure 2a. The curve shows three stages: I) In the initial stage of anodization the curve essentially follows the fluoride-free case, and if samples are removed from the electrolyte, a compact oxide layer is present (see also Figure 3). In stage II, a current increase

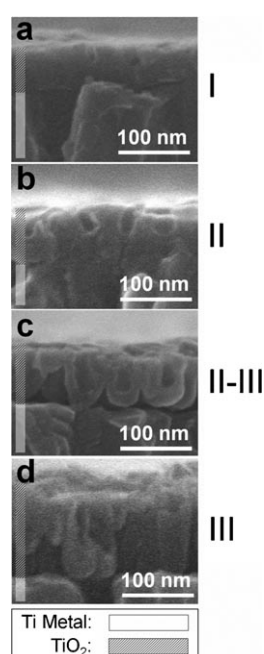


Figure 3. SEM images (cross-sectional views) of the initial phase of anodic TiO_2 nanotube growth. First, a) a compact layer is formed, then b) local thinning and c) tube embryo formation occurs before d) stable tube growth is finally established. (Reproduced with permission from Ref. [127].)

occurs, and irregular nanoscale pores are initially formed that penetrate the initial compact oxide (the current increases as the reactive area increases). In step III, the current drops again as a regular nanopore or nanotube layer forms. The penetrated compact oxide (random pore layer; initiation layer) often remains as remnants that are frequently found after anodization on the tube tops.^[103,119] Various efforts have been directed toward removing these layers,^[119–121] as they interfere with any transport process into the tubes or hamper the exploitation of tube size effects.^[122,123] After self-organization occurred, the tube growth continues at steady current densities. For extended anodization, the growth may be

determined by diffusional effects^[37,124] and thus agitation (and gravity effects^[125]) and viscosity (influence on the diffusion constant^[106]) may become important.

The initiation of the growth of TiO_2 nanotubular layers has been investigated in several works.^[117,126–128] A very recent study on the anodization of masked thin metallic titanium layers on silicon substrates enabled a detailed investigation of the very first growth stages;^[127] a typical sequence of TiO_2 nanotubular layer growth during the first 110 s is shown in Figure 3. Once the initiation phase is overcome, the tubes grow longer with time (Figure 4a) until the etching action of fluorides (permanent thinning of the tube tops) becomes apparent,^[124,126] and a steady-state situation between tube formation at the bottom and etching at the top according to Equation (6) is established (see also Section 2.7.4). When tubes are growing in phase III (Figure 2a), that is, under steady-current conditions, the magnitude of the current is significantly higher than when a compact oxide (at the same voltage) is formed. In terms of the driving force, this implies that an accordingly higher field must be present over the tube bottom (the barrier oxide), as the ion-migration rate is controlled by this oxide layer. A main role of fluorides is thus to maintain a thinner bottom oxide layer^[129] by chemical etching of the oxide layer and immediate complexation (solvatization) of Ti^{4+} species arriving at the oxide–electrolyte interface. Another important factor is that fluoride ions are very small and compete with O^{2-} migration through the TiO_2 bottom oxide (Figure 2c). In fact it has been observed that fluorides may migrate at a rate twice as high as O^{2-} ions through oxide lattices. As a result, a fluoride-rich layer is formed at the metal–oxide interface.^[118] The existence of this fluoride-rich layer was shown by Albu et al. by XPS and SEM analysis.^[118,130] In Figure 5a, a XPS sputter-depth profile through the bottom of a nanotube layer is shown, and it demonstrates two important factors: that fluoride species are present over the entire layer, and that an approximately 20 nm thick fluoride-rich layer is present at the metal–oxide interface. This layer can also be seen by SEM, where a thin salt film is visible on the dimples of the titanium metal substrate after lifting off the TiO_2 nanotubes (see Figure 5b). The very important role of this fluoride-rich layer in the development of the further tube morphology is discussed in Sections 2.3. and 2.5.

The nanotube layers, as they are grown in fluoride containing electrolytes, show a V-shaped sidewall thickness profile^[118,124] (Figure 5c) that is due to exposure of the formed tubes to the etching fluoride-containing electrolyte (permanently etching and thinning the tube walls). The general shape and composition distribution can therefore be summarized as in Figure 5c: The outer part of the shell (OST) is typically dense very pure TiO_2 , and the inner part (IST) of the tube is of a more loose nature and contains incorporated electrolyte components. Detailed SEM work showed that chemical dissolution of the inner TiO_2 layer is faster and thus contributes more to the fact that the walls become thinner towards the top of nanotubes (Figure 5d). The tube layers overall have a considerable fluoride ion content but the fluoride (or carbon) content decays strongly upon annealing.^[118,131]

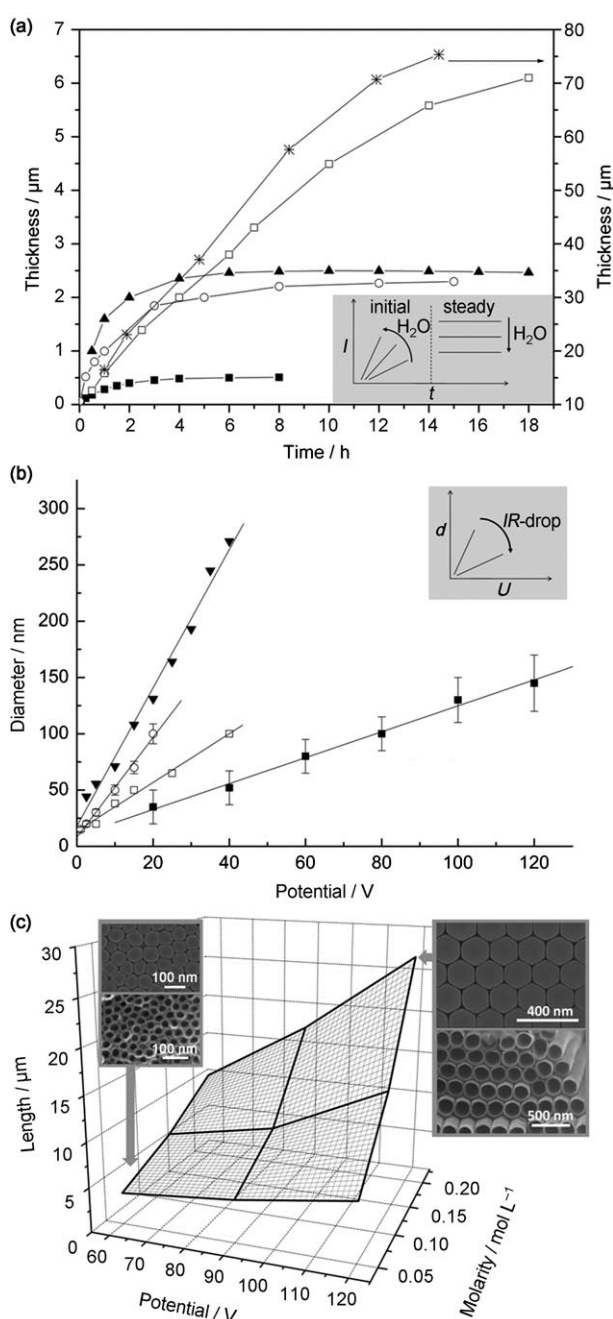


Figure 4. a) TiO₂ nanotube-layer thickness with anodization time for different electrolytes (anodization voltage for ethylene glycol electrolyte held at 60 V, and 40 V for other electrolytes): ■ water-based acidic,^[103] ▲ water-based neutral,^[105] □ glycerol,^[106] ○ glycerol/H₂O 50:50,^[129] * ethylene glycol.^[364] b) Voltage dependence of the tube diameter for different electrolytes: ○ water-based, ▼ glycerol/H₂O 50:50, □ glycerol, ■ ethylene glycol. c) Parameter study for growth rate and ordering of TiO₂ nanotube layer in ethylene glycol electrolytes. Note that for conditions beyond optimized (that is, higher voltages or higher fluoride concentrations), no ordered tube layers are obtained (reproduced with permission from Ref. [108]). The inset images in (c) demonstrate the increase in ordering with parameter optimization.

2.3. Factors Affecting Geometry and Composition

While anodization time and etching rate define tube length, as described above, the diameter of the nanotubes is controlled linearly by the applied voltage.^[124,126,129,132] Some typical results are shown in Figure 4b for some aqueous and non-aqueous electrolytes. The fact that the voltage dependence has a different slope in non-aqueous electrolytes can be ascribed to a large extent to the low conductivity of organic electrolytes and resulting IR-drop effects,^[133–136] that is, the fact that the effective voltage of the electrode is $U_{\text{eff}} = U_{\text{nominal}} - IR$, where R is the resistivity of the electrolyte and I is the current. As reaction products are formed with anodization time, the conductivity of the electrolyte changes,^[134] and thus variations in the diameter (larger diameters) are observed for longer anodization times.

Investigations into optimized conditions for tube growth usually lead to results such as those shown in Figure 4c, where the tube length as a function of anodization voltage and fluoride concentration was investigated. It is remarkable that the fastest growth conditions typically also represent conditions for optimized ordering. The nanotubes grown from organic electrolytes, such as ethylene glycol, DMSO, glycerol, or ionic liquids, show some significant differences in morphology and composition compared with nanotubes grown in aqueous electrolytes; owing to the low water content, very long tubes and large diameters (up to 700 nm)^[137] can be grown.

Most striking is, however, that in organic electrolytes, smooth tube walls can be obtained.^[106] This is due to a lower water content in the electrolyte, which controls tube splitting (see Section 2.5). While a V-shape morphology is present for aqueous and non-aqueous electrolytes, in some organic electrolytes and for higher-voltage anodization, the inner tube layer (IST) shows an extremely high uptake of carbon from the electrolyte (see the table in Figure 13c). That an inner carbon-rich contamination layer is present (for tubes formed in organic electrolytes, such as ethylene glycol) can be explained by the fact that the voltage-induced Schottky breakdown mechanism is operative for high-voltage anodization, leading to a decomposition of the organic electrolyte.^[138] In aqueous electrolytes, the inner tube layer is typically more hydroxide-rich than the outer layer.^[139–141]

In organic electrolytes, aging of the electrolyte is often required to obtain highly defined tubes. Aging involves repeated anodization of dummy titanium sheets before the target sample is prepared. Very extensive work on aging of the electrolyte was recently performed by Lee et al.^[134] Crucial factors in aging are the combined increase of the TiF₆²⁻ content in the electrolyte (reduced TiO₂ dissolution) and the reaching of a steady water content in the electrolyte (for example, ethylene glycol is relatively hygroscopic and tends to take up considerable amounts of water from environmental air).

Under steady-state conditions, the nanotubular oxide layer thickness depends linearly on the anodization time; that is, the charge passed during anodization. However, due to etching by the electrolyte, at some point an equilibrium state between the growth of the oxide and chemical dissolution

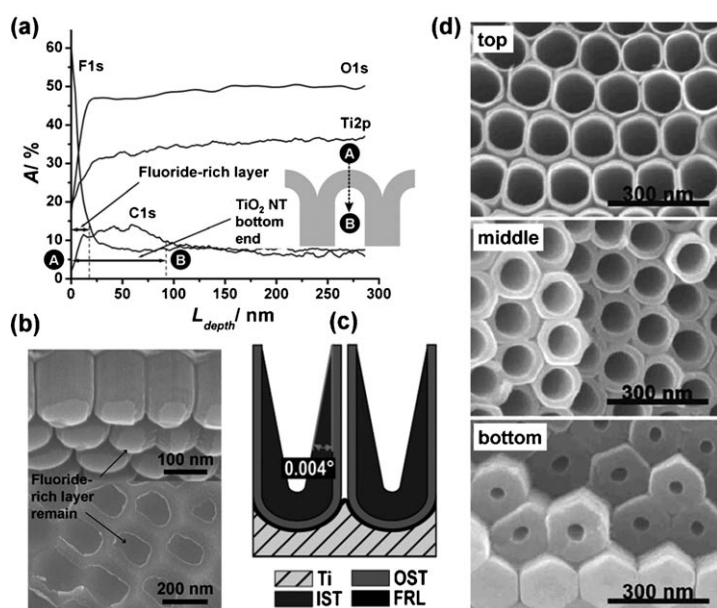


Figure 5. a) XPS depth profile taken through the bottom of a lifted-off TiO_2 nanotube layer. b) SEM images showing the fluoride-rich layer in the form of flakes on the titanium substrate and some left at the bottom part of nanotubes after lift-off the nanotube layer along with corresponding patches at the nanotube bottoms. c) Typical TiO_2 nanotube formed in organic electrolyte and consisting of an inner (IST) and outer oxide shell (OST) and a fluoride-rich layer (FRL) (reproduced with permission from Ref. [118]). d) SEM images of TiO_2 nanotubes taken at the top, from the fractures in the middle, and close to the bottom of a tube layer, illustrating the gradient in the tube-wall thickness (reproduced with permission from Ref. [110]).

exists. As the etching rate, according to Equation (6), is even faster in acidic electrolytes, tube length is limited to 500–600 nm in electrolytes at low pH. In neutral electrolyte systems, layer thicknesses of up to 2–4 μm can be obtained owing to the reduced chemical dissolution. However, owing to the hydrolysis reactions [Eqs. (2) and (3)], the pH at the tube tips is considerably lower than in the bulk electrolyte.^[105,142] Chemical dissolution can however be further decreased by anodization in glycerol or ethylene glycol based systems (reduced water content). In these electrolytes, the linear growth behavior could be significantly extended.^[106] In principle, the expected length of the tubes could be calculated by converting the charge into an oxide volume (for example, by assuming 100% current efficiency towards oxide formation and assuming the pores to be formed by purely chemical dissolution). However, the tube lengths are much larger than this estimate; that is, they would lead to a current efficiency of more than 100%. Therefore, other tube-lengthening mechanisms, as discussed in Section 2.4 (oxide flow) must come into play.

Etching of the tube at their top (in long-duration anodization experiments) leads to inhomogeneous top structures (Figure 6a–c). The formation of needle- or grass-like morphologies (Figure 6a–c) at the tube tops can be observed (which may be associated with the distribution of fluorides preferentially at boundary triple points, as outlined in Section 2.5) and collapsing and bundling tube tops (as the walls become too thin to support their own weight or

withstand capillary forces when drying; Figure 6a,b,d). As mentioned, there are various ways to protect tube tops against etching,^[119–121] and an example is shown in Figure 6.

Water content in the electrolyte affects the growth rate and the etching speed (chemical dissolution rate) of the nanotubes. In other words, the effect of water content is two-fold: it is required for oxide formation (tube bottom), but it also accelerates the dissolution of the nanotube layer (if the formed metal fluorides are water-soluble). A striking effect of the water content is that smooth tube walls are obtained for low water content, whereas side wall ripples are formed at higher contents.^[106,129,143,144] The reason for this effect is that for higher water contents, the fluoride-rich layer between the tubes shows a faster etching speed (chemical dissolution rate) than the growth speed of the tubes into the underlying substrate; that is, ripples at the walls of the tubes can be ascribed to the continuous etching and passivation of the cell boundary regions (see also Figure 9b).^[145]

In principle, tubes can also be grown under galvanostatic conditions (that is, by keeping the anodization current constant).^[146] However, this method has the drawback that the voltage may change with time and control over the tube diameter is therefore lost. Work by Taveira et al.^[146] showed that during constant current anodization, the voltage indeed increases and fluctuates. Tube growth proceeds

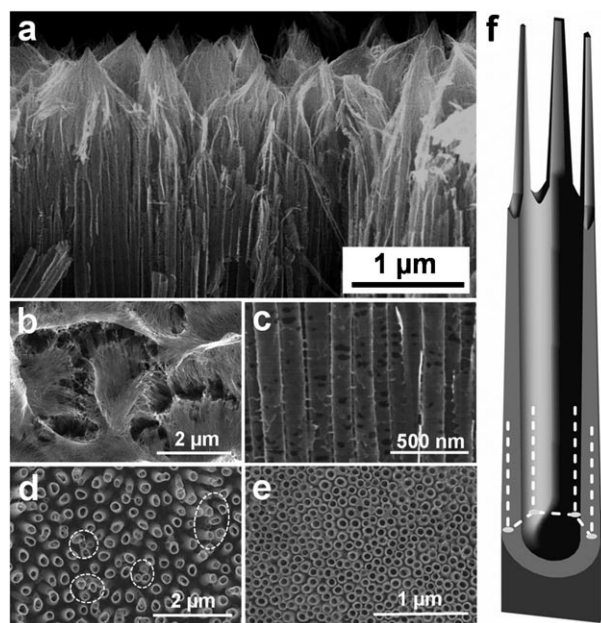


Figure 6. Typical etching effects observed with nanotube layers: a–c) Thinning of tube walls at the tops owing to etching in fluoride-containing electrolyte leads to thinning and collapse of tubes with formation of nanoglass (a,b) or perforated tube walls in the upper tube parts (c). d) Bundling at tube tops owing to a lack of mechanical support. e) Highly ordered grass-free and open tubes prepared by photoresist masking. f) Tube-wall thinning and formation of needles (grass).

up to a critical voltage, then a lift-off of the layers is observed and a new layer forms again. Other growth techniques are the use of alternating voltage (AV) techniques^[147] or support by ultrasonic treatment,^[148] the effects are interesting but overall not a very significant deviation from constant voltage results is observed.

2.4. Growth by Flow Mechanisms

A remarkable feature of TiO₂ nanotubes is that the tubes are longer than expected, as mentioned above and illustrated in Figure 7.^[127,155] The figure shows a cross-section of a lithographically defined nanotube area after anodic growth from a thin titanium layer. This approach allows the oxide expansion factors to be determined very well during the growth and they can be compared to the charge used to form the oxide. The expected expansion factor when metal is

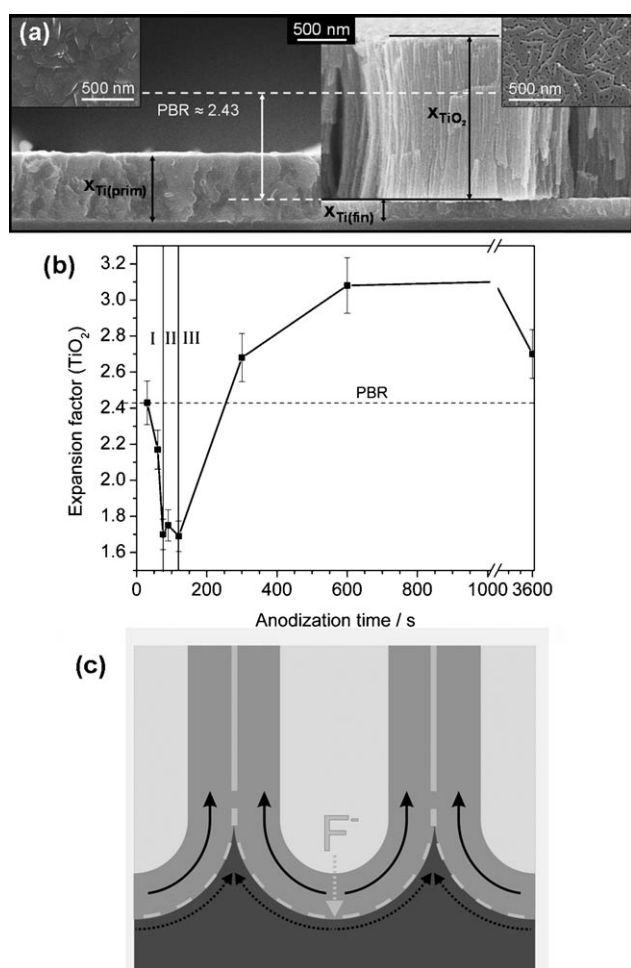


Figure 7. a) Cross-section of a titanium surface before and after anodic nanotube growth. The result indicates a much larger tube length than expected; plain volume expansion would lead to 2.4 (PBR), indicated by a dashed line (reproduced with permission from Ref. [155]). b) Dependence of the expansion factors of anodic TiO₂ layers on the anodization time (reproduced with permission from Ref. [127]). c) Diagram of the flow mechanism pushing oxide and fluoride layer up the cell walls by viscous flow.^[154]

converted into oxide is given by the ratio of the volume of the oxide to the volume of the metal consumed and is frequently called the Pilling–Bedworth ratio (PBR).^[149] The PBR of amorphous anodic TiO₂^[150] is 2.43, which corresponds to the dashed line in Figure 7a (considering the recession of the metal front from its original level). However, Figure 7 shows that the tubes grew much larger than this expectation, and an expansion factor of about 3 can be observed from the cross-section. Figure 7b shows the evolution of the oxide expansion factor (f_{exp}) with anodization time. Early oxide growth in the initial phase occurs with a volume expansion of 2.4 (as expected for a compact anodic oxide) and proceeds, after a decrease, with an increase to a steady expansion factor of approximately 3. Only after very extended anodization is a decrease again observed, which is due to noticeable influence of tube-top etching. This unexpectedly high volume expansion is ascribed to an additional lengthening of the tubes by plastic flow.

The flow concept was originally brought up for growth of porous anodic alumina in 2006 by Thompson et al.^[151,152] and was recently modeled by Hebert et al.^[153,154] For Al₂O₃, oxide flow is assumed to originate from the plasticity of the barrier layer generated by the substantial ionic movement in the high electric field together with compressive stresses induced by the volume expansion (PBR) and electrostrictive forces generated during growth. Another suggested origin for stress is the competition of strong anion adsorption with O²⁻ entrance at the growing oxide lattice.^[154] The result in any case is a force that pushes viscous oxide up the pore walls and thus extends the tube lengths. Overall, the increased volume expansion factors observed during the growth of TiO₂ nanotubes^[127,155] along with other morphological and analytical^[133,156] findings suggest a similar mechanism for the growth of TiO₂ nanotubes. Apart from length extension, another crucial implication is that the inward-migrating fluoride species will be pushed towards the cell boundaries by the flow and continuously accumulate there^[118,145,157] (Figure 7c). This accumulation of fluoride at the cell boundaries and even more at triple points leads to a chemical sensitization of these regions. Owing to the solubility of titanium fluorides in water, these regions are key in the formation of nanotubes rather than porous structures (outlined in Section 2.5 below).

2.5. Transition from Porous to Tubular Structures

At first sight, the self-organized oxide morphologies attained for aluminum and titanium seem to be considerably different (see Figure 1). However, bottom view images (Figure 1c and 8a) of TiO₂ nanotube layers show that the bottom oxide is identical to porous layers. This means that when viewing the bottom or looking at cross-sections near the bottom, a compact hexagonal oxide morphology is present without a separation into individual tubes.^[110] From a tilted bottom view (Figure 8a), it is apparent that there is a continuous transition from a hexagonal porous to a tubular structure. Several studies carried out on Ti/Al alloys (that is, alloys that contain a typical tube-forming material titanium

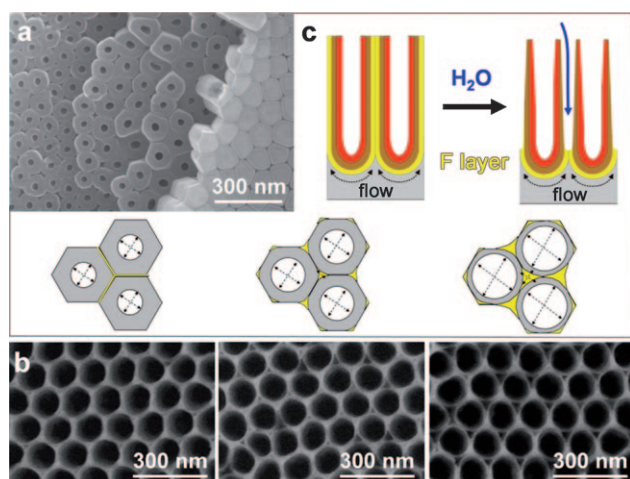


Figure 8. a) Formation of tubes from pore structures, illustrated by an SEM bottom view of a nanotube layer cracked off from the metal substrate at a slight angle. The bottom of a tube layer consists entirely of a close-packed hexagonal pore layer that is gradually converted into round tubes. b) Transition from a porous to tubular structure (left to right). c) Representation of the formation of a tubular morphology from an originally porous morphology by selective dissolution of fluoride-rich layers and preferential etching at triple points by H_2O in the electrolyte.

and a typical pore-forming material Al) were very useful in establishing why pores formed for some metals and anodization conditions but tubes formed under other conditions.^[158,159] For these alloys, oxide layers with distinct porous or tubular morphologies, or even transitional states, could be adjusted depending on electrochemical conditions (in Figure 8 b this continuous transition is shown for a Ti-54Al alloy).^[158,159]

All these findings can be explained phenomenologically by the fact that during growth of the oxide (supported by plastic flow), an accumulation of fluorides takes place at cell boundaries (Figure 8 c). These regions are sensitized, as the fluoride-rich layer is prone to chemical dissolution: Selective chemical dissolution (in aqueous electrolyte) of the fluoride-rich layer etches out the cell boundaries and thus leads to individual tube shapes. Under comparable anodization conditions, an ordered porous oxide is obtained for alumina but a tubular morphology is found for titania, which can be ascribed to the high solubility of Ti-F or Ti-O-F compounds in aqueous media, whereas Al-F species are much less soluble.^[160] In other words, separation into tubes and the etching rate (and thus the point in oxide height where pore cells are split into separate tubes) is determined mainly by the fluoride concentration and the water content in the electrolyte (fluoride solubility).

In this context, it is noteworthy that similar transition phenomena were reported on other valve metal alloys^[36,124,161,162] and also on pure valve metals, such as zirconium and hafnium.^[163–166] In each case it was found that a key parameter affecting the morphology is the concentration of H_2O in the electrolyte. By controlling the H_2O concentration, the oxide morphology of anodic ZrO_2 and HfO_2 could be completely switched from nanoporous to nanotubular.

Selective cell boundary etching was observed even for aluminum under specific conditions.^[167–170]

The effect of water concentration has also recently been studied for pure TiO_2 nanotube formation, and indeed for extremely low H_2O contents in a non-aqueous electrolyte a porous morphology is obtained.^[171] The fact that anodization voltage also affects the pore to tube transition can be ascribed to a field effect on the fluoride ion mobility (faster or slower accumulation) and stress (by electrostriction), which in turn affects viscous oxide flow (and the fluoride layer). The separation mechanism of tube splitting by fluoride dissolution is also the main factor for the formation of sidewall ripples (see also Section 2.7).^[144,152,171]

2.6. Self-Organization Length Scales (Tube Diameter)

The main point in tackling theoretically the reason of self-organization in porous or tubular oxide growth is the question of why a non-smooth surface is stable, as self-scalloping/roughening is not favored in terms of surface energy. Although considerable experimental data exist that identify crucial parameters for self-ordering of porous or tubular structures, a comprehensive fully theoretical model that directly translates into quantifiable experimental data still does not exist. From work on Al, Ti, and TiAl, and also other alloys, it is clear that once tube or pore formation is possible (experimental conditions established), the applied voltage linearly determines the length scale of self-ordering (see also Figure 4). The difference in the various materials can be explained by the different high-field growth factors of the oxides.^[124,126,172] Very elaborate theoretical work has been performed for self-ordering of porous alumina. To explain self-ordering, perturbation methods, and in particular long- and short-wave stability analyses were used, but only in a few cases also associated with specific physical phenomena:^[173,174] to explain why a specific wavelength (tube or pore spacing) becomes stabilized over a flat surface. In light of the contemporary experimental findings, approaches that base stable self-ordering either on the specific ion-flux conditions^[174b] (electromigration) or on the stress generated during oxide growth^[174a] seem most adequate. In ion-flux models, a crucial component is adjustment of ion flux through the oxide and flux across the interfaces versus the interface shape, which under certain conditions can stabilize a short-wave instability. In stress-based models, a key question is whether purely mechanical (volume expansion) or electrostrictive effects dominate. While the length scale (wavelength) for pure Pilling–Bedworth volume expansion is far from accounting for the observed self-ordering length (100 nm range), scales estimated for observed electrostrictive forces are very likely to be in the required range ($\lambda \approx 100$ nm).^[174b] In other words, the compressive electrostrictive stresses occurring in the oxide film, and in particular at the film surface, could be minimized by an increase of the surface area, that is, scalloping of the oxide film. However, the fact that optimized self-organization is typically observed for an optimized set of voltage combined with a specific current situation^[110,175] (see also Figure 4 c) and some preliminary stress measurements^[176]

supports ion flux models that possibly need to be linked with approaches describing the final steady-state (growth) ordering by saturation effects.

2.7. Advanced Geometries

2.7.1. Tube Stacks, Bamboo, Nanolace, and Branched Tubes

Various modifications in the tube geometry can be achieved by changing the anodization voltage during the tube growth process, and some examples are shown in Figure 9. Applying voltage steps can be used for example to generate tube stacks,^[126,144,177,178] or stratification layers

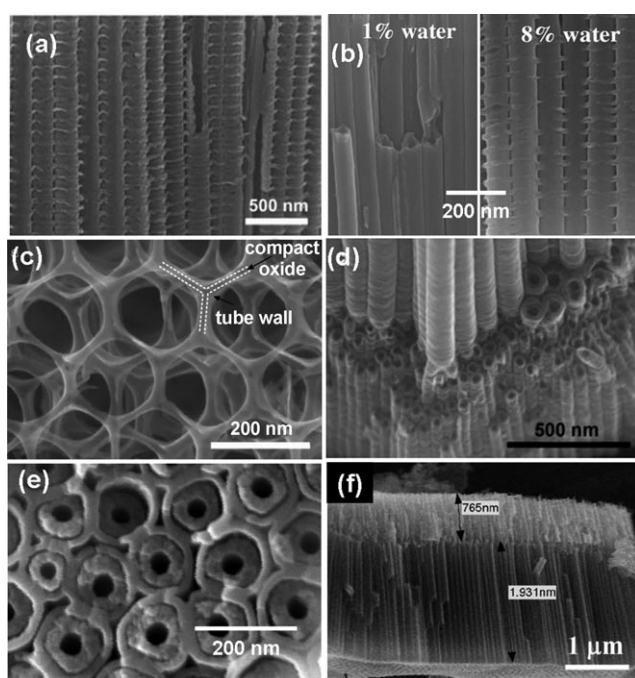


Figure 9. Advanced TiO₂ nanotube morphologies: a) Bamboo nanotubes fabricated by alternating voltage anodization (reproduced with permission from Ref. [178]), b) smooth to bamboo-tube transition induced by variation of H₂O content in the electrolyte (reproduced with permission from Ref. [144]), c) nanolace (reproduced with permission from Ref. [178]), d) branched nanotubes by voltage stepping (reproduced with permission from Ref. [178]), e) double-walled nanotubes, f) amphiphilic double-layer tubes (reproduced with permission from Ref. [177]).

(bamboo).^[178,179] In tube stacks, a second tube layer can be grown underneath the top layer, if desired with a different diameter. Key to whether a second tube layer grows through the bottom of the top layer or starts in the V-shaped open space between the tubes depends critically on the experimental conditions.^[36,178]

If the voltage is lowered during anodization, tube growth will be stopped or drastically slowed down, as the driving field across the bottom oxide is too low to maintain growth. However, owing to the permanent etching of the tube bottom in the fluoride environment, at some point the oxide is

thinned down sufficiently to continue growth under lower field conditions (the tube diameter will in this case adjust to the lower field and thus tube branching may occur). If tube-wall separation (tube splitting) is faster than the etching process through the tube bottom, then the second tube layer will initiate in the space between the tubes.

Stratification layers^[36,178] can be generated when stepping first to a lower voltage while holding the lower voltage for a time that is sufficient to establish diffusion and field conditions corresponding to the lower applied voltage, and then stepping back to the original high voltage. This process has of course to be carried out before tube bottoms are penetrated and a second tube layer grows. In this case the result is the formation of a new initiation layer between the tubes. There are two reasons for this: 1) When the voltage is stepped up, the thinned tube bottom immediately thickens in all directions as new high-field oxide is forming, or 2) because tube separation has reached the bottom but no secondary tube formation has yet been initiated.

By exploring this behavior, regular tube structures with bamboo-like features can be fabricated by pulsing between two appropriate voltages.^[178,179] The distance between the bamboo rings can be altered by adjusting the holding times at different voltages. Bamboo-type nanotubes, with higher surface areas compared to normal TiO₂ nanotubes, are promising in the field of dye-sensitized solar cells.^[179] The oxide quantity formed during initiation process is different^[119,121,128,180] and more etch-resistant in fluoride electrolytes; therefore, after extended exposure to a fluoride containing environment, the tubes are selectively etched out, leaving behind the stratification layers that form a large uniform nanolace structure, which can be converted into large anatase networks.^[178]

2.7.2. Double-Walled Tubes

As mentioned in Section 2.3., in some organic electrolytes formed at sufficiently high voltages, the nanotubes contain an inner carbon-rich shell (Figure 9e) originating from electrolyte decomposition. Upon annealing, the carbon-rich layer can be thermally decomposed, leading to a remaining nanoparticulated inner tube wall.^[118] This effect can be used to increase the inner surface area of the tube layers substantially. The exact structure of these double-walled tubes upon annealing is very sensitive to the annealing conditions, and in particular the temperature ramping speed and holding time, which allows for the fabrication of very robust membranes or entirely separated inner-shell/outer-shell structures.^[118]

2.7.3. Amphiphilic Tubes

Recently, it was reported that growing a first layer of nanotubes, treating them with an organic hydrophobic monolayer (octadecylphosphonic acid; ODP), and re-growing tubes again in an organic electrolyte allows amphiphilic tube stacks to be fabricated^[177] in which the lower tube layer grows through the bottom oxide of the first layer (Figure 9f). Owing to the hydrophobic coating of the top layer and the naturally hydrophilic character of the freshly grown tubes, the

double-layer stacks have a highly amphiphilic behavior (see Section 6.5 for applications). Furthermore, the hydrophobic nature of the top layer strongly aids directing the initiation of the secondary layer. The tube walls are to a certain extent protected against the etching effect from the fluorides, but the voltage-induced chain scission effect (see Section 6.1) leads to preferential removal of the monolayer at the tube bottom. Furthermore, the V-shaped openings between the tubes are even more protected by monolayers owing to suppression of preferential wetting of the space in between the tubes (see Section 4.5).^[181]

2.7.4. High-Order, Defined Tube Tops

The highest level of ordering in TiO₂ nanotube layers is achieved in non-aqueous electrolytes, such as glycerol or ethylene glycol, and in fact by using ethylene glycol electrolytes under optimized conditions (electrochemical and electrolyte),^[108,118] very closely packed tubes with a hexagonal symmetry can be obtained (see Figure 4c). The key for a high degree of ordering is to grow under optimized electrochemical conditions, which are typically conditions under which maximum current is achieved but oxide dielectric breakdown (sparking) is avoided. This is entirely in line with observations by Ono et al. that were made for highly ordered alumina growth that also is optimized at maximum current but avoiding burning events.^[175,182] Even further improved ordering of the tubes can be achieved using pre-structured surfaces that provide geometrical guiding. This was demonstrated^[110] for example by tube formation followed by a removal of the tube layer and a second anodization. The organized dimpled titanium metal surface after removal of the first tube layer acts as initiation sites for tube growth in the second anodization step, which results in an optimized hexagonal arrangement. This procedure was originally established for aluminum by Masuda et al.^[116] and has been used frequently since then to obtain highly ordered alumina arrays.

A commonly undesirable feature is the presence of non-ideal tube tops (as shown in Figure 6), and three different origins should be distinguished: 1) Initiation layer remnants that may cover the tube tops while highly ordered layers are growing underneath. These initiation layer remnants are etched off in the fluoride-containing electrolytes with time, and their creation can be minimized by using a voltage sweep approach^[105] to the desired final anodization voltage rather than using direct voltage steps. In some cases these layers can be removed by adequate polarization/sonication techniques^[183] or can be minimized by using sacrificial layers.^[119–121] 2) Collapsing tubes: the tube tops are exposed to the electrolyte for the longest time and therefore are etched by fluorides the most. If the tube tops are considerably thinned down, the tube walls become comparably flexible and tend to stick together in irregular bundles (see Figure 6d) owing to capillary effects while drying samples by gas streams or heating. This effect can to a large extent be avoided by supercritical drying^[184] or keeping tube tops sufficiently rigid.^[119–121] 3) Grass or needles: if etching thins down the tube tops even more, the tube walls start becoming perforated and disintegrate. The etching is not entirely uniform and

typically some needles (often called nanograss or even nanorods^[185]) remain on the tube top (see Figure 6a,b). To counteract the formation of nanograss, various approaches have been reported^[119–121] that often rely on protecting tube tops by some sort of etching resistant layers. These involve thermal rutile layers, sacrificial tube layers, or photoresist layers: these layers not only provide enhanced protection against etching of the tube tops but also suppress undesired local convection effects from the electrolyte.

2.7.5. Self-Organization on Two Size Scales

A very spectacular effect, two-size-scale self-organization, was first observed when growing tubes on a complex biomedical titanium-based alloy.^[186,187] In this case, tubes of two distinct different diameters were formed under some anodization conditions that were highly ordered and arranged. This effect was later also reported for a range of more simple binary^[124,188–190] and ternary^[191,192] alloys. The origin of this highly unusual effect is still not entirely clear. While this effect was originally attributed to alloy composition, it seems however more related to geometry stabilization effects under certain anodization conditions.^[36] This is most evident from very recent findings on two-level size-scale stabilization on pure titanium.^[137,193]

2.7.6. Membranes

The defined geometry (length and diameter) make nanotube layers very interesting for membrane-type applications, such as filtration or microphotoreactors (see Section 6.1). The strategy to produce such membranes typically consists of the formation of a tube layer, its separation from the substrate, followed by opening the tube bottoms. A typical free-standing membrane is shown in Figure 10. In the first report on the fabrication of such free-standing flow-through membranes,^[123] nanotubes of 50–100 μm length were grown, then the underlying titanium metal was selectively dissolved in Br₂/CH₃OH, and then the oxide bottom of the tubes was etched open by HF vapor. Flow-through and photocatalytic activity was demonstrated for such membranes. Thereafter, several other approaches were reported, which mostly involve modifying the lift-off and opening procedure using for example sonication or voltage pulses.^[194–196] However, the main problem remains the lift-off process (particularly if the membrane is thinner than 50 μm), which is increasingly difficult to handle without causing membrane rupture, and this becomes an even bigger challenge if larger membrane areas are desired. Furthermore, opening the tube bottoms uniformly over a large area by a chemical etching process (using HF, oxalic acid, or any other etchant) is difficult because as soon as tube bottoms are etched open at one location, the etchant creeps up the tube walls by capillary forces. This problem is most severe for thin membranes.

A fundamentally novel approach was reported recently that eliminates these difficulties.^[121] Albu et al. evaporated an aluminum film on a thin titanium foil, anodized from the titanium side, and grew tubes through the titanium into the underlying aluminum (using to advantage the fact that

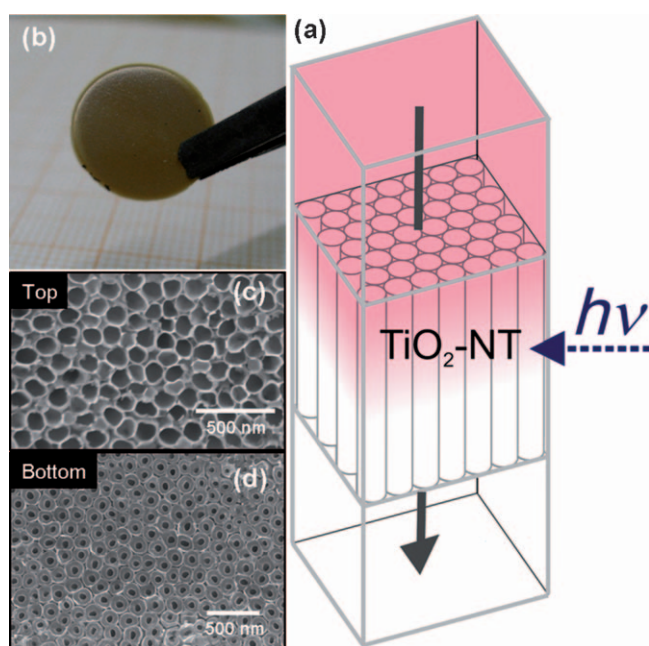


Figure 10. A TiO₂ nanotube membrane produced by anodic tube formation, lift-off, and bottom-opening processes. a) Flow through a membrane, b) optical image of a robust membrane (reproduced with permission from Ref. [118]) c, d) SEM images of a membrane open on both sides: c) top view, d) bottom view.

ordered porous alumina can also be formed in fluoride-containing electrolytes).^[158] The remaining aluminum metal and oxide were then selectively chemically dissolved. Another highly beneficial feature introduced by Albu et al. is that the etched area was defined by a photolithographic process to form a grid structure. The remaining titanium metal frame allows for a high mechanical flexibility and excellent electrical contact to the enclosed nanotube packs. This strategy allowed large-scale membranes to be reliably created for the first time.

3. Properties of TiO₂ and TiO₂ Nanotubes

The main reason why TiO₂ nanotubes are currently attracting such a high interest is that some of the intrinsic properties of TiO₂ provide the basis for many outstanding functional features. In the following, we will briefly discuss some of the most relevant material properties of TiO₂; for more detailed material properties, the reader is referred to some excellent reviews.^[16, 22, 28, 40, 197, 198] However, in the following sections, we will address several specific features relevant to TiO₂ nanotubes.

3.1. Crystal Structure

TiO₂ exists naturally mainly in three crystalline phases: anatase, rutile, and brookite. Other than these, a synthetic layered phase, called TiO₂(B),^[199] and some high-pressure polymorphs also exist.^[200] Moreover, TiO₂ structures formed

at room temperature (sol-gel techniques, or anodic oxides) often are obtained in an amorphous form. Among the different polymorphs, rutile is generally considered to be the thermodynamically most stable bulk phase, while at the nanoscale (< 20 nm), anatase is considered to be stable, although there are some arguments in literature.^[200, 201] Regarding nanoscale materials, it is important to realize that surface energy and stress have a significant effect on phase stability. The surface energy depends on the number of uncoordinated titanium cation sites. Fourfold-coordinated centers have larger surface energy than those with fivefold coordination, and the surface energy increases with the number of uncoordinated positions. In case of anatase crystals, the surface energy is lower than for rutile. However, the stress energy shows the opposite behavior. Both energies have some compensational effect; therefore, it is not surprising that a somewhat unclear picture exists regarding the most stable phase in nanoscale materials.^[201, 202] Moreover, the presence of some ionic species in the lattice, such as Cl⁻ or F⁻, also influences the stability of particular polymorphs.^[180, 203–205] For example, rutile is more stable in presence of chloride ions.^[203–205] In the case of anodic oxidation of titanium, the amorphous oxide layer can be converted by extended anodization times into rutile in fluoride-containing electrolytes, whereas in fluoride-free electrolytes, anatase can be obtained.^[180] In anodic layer formation, the conversion from an amorphous TiO₂ film into a crystalline anatase phase and dehydration effects are reported to depend not only on time but also on the applied voltage.^[101, 206–209]

Apart for stoichiometric TiO₂, various suboxide phases exist that have very interesting properties. Substoichiometric compositions of titania may be described by the general formula Ti_nO_{2n-1} (4 ≤ n ≤ 10), but some defined phases are most remarkable, such as Ti₄O₇, Ti₅O₉, Ti₆O₁₁, Ti₇O₁₃, Ti₈O₁₅, Ti₉O₁₇, which are usually called Magnéli phases.^[210, 211] Such phases are made up of two-dimensional chains of titania octahedra; for example, Ti₄O₇ can be considered as three TiO₂ octahedra and one TiO octahedron with oxygen vacancies at the edge of the unit cells. Such Magnéli-phase titanium oxides are highly conductive (almost as high as graphite) and can be formed under reductive high-temperature treatment in H₂^[210] or C₂H₂.^[212, 213]

In fact, many properties of TiO₂ strongly depend on bulk or surface structural defects, and in particular on the formation or presence of bulk or surface Ti³⁺ states or O²⁻ vacancies.^[40] On the surface of TiO₂, unsaturated titanium cations, such as Ti³⁺, Ti²⁺, and Ti⁺, may for example be generated during vacuum or inert-gas annealing (TiO₂ surfaces at low oxygen partial pressures tend to split off O₂ or H₂O from terminal oxide or hydroxide groups and form bridged oxide and Ti³⁺ states). Such effects can also be obtained under inert gas sputtering (for example, with Ar⁺) or e-beam exposure etc. Usually, Ti³⁺ states are found after such treatments, which are crucial for electronic and optical properties and also the surface reactivity. Under UV irradiation and in the presence of O₂, adsorbed oxygen can be reduced to O²⁻ and thereby inhibit the generation of Ti³⁺ sites. During long-time annealing, Ti³⁺ atoms may diffuse from the surface into the bulk of TiO₂.

TiO₂ nanotubes, after electrochemical formation, are amorphous, and some reports^[103,118,214] indicate the presence of nanocrystallites in the tube wall, particularly if anodization is carried out at higher voltages. For example, in acidic electrolyte (H₂SO₄), depending on the anodization conditions (sparking, potentiostatic, or galvanostatic), the as formed oxide film may consist of anatase, a mixture of anatase and rutile, or rutile crystallites.^[129,215–217] Reports that suggest the presence of crystallites in as-formed oxide nanotubes and which are based on HRTEM investigations need to be examined very critically, as amorphous TiO₂ seems to be particularly prone to electron-beam-induced crystallization.^[214]

Intended conversion of the tubes into crystalline material (anatase/rutile) by annealing is discussed in Section 4.1. In general, amorphous material (such as tubes and powders) can be converted into anatase (ca. 300–500 °C) or rutile (> 550 °C) by a thermal treatment in air. It should be noted however that surprising size effects on these transitions have been observed for nanotubes^[201] and that several alloying elements affect the transition temperature.^[188,189,218] There are some reports that show that doping with Nb, Al, Ni, Ga, Ta, and W retards the growth of anatase and rutile crystallites and delays the anatase-to-rutile phase transformation.^[219–221] On the other hand, Mn, Fe, Cu, and Zn are generally believed to promote the phase transformation. For TiO₂ nanotubes, niobium addition in particular was reported to lead to a significant temperature shift for anatase conversion.^[188] The process is believed to be due to the inhibition of nucleation of anatase crystallites by the niobium dopants.^[222,223] In the case of zirconium^[189] and tungsten,^[224] slightly elevated temperatures are also needed to convert the tubes into anatase.

3.2. Optical and Electrical Properties

In TiO₂, the relevant energy levels that form the band edges and thus define the bandgap are considered to be the Ti 3d states and O 2p levels. The lowest empty energy levels are Ti d_{xy} and thus they are representative of the conduction band (CB) edge, whereas full O 2p states (in particular, non-bonding p_π states) define the valence band (VB). Both anatase and rutile show this general distribution of states.^[225,226]

TiO₂ has an indirect optical bandgap for anatase of 3.2 eV, for rutile of 3.0 eV, and amorphous material is reported to have a mobility gap of about 3.2–3.5 eV.^[225,227–230] Crucial for the optical and electrical properties is the presence of defects that provide additional states in the bandgap near the CB or VB. Particularly important in TiO₂ are oxygen vacancies and Ti³⁺ states, which to a large extent dominate optical and electrical properties of the material. Typically Ti³⁺ states are situated about 0.2–0.8 eV below the conduction band (see also Figure 14a).^[197,231] Electrons may be trapped in the Ti³⁺ sites or the holes may be trapped in oxygen states, leading to radicals covalently linked to the TiO₂ surfaces. Such shallow defects can release trapped charge carriers easily to the nearby conduction or valence bands by thermal excitation.

The Ti³⁺ content seems to entirely dominate the conductivity of TiO₂ crystals. Investigations on the typical

conductivity of anatase and rutile TiO₂ films reveal that the conductivity of undoped anatase and rutile is more or less similar (range of 10⁴–10⁷ Ω cm). When thermally reduced, the conductivity for anatase and rutile is significantly different (in the range of 10⁻¹ Ω cm for anatase and 10² Ω cm for rutile); for anatase the conductivity becomes independent of the temperature.^[227,232]

A wide range of studies investigate the optical properties of TiO₂ nanotubes, mainly in photoelectrochemical arrangements in an electrolyte, or by measuring optical absorption coefficients in reflectivity or transmission mode in air. For as-formed tubular layers, a photocurrent behavior (Figure 11a) is often obtained with a band (mobility) gap of approximately 3.1–3.3 eV for the amorphous tubes.^[233] After conversion to anatase, the photocurrent strongly increases and a gap of 3.2 eV results. If annealing is performed to form rutile, the gap is correspondingly narrower and is about 3.0 eV.^[233] There are two major observations for tubes in comparison to

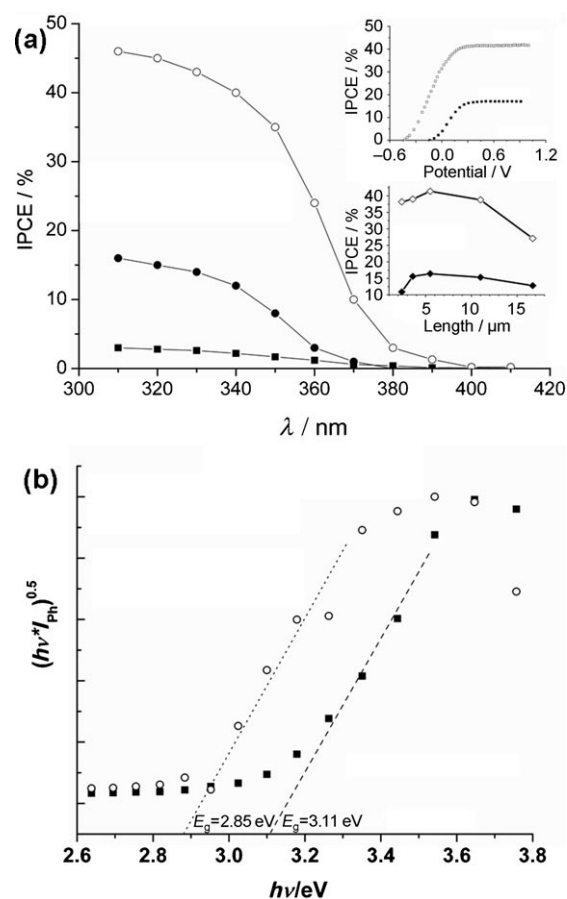


Figure 11. Photocurrent response from TiO₂ nanotubes:^[235] a) IPCE versus wavelength spectra of different TiO₂ nanotube layers (amorphous and annealed) in 0.1 mol dm⁻³ Na₂SO₄: ■ amorphous (NTs or compact oxide), ● 2.4 μm (annealed), ○ 2.4 μm (annealed) with CH₃OH. Inset: Incident photon-to-current conversion efficiency (IPCE) dependence at 350 nm on the applied voltage and different tube lengths in 0.1 mol dm⁻³ Na₂SO₄ in presence (◇) and absence (◆) of 2 mol CH₃OH. b) Photoresponse spectra of TiO₂ nanotubes (thickness ca. 1.8 μm) fabricated in aqueous Na₂SO₄ solution (■) and in ethylene glycol (○), showing altered sub-bandgap response in carbon containing electrolytes.

compact layers: 1) To obtain a contribution to the photoresponse from the tube walls, the tubes need to be annealed; the amorphous material contains such a high density of recombination centers that there is virtually no photoconductivity in the tube walls; 2) for tubes annealed to a crystalline material, the doping level is typically very high (10^{18} – 10^{19} cm⁻³); that is, if in a photoelectrochemical configuration a voltage is applied at relatively moderate bias (ca. 0.3 V anodic to the flat band potential), total carrier depletion of the walls is reached^[235] (using capacitance data and the Schottky approach).^[234,236–238] In other words, the space charge layer follows the wall contours only up to this threshold voltage (and may aid charge separation); at higher voltages the depletion layer cannot extend any further. This is the key reason why for tubular shapes a deviation from the classical Gärtner model^[239] for the potential dependence of the photocurrent is observed.^[235]

In general, the determined density of bulk states (10^{18} – 10^{19} cm⁻³) is much higher for nanotubes than for conventional nanoparticles. As a result, charge-carrier transport in TiO₂ nanotubes is much slower than in comparable nanoparticulate systems, as the bulk states strongly affect the trapping/detrapping-dominated majority-carrier transport. However, the electron diffusion length under UV illumination is up to 30 times higher than for comparable nanoparticle layers owing to lower surface recombination.^[235] The overall photocurrent in tubes and particles is determined to a large extent by surface recombination effects, as is evident from measurements carried out in presence of a hole scavenger (Figure 11 a). When methanol is added to the electrolyte, the diffusion length for photogenerated electrons is drastically enhanced owing to a reduced recombination probability with surface-trapped holes.^[235] For tubes, the electron diffusion length depends extremely on the type of tubes used, whereas rough-tube walls (first-generation tubes formed in aqueous electrolytes) lead to a diffusion length of $L_n \approx 1$ – $2 \mu\text{m}$; for second-generation (organic electrolyte) tubes, $L_n \approx 25 \mu\text{m}$ can be obtained.

Another interesting point is that photocurrent spectra for different types of nanotubes show a slightly different sub-bandgap response. For nanotubes prepared under double wall conditions,^[118] that is, in some organic electrolytes at higher voltage, a tail in the photoresponse is observed owing to carbon remnants (Figure 11 b; see also Section 4.2 on carbon doping).

Another optically interesting feature of TiO₂ is its comparably high refractive index ($n = 2.5$ for anatase to 2.9 for rutile)^[240] in comparison with other materials that are used to manufacture 3D optical structures (SiO₂, $n = 1.5$; Al₂O₃, $n = 1.7$).^[241] This high refractive index should allow to create very interesting photonic materials that for example are predicted to show a negative-refractive-index photonic crystal structure.^[242] In practice, however, to fully experimentally realize such structures, some additional control over geometry and order of the tube arrays is needed.

Optical nanosize effects in terms of bandgap widening have not been observed for TiO₂ nanotubes, although the tube walls in some cases come close to the dimensions (5–10 nm) where effects could be expected.^[243–245] The size, however, is

sufficient to observe phonon confinement in tube walls,^[222,223,246] which is dependent on crystallite size in the wall and depends on whether 1D or 2D confinement is established. Most remarkable, however, is an unexpected phase stabilization upon annealing.^[201] While annealing for nanotubes at moderate temperatures ($> 200^\circ\text{C}$, $< 550^\circ\text{C}$) usually converts nanotubes with a diameter of more than 30 nm to anatase, for smaller diameters, rutile can be stabilized.

The electrical conductivity of self-organized TiO₂ nanotubes on titanium metal has been estimated by two-point measurements between a metallic contact on the top of the tubes and the back metal substrate.^[247] Some results as a function of annealing temperature are shown in Figure 12 a. Although two-point measurements may not yield entirely reliable values (in absolute terms), the behavior shown is very characteristic for all TiO₂ nanotube layers. For low temperatures ($< 200^\circ\text{C}$), the resistivity increases with temperature, owing to evaporation of surface water. At about 300°C , conversion of the amorphous material to anatase occurs, and a significantly higher conductivity is obtained. At temperatures higher than 500°C , the anatase material is increasingly

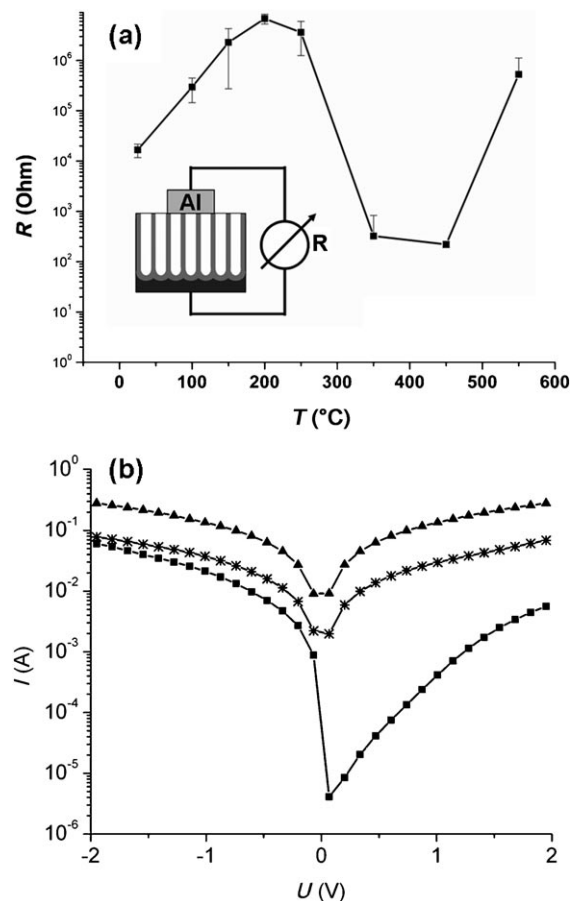


Figure 12. Two-point conductivity measurements for TiO₂ nanotube layers a) annealed for 2.5 h at different temperatures in air^[247] and b) I – U characteristics for anatase tubes before (■) and after (*) carbon doping in C_2H_2 and conversion into semimetallic tubes (▲); high-temperature C_2H_2 treatment; reproduced with permission from Ref. [212].

converted into more resistive rutile, which leads to a considerably lower conductivity. Using reducing and carbonizing annealing conditions, the conductivity strongly increases,^[247] and reduction to titanium oxocarbides can even provide a virtually metallic behavior.^[212]

3.3. Reactivity

TiO₂ surfaces have been extensively studied regarding gas-phase adsorption and catalytic effects on various reactions (for a comprehensive overview, see reference [40]), such as CO oxidation,^[248,249] selective reduction of NO_x^[250] and O₂ and water decomposition.^[251–253] Rutile TiO₂ (110) in particular is the preferred substrate for UHV studies owing to the comparable ease with which these single crystal surfaces can be properly prepared. Overall, it has been shown that surface defects are the crucial reactive sites for many reactions. For example, on defective (110) rutile surfaces OH-surface groups can be formed after H₂O adsorption,^[254–256] which is proposed to be due to a reaction of bridged oxide with an adsorbed water to form hydroxides. For H₂ adsorption, oxygen vacancies were reported to act as electron donors,^[256,257] and Ti–H can be formed. Such hydrogen atoms may recombine or diffuse into the bulk of the TiO₂ and dope the material; an according increase of conductivity is observed^[258,259] (see also Figure 14a). Studies on rutile surfaces with very low defect densities showed that defects (oxygen vacancies) were crucial for CO adsorption.^[256,260] Similarly, NO oxidation^[256,261] and SO₂ reactions^[256,257] strongly depend on the presence of oxygen vacancies or presence of Ti³⁺ on the surface. Whereas NH₃ only weakly interacts with defects,^[240,256] H₂S may be dissociated.^[256,262] Ti³⁺-rich surfaces show considerable reactivity regarding deoxygenation reactions of organic molecules, such as alcohols.^[256,263,264] Regarding O₂ adsorption, significant adsorption and O₂ formation^[256,257] was only observed on defective surfaces, and no oxygen adsorption could be detected on intact surfaces.^[256,265] Some reports exist regarding O₂ dissociation at elevated temperatures, and this fact is in line with the observation that Ti³⁺ states can be easily annealed out (oxidized) using high-temperature O₂ exposure.^[256,266]

These examples may illustrate why reactions on nanoscale TiO₂ particles and nanotubes are highly promising. Nanoscale materials can have an extremely high density of defect sites (lattice corner and kink sites), may possess extreme surface curvature, and may stabilize unusual crystal orientations or crystal phases.

For TiO₂ nanotubes, proper UHV surface studies were mainly carried out by Burghaus et al.^[248,249,251–253] They investigated CO, CO₂, H₂, O₂, and alkane activity on different crystal structures of TiO₂ nanotubes. Currently, reports on unexpected O₂ adsorption on anatase TiO₂ nanotubes are highly interesting.^[251] TiO₂ nanotubes are the first example of an intrinsic TiO₂ nanostructured material for which active O₂ adsorption could be observed; this can usually only be observed for samples where active defects were introduced, for example by ion bombardment or for some powders.

In solution, the most important reactive features of TiO₂ are: 1) its solubility in some complexing agents (HF, organic acids), 2) the possibility of modifying the surface with organic monolayers by surface hydroxy group reactions (discussed in Section 4.5), 3) the feasibility of inducing apatite formation (see biomaterials in Section 6.5), and 4) its electrochemical properties. Electrochemically, anodically formed amorphous TiO₂ layers behave like a highly defective n-type semiconductor, and annealed to anatase or rutile like a highly doped n-type semiconductor.^[233,234,237,238,267,268]

A very important electrochemical feature is the ability to reduce Ti⁴⁺ in the TiO₂ lattice to Ti³⁺ if a sufficiently negative potential is applied. The reduction reaction is accompanied by insertion of small cations (Y⁺ = H⁺, Li⁺ from the solution) into the TiO₂ lattice [Eq. (7)]:



There is a color change associated with formation of the reduced Ti^{III} material (usually dark blue to brown) that can be exploited for suitable electrochromic devices.^[269–273] For TiO₂ and other transition-metal oxides, the electrochemical reduction and re-oxidation are reversible with a switching time that is determined by the solid-state diffusion/migration of Y⁺ into and out of the lattice. Therefore, nanotube surfaces with nanoscale wall thicknesses allow comparably fast switching in the millisecond to second range (see also Sections 4.4 and 6.3).

Under anodic polarization, a current blocking situation is established in n-type TiO₂ electrodes. The material can thus be exploited for photoelectrochemical reactions, such as for photocatalysis (Section 6.1) or in solar cells (Section 6.2). In all these applications, the directionality of the nanotube layers may be beneficially exploited.

TiO₂ nanotubes have some beneficial effects as a substrate for noble metal catalysts in electrocatalysis. For example, it has been shown that for TiO₂ nanotubes decorated with gold, a more facile O₂ reduction reaction can be observed,^[274] or that a highly accelerating effect for methanol oxidation catalysts can be obtained.^[212,275–278] Such electrocatalytic effects of TiO₂ nanotubes have also been explored for glucose sensing.^[279] All of these applications rely on the fact that owing to carrier depletion conditions in the TiO₂ substrate, a high overpotential for the oxygen evolution reaction is provided. A particularly beneficial effect of the tubular substrate as a support for nanoparticles is not only the large surface area, but may be even more importantly the compartmentization of the electrode surface. The nanotubular arrangement can contribute to avoid catalyst aggregation and thus lead to an increase in reactivity and specific reaction rates. The loadings of expensive noble metal catalysts can be therefore considerably reduced.

4. Modification of Tube Properties

Modification of the TiO₂ nanotubes is mainly carried out by 1) heat treatments, 2) introducing other elements, or 3) by tube-wall decoration. The aim is to make the material suitable

(or even more suitable) for various applications that rely on specific electrical, optical, or chemical properties. In view of electronic properties, annealing to a crystalline structure mainly changes the conductivity and lifetime of charge carriers, while active doping or bandgap engineering by introducing other elements targets decreasing the optical bandgap, thus enabling a visible-light photoresponse. Particle decoration is often used to increase surface catalytic effects and to create solid-state junctions. Some of the modification approaches are borrowed from techniques that are already established for bulk or nanoparticulate TiO₂; others are specific for anodic nanotubes. For anodic nanotubes, the fact that the synthesis route for the nanotube arrays is an electrochemical oxidation of a metal piece can be taken advantage of, and therefore some specific doping principles become feasible (for example using an alloy of TiX for anodization, where X is another metal that may act in its oxidized form as a doping species).

In many conventional applications, nanoscale TiO₂ is either used as isolated nanoparticles (for example, in a suspension) or as an electrode consisting of TiO₂ nanoparticles that are compacted or sintered on a back contact. The latter case significantly differs from isolated particles in a solution, as the charge transfer for electrodes through the entire layer to the back contact is crucial. This, of course, also applies to nanotubular oxide electrodes, where charge transfer in the tube walls along the tubes to underlying titanium or the back contact is very important. Therefore, intense efforts focus on modifying the electrical properties of TiO₂ nanotubes.

4.1. Annealing

As mentioned above, the as-prepared TiO₂ nanotubes are amorphous in nature but can be annealed (under oxidizing conditions in air or O₂) to anatase or rutile.^[104,118,233,247,267] Examples of typical structural and compositional characterization before and after annealing are shown in Figure 13. Detailed XRD investigations show that significant conversion of nanotube layers into anatase begins at around 280 °C. With an increasing annealing temperature, anatase formation is enhanced.^[280] Above about 500 °C, the rutile phase starts to appear, and with a further increase in the annealing temperature the quantity of rutile increases; for example 12 h annealing in air results in 4% rutile at 500 °C, 17% at 600 °C, 30% at 700 °C, and 46% at 800 °C. At 900 °C and relatively short-time annealing (2 h) and with a ramping speed of 1 °C s⁻¹, the TiO₂ nanotube layer is completely converted into a rutile structure. The annealing duration and ramping speed also has a significant effect on the crystal structure of TiO₂ nanotubes and furthermore affects the composition of the nanotubes. As-formed nanotubes contain a significant amount of fluoride species^[104] (Figure 13b,c), and if formed in most organic electrolytes (see Figure 13c), a significant amount of carbon is contained, being decomposition products of the electrolyte.^[137] These species can be driven out to a large extent by annealing.^[118] Typically, the as-formed tubes also contain some surface hydroxide groups (evident for

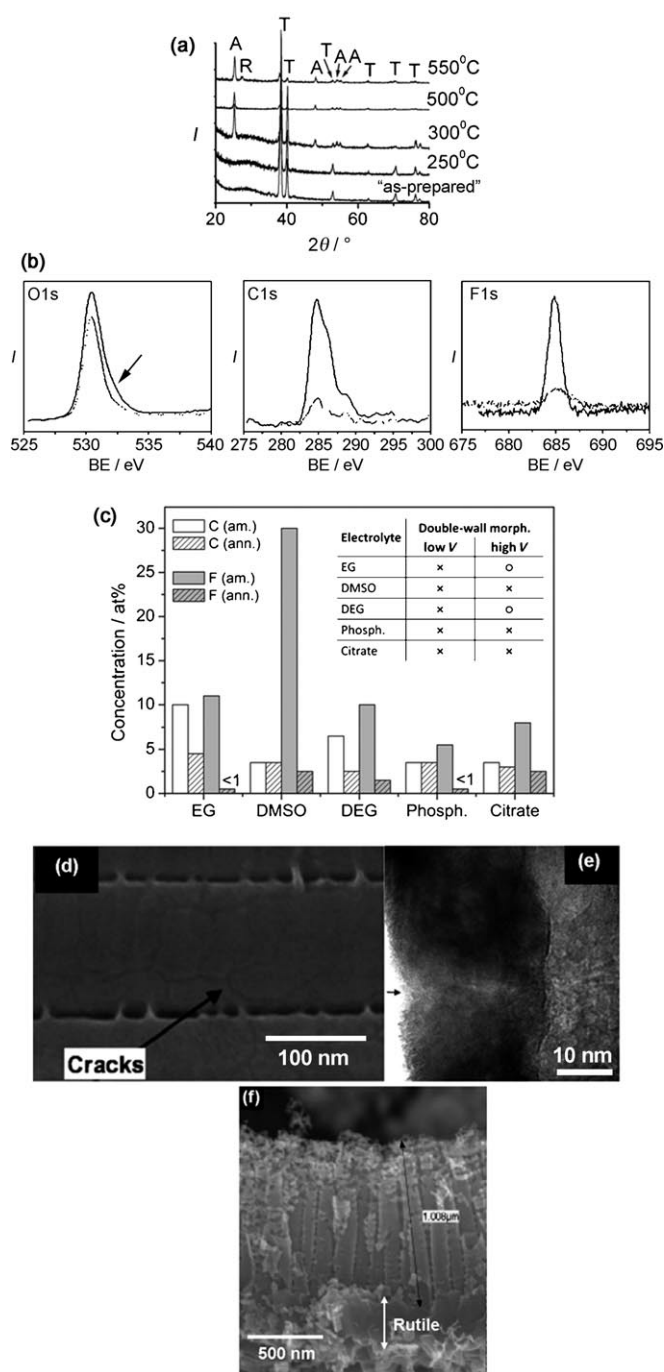


Figure 13. Annealing of TiO₂ nanotube layers: a) XRD pattern of TiO₂ nanotube layers as-formed and after annealing at different temperatures in air (reproduced with permission from Ref. [280]). b) XPS spectra of O1s, C1s, and F1s peaks before (—) and after annealing (----). The arrow denotes an OH shoulder peak; BE = binding energy. c) Composition of tubes (according to the EDX analysis shown at the bottom) after formation in different electrolytes (the degree of natural carbon contamination is about 2–3 atom%). Inset: conditions for double wall formation; O yes, X no (reproduced with permission from Ref. [137]). d, e) SEM and TEM images of TiO₂ nanotubes showing cracks at the tube wall after annealing at 450 °C (reproduced with permission from Ref. [35]). f) Rutile layer formed underneath the TiO₂ nanotube layer after annealing at 650 °C for 3 h.

example in the O 1s XPS peak); this amount is also considerably decreased when the material is annealed.^[140,281]

Two undesired effects that can occur in annealing are shown in Figure 13d–f. When annealing tubes at temperatures above 450 °C, some cracks can occur in the tube walls (Figure 13d,e), mostly in the OST layer (compare with Figure 5); these cracks were considered to slow down electron transport.^[35] Furthermore, by annealing in O₂-containing atmospheres, thin rutile layers underneath the nanotube bottoms are formed (Figure 13f). This formation is due to direct thermal oxidation of the titanium metal substrate to rutile TiO₂ during annealing. The higher the temperature and the more oxidizing the conditions, the thicker the solid layer. While the layer is typically in the range of 20–100 nm at 300–450 °C, at higher temperatures and in an O₂ environment, it can reach micrometers in thickness. Such a rutile layer under the nanotube bottom can detrimentally affect various applications that use electrode configurations, such as solar cells,^[35] owing to the inferior electronic properties of rutile layers compared to anatase.

Annealing can also affect the nanotube morphology. Usually, for extended annealing, TiO₂ nanotubes are stable up to 650 °C, but at higher temperatures the tubes start collapsing.^[118] For tubes formed in ethylene glycol, the morphology strongly depends on the ramping rate. Single-walled, double-walled, or fused membrane structures may be obtained.^[118] Depending on the annealing ramping rate, the TiO₂ nanotube walls consist of crystallites of the range of few nm to 200 nm.^[118] As shown above (Figure 12a), conductivity along the tubes is affected to a large extent by the heat treatments, and therefore appropriate annealing is essential for many applications.^[35,247] A crucial point is the formation of Ti³⁺ species during heat treatments. Heat treatment in absence of oxidizing species or in vacuum usually leads to loss of O₂ from the material and formation of Ti³⁺ (at least in the near-surface region). The reduced material that is formed shows visible light absorption and enhanced conductivity. This effect can be regarded as introducing a doping band or a high density of localized donor states (Ti³⁺ being an electron donor species located close to the conduction band of TiO₂; see Figure 14a). By usual thermal treatments, approximately 1% of the lattice atoms may be reduced to Ti³⁺. A very noticeable effect of annealing temperature is also observed in the detailed tube wall morphology after annealing. Annealing in different gas atmospheres, such as air, N₂, O₂, or a N₂/H₂ mixture, leads to a different anatase/rutile ratios of TiO₂.^[282]

4.2. Doping

Over the past 10–15 years, considerable effort has gone into doping or bandgap engineering of TiO₂ by introducing a secondary electronically active species into the lattice. The main thrust comes from photocatalytic or photovoltaic applications: To exploit the solar spectrum much better, the onset energy for light absorption needs to be decreased. The intrinsic bandgap of 3.2 eV allows the material to absorb light only in the UV range, which means that only about 7% of the solar spectrum can be absorbed.

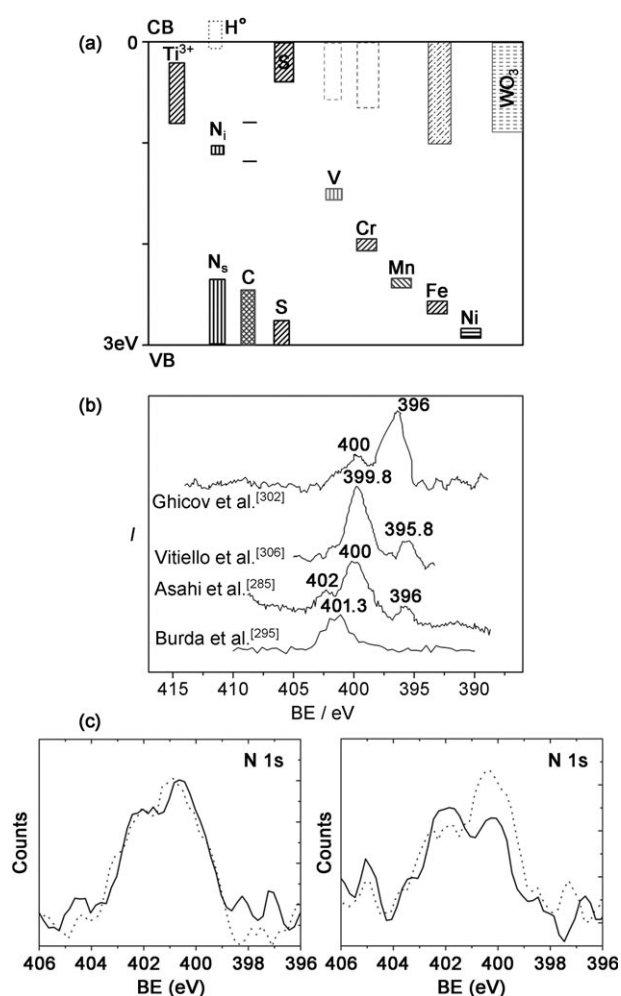


Figure 14. a) Distribution of energy levels introduced into the bandgap of TiO₂ (ca. 3 eV) according to various DOS calculations.^[283,286–294] Solid lines are generally assumed to act as electronically active donor/acceptor states. Dashed lines represent more unclear contributions (for example, traps or uncertain position of the energy level relative to the conduction band (CB) or valence band (VB)). s = substitutional, i = interstitial. b) XPS spectra of various nitrogen-doping approaches for TiO₂. c) Illustration of contradicting findings to claims of a successful solution doping approach for TiO₂ nanotubes. ----- 2 h at 1 V (left panel) and 20 V (right panel); — 20 h at 1 V (left panel) and 20 V (right panel) (reproduced with permission from Ref. [416]).

After various early findings,^[283,284] the first report on successful band-structure modification was by Asahi et al. in 2001.^[285] The authors used nitrogen doping and interpreted the results in terms of a valence band rise owing to a mixing of the introduced p states of nitrogen with the O 2p states (Figure 14). In the following years, a wide range of other elements were explored, including other nonmetals, such as carbon or sulfur.^[286–291] At the same time, a variety of transition metals, such as V, Cr, Mn, and Fe^[283,292–294] were investigated, and among the transition metals, chromium and vanadium in particular were reported to be successful in activating a response to visible light.

The most typical methods to prepare doped TiO₂ nanostructures are: 1) treating the final or growing TiO₂ nano-

2) thermal treatments or synthesis in gas atmospheres of the doping species; 3) production of the nanomaterials by co-sputtering or sputtering in an atmosphere of doping species; 4) high-energy ion implantation; and 5) the use of a substrate of a suitable alloy or the incorporation of active electrolyte species for TiO₂ structures that grow from the metals by electrochemical oxidation. This method will be discussed in more detail in the section on growth of oxide tubes on alloys (Section 5).

Approach (1) is often successfully used in precipitation reactions, that is, hydrothermal or sol-gel processes while growing the crystallites. A post-synthesis processing seems to be successful only in some specific cases and only if the TiO₂ crystallites are in the range of a few nanometers.^[295–297] Approach (2) is frequently used for nitrogen or carbon doping using predominantly treatments in NH₃, CO, or acetylene.^[298–301] Approach (3) is the classic approach used by Asahi for the first successful nitrogen doping.^[301] Approach (4) is indeed a very reliable way to properly incorporate nitrogen-containing species into the TiO₂ lattice at lower to medium doping levels.^[302,303] The drawbacks are that maximum (reasonable) fluences of high energy accelerators, operating at 50–1000 keV, are limited to about 10¹⁸ ions cm⁻², and an implantation depth into the substrate limited to several micrometers, with a somewhat inhomogeneous dopant distribution.

The most successful and most studied approach is currently nitrogen doping. Carbon doping recently became subject to a well-justified dispute,^[291] where the effectiveness of the approach was mainly questioned. For nitrogen and carbon, states close to the valence band are typically considered to be responsible for optical gap narrowing (Figure 14a).

There has been discussion regarding the mechanistic nature of nitrogen doping in view of true bandgap engineering. Considering that non-metal doping typically leads to some 2% of nitrogen in the structure, and although this corresponds to a comparably very high doping concentration for a classical semiconductor, it is problematic to assume that this concentration is sufficient to raise the bulk valence band level by more than 0.5 eV. Therefore, it may be more appropriate to describe the situation of nitrogen-doped material as a high density of localized states.

Another challenge in nitrogen doping is that the various methods to synthesize nitrogen-doped material lead to different states of nitrogen in the TiO₂ bulk or on the TiO₂ surface. This may be best illustrated by considering the XPS N 1s peak after doping treatments (Figure 14b). Proper ion implantation of N⁺ and annealing leads to a peak at about 396 eV^[302] that is in line with results from sputtering TiO₂ in N environments^[285] or peak positions obtained for titanium nitrides.^[304] Wet treatments in for example amine-based solutions typically lead to peaks above 400 eV; these materials were also found to be active under visible-light illumination.^[297] Peak positions above 400 eV can in many cases be interpreted as a surface doping or sensitization, with for example an N–C compound. Nitrogen doping reactions that result in an XPS peak of about 400 eV are very ambiguous. This peak position is also found for molecular N₂ adsorbed on

TiO₂. Although several groups reported on successful nitrogen doping with this peak position, most results show neither visible photocurrent nor convincing visible photocatalytic activity. One of the main difficulties in obtaining reliable information of effective doping is that many results that have been reported are based on plain absorption or reflectivity measurements. In many cases, although absorption spectra show strong alternation for any sort of treated sample, the corresponding photocurrent spectrum does not show any significant response (absorption that is due to, for example, contamination of the TiO₂ substrate with a visible-light-absorbing material does not mean that electronic coupling with TiO₂ occurs). This point may indicate how critical many claims of successful doping that are based purely on absorption measurements rather than an optoelectronic or electrical characterization should be regarded.

Moreover, a visible photoresponse does not automatically imply activation for visible-light photocatalysis. Ion implantation has been reported to lead to most effective doping of TiO₂ nanotubes^[302,303] with nitrogen, and to some extent with chromium.^[305] After ion implantation, amorphization of TiO₂ nanotubes occurs, and reannealing is needed to make the nanotubes defect-free. Simpler are thermal treatments in NH₃^[306] or modification by urea pyrolysis.^[307] While treatment in NH₃ indeed leads to the signature of Ti–N formation at 396 eV in XPS spectra, urea treatments seem to lead mainly to some surface sensitization with C–N=C and C–NH₂ groups. However, such surface-modified nanotubes show a significant photoresponse in the visible range compared to non-modified nanotubes.

A particularly straightforward approach to dope anodic oxides is the use of an alloy as a substrate. For example, nitrogen doping of TiO₂ nanotubes can also be carried out by using TiN containing titanium alloy substrates.^[205] Such substrates can be made with pure titanium and TiN powder by arc melting. Other elements were also explored for alloy doping, such as tungsten and niobium.^[224,308] Regarding bandgap engineering, a most interesting element is tungsten, as the introduction of WO₃ into the TiO₂ structure can be expected to lead to conduction band lowering (Figure 14a).

For tubes, considerable effort went into solution-based doping; however, efforts are questionable, as XPS peaks located at 400 eV (adsorbed species) were mostly obtained for nitrogen; visible absorption can be ascribed to carbon contamination for tubes prepared in organic electrolytes, which originates from decomposition of the organic electrolyte under the applied voltage.^[118,138] Some reports claim an increase in nitrogen doping by extended anodization:^[309] such results however could not be convincingly confirmed (Figure 14c). Highly successful carbon doping and conversion of the tubes can be achieved using acetylene.^[212,299]

4.3. Conversion of Tubes (Titanates, Semimetallic Phases)

TiO₂ nanotubes can comparably easily be converted into their perovskite oxide. Perovskite materials, such as lead titanate (PbTiO₃), barium titanate (BaTiO₃), strontium titanate (SrTiO₃), and lead zirconium titanate (PbZrTiO₃), show

a variety of interesting piezoelectric or ferroelectric properties.^[310] There are several chemical approaches to fabricate MTiO_3 ($M = \text{Sr}, \text{Ba}, \text{Pb}$) directly from the TiO_2 bulk powder, for example by the sol-gel method or hydrothermal/solvothermal process, or template-assisted processes.^[173,174,311–313] However, a simple way to convert anodically grown TiO_2 nanotube arrays into their titanates is to treat them hydrothermally in presence of corresponding precursor solution. For example, fabrication of BaTiO_3 , SrTiO_3 , or mixed $\text{Ba}_x\text{Sr}_{(1-x)}\text{TiO}_3$ perovskites by a hydrothermal treatment of TiO_2 nanotube arrays has been reported.^[314–318] Although comparably successful, there are concerns that the high-pressure autoclave environment affects the bonding of titanate tubes to the surface, and therefore other approaches to convert self-organized TiO_2 nanotubes into PbTiO_3 were explored.^[317] For example, lead was electrodeposited into the TiO_2 nanotube arrays, followed by an appropriate heat treatment. By this approach, highly ordered piezoelectric PbTiO_3 nanocellular layers with uniform structure and defined dimension over large surface areas were achieved. Titanium zirconate tube formation was reported by anodization of an appropriate alloy followed by adequate heat treatment.^[124,172,189] Moreover, alkaline hydrothermal treatment of TiO_2 nanotubes can convert the material into protonated titanates, which are also promising for applications in catalysis, photocatalysis, electrocatalysis, lithium batteries, hydrogen storage, and solar-cell technologies.^[15,65,319]

A highly promising approach of converting the semiconducting TiO_2 nanotubes into semimetallic TiO_xC_y has been reported recently.^[212] By a carbothermal reduction treatment in acetylene at temperatures above 800°C and by using short times to prevent collapse of the tubes, nanotube layers were attained that showed stable metallic conductivity. The conductivity of the TiO_xC_y tubes is in the range of graphite; optically the material shows a metal-type of photoresponse, and also capacitance measurements of TiO_xC_y nanotube electrodes shows a semimetallic behavior. The material possess a high overpotential for oxygen evolution and thus is promising for a wide range of electrochemical applications, such as a catalyst support in the field of fuel cells and other applications that require very high electron conductivity.

4.4. Filling and Decoration

An approach related to doping is the modification of TiO_2 surfaces with nanoparticles (metals, semiconductors, polymers). In all of these cases, essentially three beneficial effects are expected: 1) heterojunction formation that either changes the band bending (metal clusters on semiconductor) or provides suitable energy levels for charge injection, such as in dye-sensitized solar cells (DSSCs); 2) catalytic effects for charge-transfer reactions, such as reaction of O_2 in photocatalytic particles; 3) surface plasmon effects, leading for example to field enhancement in the vicinity of metal particles and thus allowing more efficient charge transfer.

For TiO_2 nanotubes, several approaches for decoration or filling with different foreign materials (metals or metal oxides) have been reported (Figure 15). Electrodeposition reactions into TiO_2 nanotubes essentially provide a very versatile way to fill or decorate oxide nanotubes. In the case of

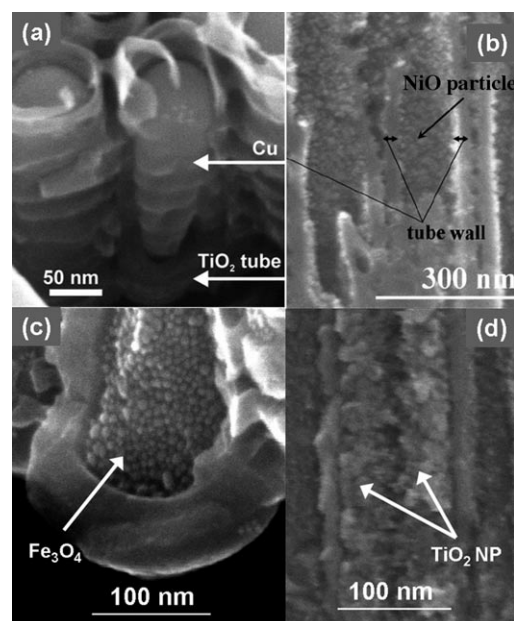


Figure 15. Examples of TiO_2 nanotube filling with a) electrodeposited copper (reproduced with permission from Ref. [320]), b) decoration with NiO nanoparticles (reproduced with permission from Ref. [323]), c) Fe_3O_4 nanoparticles,^[324] and d) TiO_2 nanoparticles (reproduced with permission from Ref. [322]).

TiO_2 nanotube layers, several factors hamper an easy, direct electrodeposition: TiO_2 is an n-type semiconductor, thus a cathodic potential needed for electrodeposition of metals represents forward bias; as a result, the tube walls have such a high conductivity that deposition occurs preferentially on top of the layers rather than within the tubes.^[320] This effect is even amplified if the cathodic potential is negative to the $\text{Ti}^{4+} \rightarrow \text{Ti}^{3+}$ potential, as the formed Ti^{3+} species acts as additional dopant. Therefore, careful consideration of the experimental conditions is essential to achieve successful metal filling. A successful strategy for complete filling is to first carry out reductive self-doping of only the nanotube bottoms by selective Ti^{3+} formation, which then allows electrodeposition to start at the tube bottom and then fill the tubes from bottom to top.^[320] This approach was used to electrodeposit Cu in the tubes, and this kind of copper-filled nanotubes may be used as one step for establishing the p–n heterojunctions ($\text{Cu}_2\text{O-TiO}_2$) in solid-state solar energy devices.

Oxide nanoparticle decoration of for example WO_3 ^[321] or TiO_2 ^[322] can be obtained by slow hydrolysis of precursors, such as TiCl_4 or WCl_5 . In DSSCs, the TiO_2 nanotubes decorated with TiO_2 nanoparticles show higher solar cell efficiency in comparison to neat TiO_2 nanotubes. The TiO_2 nanoparticles 2–3 nm in size can be deposited inside as well as outside of the tube wall by hydrolysis of a TiCl_4 solution,

which significantly increases the surface area and thereby improves the solar-cell efficiency.^[322] While the beneficial effect is surface area increase in the case of TiO₂ nanoparticle decoration, with WO₃ nanoparticles, junction formation between TiO₂ and the misaligned bands of WO₃ can also be expected.

An approach to TiO₂ nanotube filling with nickel oxide nanoparticles by using a sufficiently slow precipitation reaction of Ni(OH)₂ followed by a suitable thermal treatment has recently been presented.^[323] Such nanotubes show significant photoelectrochemical activity under visible light, possibly by charge injection from NiO states to the conduction band of TiO₂.

A very simple but highly successful approach involves filling TiO₂ nanotubes with a suspension of magnetic Fe₃O₄ nanoparticles.^[324] By placing a permanent magnet under a tube layer, a ferrofluid swiftly enters the tubes and the TiO₂ nanotubes can be very homogeneously filled with magnetic nanoparticles. Such magnetic tubes can be used in guiding and release applications.^[324]

Decoration of TiO₂ nanotubes by noble metal nanoparticles (such as Au, Ag, and Pt) also can be carried out to enhance their photocatalytic activity.^[275,325,326] Silver nanoparticles can be deposited on the tube wall by photocatalytically reducing Ag⁺ on a TiO₂ surface by UV illumination.^[325] Other metal nanoparticles are preferably deposited by UHV evaporation or chemical reduction techniques.^[274,325] Ag/TiO₂ nanotubes show a significantly higher photocatalytic activity compared with Au/TiO₂ nanotubes.^[325] Silver-decorated tubes significantly enhanced the performance of DSSCs.^[327] TiO₂ nanotubes filled with zeolites were also very promising and show an interesting photocatalytic activity.^[328]

TiO₂ nanotubes can also be decorated by narrow-bandgap semiconductors, such as CdS, CdSe, PbS quantum dots.^[329–332] These quantum dots can be deposited on the nanotube wall electrochemically, by sequential chemical bath deposition methods, or by chemical treatment in presence of cadmium precursors. Such CdS/CdSe quantum dots with a bandgap of 2–2.4 eV can absorb light in the visible range and inject the excited electron quickly into TiO₂, thus performing as a photoelectrochemical solar cell. To date, such photoelectrochemical solar cell shows efficiencies of about 4%.^[330]

Another very useful principle is to attach organic dyes (or any other molecule that has suitable HOMO–LUMO orbitals) to TiO₂ surfaces. The principle is that optically stimu-

lated electrons from a HOMO–LUMO transition in the adsorbed molecule can be injected to the conduction band of the TiO₂, as will be discussed in more detail in Section 6.2.

4.5. Monolayers

TiO₂ and TiO₂ nanotube surfaces can be modified relatively easily by covalent attachment of organic monolayers.^[138,177,333–336] The attachment typically occurs at hydroxide-terminated surface sites by a condensation reaction with phosphonates, silanes, or carboxylates (splitting off small molecules, such as H₂O or HCl) and leading to a covalent bond between a substrate oxygen and the anchor group (Figure 16a). Organic monolayers are attached onto TiO₂ surfaces mainly because of one of the following intentions: 1) to change the surface wettability, 2) to modify the biocompatibility (drug delivery, bioactivation), 3) to obtain chemical or biochemical sensors, and 4) to attach an electron injection system (DSSCs).

In general, the quality of the monolayer (packing density, attachment strength) is in the order phosphonate > silane > carboxylate. It should, however, be noted that if charge-transfer reactions across the attached molecule are important, such as in charge-injection sensors^[337] or DSSCs (see Sec-

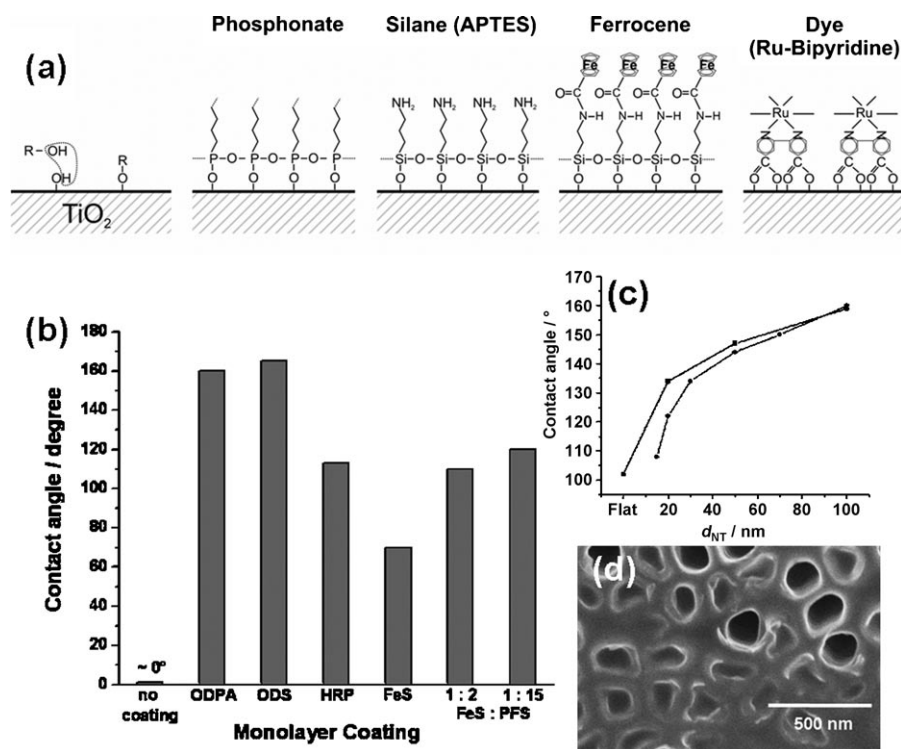


Figure 16. a) Examples of monolayer attachment on TiO₂ (from left to right): surface condensation reaction; alkane phosphonate attachment (creating hydrophobic surface); APTES attachment (bifunctional linker for other molecules, (e.g., proteins etc.); APTES coupled to ferrocene (electrochemically switchable group); and carboxylate coupling (DSSCs). b) The effect of different monolayers on wetting of TiO₂ nanotube surfaces and c) the effect of the tube diameter on ODPA-coated NTs d_{NT} . ■ as reported in Ref. [343], ● as reported in Ref. [417]. d) SEM image of microscopic wetting of TiO₂ nanotube surfaces, showing that wetting takes place preferentially between tubes (reproduced with permission from Ref. [181]).

tion 6.2), the electronic properties of the anchoring groups are crucial. For example, in DSSCs charge transfer from a dye molecule to the TiO₂ conduction band is significantly faster for COO⁻ groups than for silanes.

As Ti/TiO₂ is the most used biomedical implant material worldwide, it is highly interesting to modify the surface with additional biorelevant molecules. To link active organic entities (mainly enzymes, proteins, or DNA) to TiO₂ surfaces, bifunctional molecules such as APTES^[138,144,177,281] that carry for example a terminal NH₂ group are attached. These or similar linkage methods enable further covalent attachment of virtually any organic species.^[338–341]

Of interest in this context is the fact that some linker molecules, such as APTES with a silane and an opposite NH₂ linker group, show a different reactivity on amorphous, anatase, and rutile polycrystalline surfaces,^[281] even the degree of reverse attachment (coordination of the NH₂ group) varies with TiO₂ crystal structure. A specific feature of almost all monolayers attached on TiO₂ is that they can be cut by photocatalytic reactions^[177,335,342,343] or by voltage-induced reactions.^[138] This principle was used for various drug and other payload release processes from dispersed TiO₂ nanotube bundles or from nanotube electrode surfaces.^[144,177,324,344]

The organic modification of nanotubes combined with a photocatalytic reaction was used to create surfaces that could be adjusted to have essentially any desired wettability property^[335,343] (that is, a water contact angle from 0° to 170°).^[335,343] Nanotube layers as such (amorphous or crystalline) are super-hydrophilic; only when treated with a suitable monolayer do they become superhydrophobic.^[335,343] Upon UV irradiation, chain scission occurs, which makes the surface increasingly hydrophilic with the duration of illumination. In this approach, the achievable superhydrophobicity depends on the tube diameter^[343] (Figure 16c), and overall wettability behavior is in accord with the Cassie–Baxter model.^[345]

To fill super-hydrophobic tubes with a liquid (with for example an electrolyte), organic solvents are needed, which is the key to filling hydrophobic tubes or to fabricate amphiphilic tubes (see Section 6.5).^[177] Of interest in this context is, however, a very recent observation that on the microscopic level, all TiO₂ nanotube layers (non-modified and modified) show preferential wetting between the tubes rather than inside the tube.^[181] This observation is in line with those for dry anatase tubes: the inside of the tubes is not easily filled by aqueous electrolytes.^[346]

Another elegant way to adjust the wettability of nanotube layers is by applying mixed monolayers with a different degree of polarity or even actively switchable polarity. Such mixed monolayers of *N*-(3-triethoxysilyl)propylferrocenecarboxamide and perfluorotriethoxysilane were used to demonstrate electrical redox switching of attached ferrocene molecules and thus to induce alterations of the wettability on TiO₂ nanotube layers accordingly.^[347]

5. Oxide Nanotube Layers on Other Transition Metals and Alloys

The principle used to grow oxide nanotubes on titanium by using a dilute fluoride electrolyte can be transferred to a considerable range of other metals and alloys (Figure 17). Depending on the exact electrochemical conditions, organized nanotubular or nanoporous structures were reported for several other valve metals, such as Zr,^[164,348–352] Hf,^[163,166] W,^[74,353–356] Nb,^[357,358] Ta^[359–363] Fe,^[364–366] and Mg.^[367] To obtain highly organized high-aspect-ratio structures for each case, some optimization of the electrochemical conditions specific to the element or alloy is needed, and this has not yet been achieved for all of the elements, which is also apparent from the SEM top and cross-sectional images shown in Figure 17. The optimized conditions are different for each case and the ease by which optimal self-organizing conditions

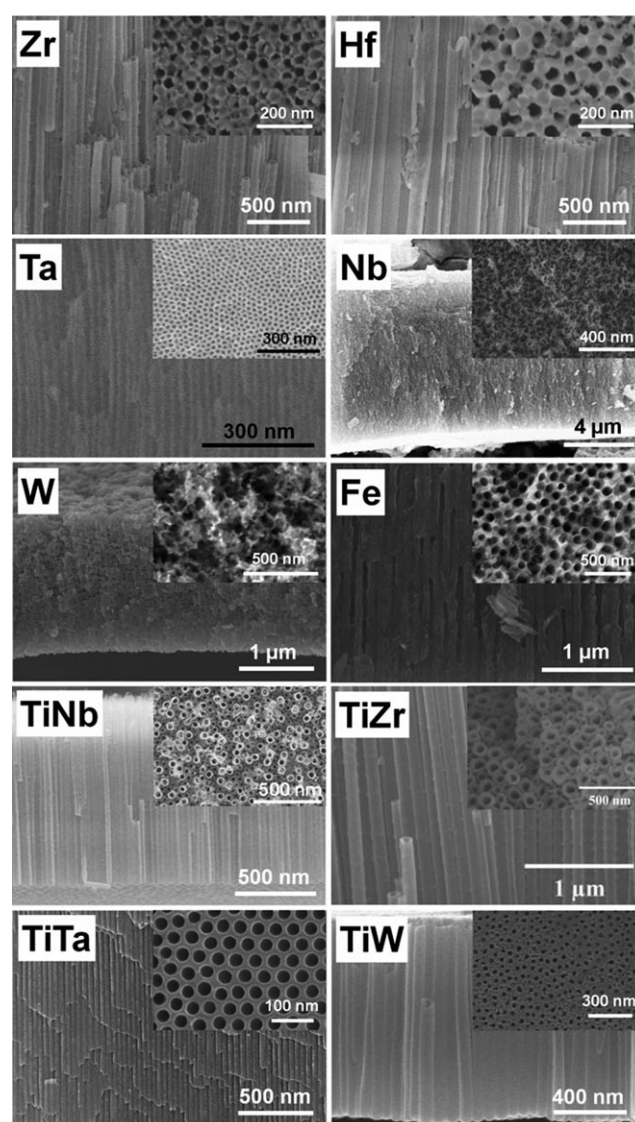


Figure 17. Cross-sectional and top-view SEM images of ordered nanotube or nanopore layers electrochemically grown on different valve metals and metal alloys.

and high aspect ratios can be established varies significantly for the different elements. For zirconium and hafnium, high-aspect-ratio smooth tubes can be achieved very easily under a wide range of parameters. Other extremes may be non-valve metals, such as iron, where high-aspect-ratio oxide structures were reported only very recently,^[364–366] or WO₃ structures, for which still no highly ordered and only comparably short tube structures were reported.^[353,355,368–370] The main reasons for this different behavior can be ascribed to following factors: 1) the solubility of a formed oxide structure in the anodizing electrolyte affects the aspect ratio, 2) the solubility of the fluoride species (or any other sensitizer) at cell boundaries affects tube or pore morphology and the observation of sidewall ripples, 3) different Pilling–Bedworth ratios that affect stress that is generated when the oxide is formed, thus the adhesion of the tube layer to the substrate or the tube length (overshoot by plastic flow) and the self-organization length scale are also affected.

Many of the nanostructures that are formed have very interesting properties. For example, WO₃ nanotubes/pores show excellent ion intercalation properties (electrochromic devices, charge storage)^[66,69,70,224,321,355,371–373] or enhanced photoelectrochemical properties.^[374,375] For ZrO₂ nanotubes, bright visible luminescence^[376] has been reported. An even wider field, in view of varying properties, is provided by using alloyed metal substrates for anodization, for example to tune ionic, electronic, or optical properties of the tube layers. However, to obtain ideal tube layers and defect-free homogeneous ordering of tubes over a large surface area, the alloys should be single-phase (to avoid different etching/anodization rates on different phases), and growth is achieved more easily if the elements involved are valve metals.

Accordingly, self-organized oxide nanotube/pore layers of a reasonable quality have been reported on binary alloys, such as TiNb,^[188,308] TiZr,^[124,126,172,189] TiTa,^[190,361,377] TiW,^[224] TiMo,^[378] TiAl,^[158,159] and on ternary^[191,192] and more complex alloy systems.^[379,186] Alloy anodization thus enables the growth of mixed anodic oxides with tailored and improved properties for a wide range of applications.^[190,192,224,308,378,379] For example, nanotubular layers grown on TiNb and TiW show not only the feature that geometry can be adjusted over a wider range,^[224,308,380] but also show highly enhanced intercalation properties.^[308] It is also interesting that in the case of titanium alloys, small amounts of the alloying element can drastically affect the properties while the unique nanotubular morphology is completely retained. For example, TiW (0.2 atom %) and TiMo (7 wt %) alloys show a strongly enhanced electrochromic response and improved photocatalytic properties.^[224,371,378,381]

On all of the pure metals and alloys that have been explored to date, the nanotubular oxide layers are amorphous, and in each case they can be easily transformed to a crystalline structure by an adequate annealing treatment.^[189,224,308,368,376,378] After alloy anodization, the composition of the oxide in general is consistent with the ratio in the alloy. In the case of anodic oxide layers on TiAl alloys, the film is composed of (TiO₂)_n and (Al₂O₃)_m, where *m* and *n* are the respective fractions of the base alloy Ti_nAl_m.^[382] In some cases, minor amounts of mixed oxides may also be present in

the anodic oxides. Full conversion to a mixed oxide was only reported for TiZr.^[189] It is also interesting to note that for most elements and alloys, ordered tubular and nanoporous morphologies have been observed, and transitions from one to another can be achieved (for example, TiAl, TiNb, and TiTa).^[159,308,361,383] However, owing to the difference in chemistry (solubility of the oxide in fluoride and solubility of the respective metal fluorides in different solutions), most elements appear to have a preferred morphology, that is, a morphology that dominates under most anodization conditions. For example, on zirconium and hafnium, nanotubular anodic oxides are usually observed, whereas on aluminum, niobium, and tantalum, nanoporous morphologies are usually obtained. For tantalum, extreme conditions are required to obtain a tubular morphology.^[363] In the case of alloys, the morphology follows the specific oxide morphology of the major alloying element.

A highly interesting phenomenon that was observed for several alloys but is still not well understood is self-organization at two length scales,^[37,186,187,190,191] by which two distinct tube diameters are formed during anodization (a large center tube surrounded by smaller tubes, repeated over the entire anodized area). The simultaneous ordered formation and stabilization of two tube diameters is currently ascribed to availability of current at the different tips,^[37] but the phenomenon seems to be far from satisfactorily explained.

In general, it can be said that all investigated organized oxide structures grown by anodization in fluoride-containing electrolytes on different metals or alloys seem to follow the same growth principles and key factors: The diameter of the tube is determined by the anodization voltage, etching of the tubes (and thus the achievable length of the tubes) depends on the chemical resistance of the oxide against fluoride etching (in a particular electrolyte), and water plays the key role for providing the oxygen source for tube growth, splits pores into tubes, and is responsible for sidewall ripple formation.

Obviously, anodization techniques in fluoride-containing electrolytes allow the fabrication of nanostructured oxide layers on an extremely wide range of alloys that enable the tailored fabrication of mixed nanostructured oxides with virtually endless possibilities to create enhanced properties, and therefore have also a very high and widely unexplored technological potential.

6. Applications

Applications of TiO₂ nanostructures usually involve the exploitation of some unique feature of TiO₂ (electronic, ionic, or biocompatibility properties) and a significant enhancement of some reaction or transport rates that is obtained by using small scale dimensions (large surface area, short diffusion path, or size confinement effects). Using nanotubular assemblies also provides a preferred dimensionality to the system. Tubes grown on a metal substrate are vertically aligned to a back contact; that is, a direction for charge transfer towards the electrode is established. Nanotube layers provide well-

defined top openings and are thus suitable for size-selective applications (filters) or for templating secondary material. The inside volume is well-defined and regular, thus applications, such as nano test tubes^[384] are promising. In the following sections, we give an overview of current efforts towards TiO₂ nanotube applications.

6.1. Photocatalysis and Dark Photocatalysis

TiO₂ is the most photocatalytically active material for the decomposition of organic materials (for example, it is used for degradation of organic pollutants).^[28, 38, 197, 198, 385–387] The reason for this high activity are the band-edge positions relative to typical environments (such as water). The basic principles involved in the photocatalytic mechanism are shown in Figure 18. UV light promotes electrons from the valence band to the conduction band; holes and electrons will be separated (under the field of the Schottky junction with the environment), reach the semiconductor–environment interface, and react with appropriate redox species in the environment. Several highly reactive species are generated for example from the surrounding water by charge exchange at the valence band ($\text{H}_2\text{O} + \text{h}^+ \rightarrow \text{OH}^\bullet$) and at the conduction band ($\text{O}_2 + \text{e}^- \rightarrow \text{O}_2^-$). These radicals and peroxy ions are able to virtually oxidize all organic materials to CO₂ and H₂O. Furthermore, at the valence band, direct h⁺ transfer to adsorbed species to initiate decomposition may also be considered.

Alternatively, apart from decomposition of organics, h⁺ and e⁻ can react with H₂O to form H₂ and O₂; that is, direct splitting of water can be achieved. At the conduction band, the situation is such that the redox potentials for O₂ → O₂⁻ and H⁺ → 1/2H₂ are very close. In other words, H₂ generation and O₂⁻ formation are typically competing. At the valence band, O₂ can be formed from water by various pathways, including radicals that can (if not otherwise used) react finally to O₂. The reaction rates of the photocatalytic processes on pure TiO₂ are typically limited by the charge-transfer process to a suitable redox species. Therefore, at the valence band, catalysts such as platinum are used to promote for example H₂ evolution, and hole-capture agents such as CH₃OH are often used to promote the overall reaction rate.

However, as discussed in previous sections, although TiO₂ has very suitable band-edge positions for high photocatalytic activity, the bandgap of about 3 eV allows only UV light to be efficiently used. To achieve visible-light-driven processes, a large number of bandgap-engineering (doping) approaches, as discussed in Section 4.2, have been explored with TiO₂. The method that has been most investigated for photocatalysis is N-doping, as it is perceived to be the most efficient measure to stimulate a visible photocurrent response. However, the success of N-doping to achieve visible photocatalytic activity is somewhat questionable if the photocatalytic reaction is indeed valence-band-dominated (that is, h⁺ transfer to the electrolyte is the dominating reaction). As N-doping raises the valence band edge (Figure 14), the h⁺ leaves the semiconductor at a lower energy (less anodic redox potential), which is possibly not sufficient to decompose H₂O to OH[•] or

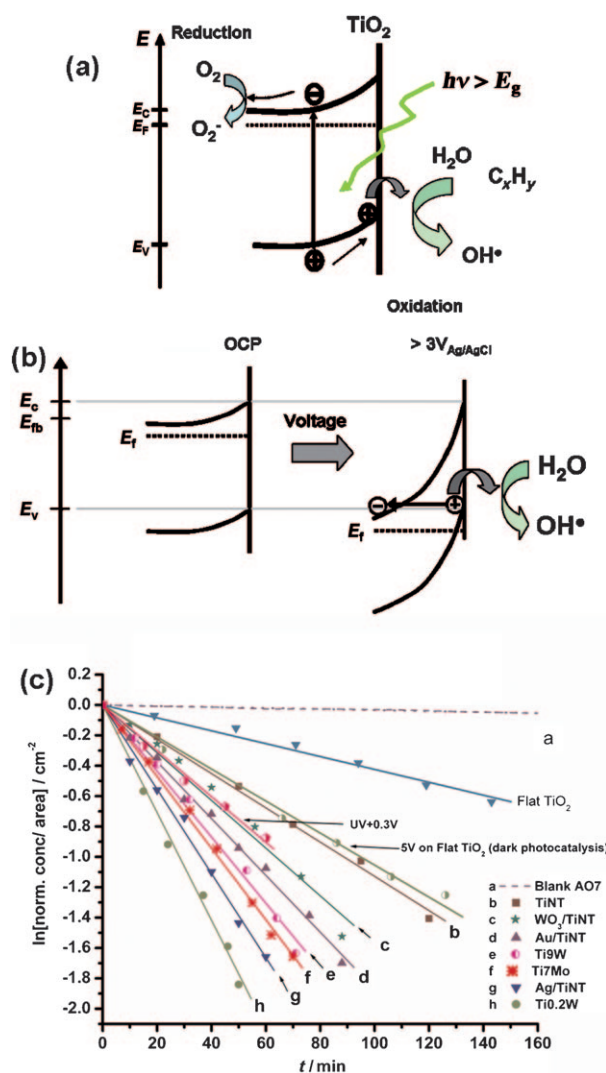


Figure 18. Photocatalytic activity of TiO₂ nanotubes: a) the mechanism (photoinduced formation of electron–hole pairs and reaction with surroundings). b) Dark photocatalysis: sufficient voltage-induced band-bending creates valence band holes (h⁺) that can react with the environment, in analogy to photon-induced hole (h⁺) generation.^[138] c) Photocatalytic activity of various nanotubes measured as decomposition rates of organic compounds (AO7; C₀ = 2.5 × 10⁻⁵ M) and including a comparison to the dark photocatalysis mechanism.

to achieve direct decomposition of the organic material. The fact that in some cases a visible photocatalytic effect (mostly very mild) was found for N-doped material could then be attributed to O₂⁻ generation by the conduction band. In other words, in many cases of photocatalytic degradation of a specific organic molecule, the active reaction path depends on the molecules energy states that may prefer to interact (overlap) with either valence-band or conduction-band levels.^[198]

Nevertheless, all of the photocatalytic applications have in common the fact that a higher overall reaction rate is achieved using high-surface-area geometries. Thus, reactions are commonly performed using suspended nanoparticles or nanoparticulate electrodes. Ordered nanotube arrangements offer various advantages over nanoparticulate assemblies, as

their defined geometry provides very defined retention times in nanoscopic photoreactors.^[123,388] Moreover, the 1D geometry may allow a fast carrier transport and thus less unwanted recombination losses.

A first investigation to this end^[388] has shown that TiO₂ nanotubes can indeed have a higher photocatalytic reactivity than a comparable nanoparticulate layer. Although various factors may be responsible for this effect (optimized reaction geometry for charge transfer, UV absorption characteristics over the tube, solution diffusion effects), the work triggered intense follow-up investigations. It was shown that particle decoration with silver or gold led to a significantly increased photocatalytic activity,^[325] and that also applying an external anodic voltage drastically enhances the photocatalytic activity.^[138,389] These findings suggest that in the investigated cases, a valence-band mechanism dominates, and the observed accelerating effects have a common origin in increased band bending, either by junction formation or by the applied voltage.^[38]

To increase the photocatalytic activity, various mixed-oxide tube layers were used, such as TiMo or TiW.^[381,390] A compilation of the photocatalytic results is shown in Figure 18c. Clearly, a highly beneficial effect is observed for tungsten and molybdenum that cannot be explained by a better charge transport in the tubes but must be ascribed to modification of the surface state distribution at the nanotubes.^[38,381,390] Visible photocatalysis was shown for TiW oxide tubes^[390] and to some degree for carbon-doped TiO₂ nanotubes regarding water splitting,^[298,21,391,392] although there is considerable dispute on its effectiveness,^[291] and for TaON nanotubes.^[393]

A very spectacular possibility to use TiO₂ nanotubes in photocatalytic applications is to produce free-standing flow-through membranes,^[123,193] as they allow extremely defined photocatalytic interactions (highly defined interaction times) combined with a filtration capability.

Another intriguing specific feature of TiO₂ photocatalysis is the ability to induce chain scission in attached organic monolayers (see Section 4.5). This feature can be used to create extremely well-defined wettability on surfaces^[335,343] or to liberate terminal payload molecules from the surface upon UV illumination. This was used for example to construct various drug-release systems.^[138,177,333–336] Of interest and common to all approaches is the fact that chain scission (photocatalytic or voltage-induced) occurs after the anchoring group (a silane or phosphonate). The reaction may thus be based on a direct h⁺-induced chain scission as the diffusion range (lifetime) of OH[•] radicals is typically comparably long (0.1–10 μm).^[22] This hypothesis is further supported by the fact that a release of intact activemolecules, such as dyes, from TiO₂ nanotubes can be observed after chain scission;^[144,177,324] if OH[•] formation was the main mechanism, the dye would be decomposed before it is able to leave the tubes.

A particularly interesting concept in the field of photocatalysis is the combination of the TiO₂ nanotube geometry with molecule-selective binding units, for example zeolites.^[328,394] Considering that zeolite structures can be tailored for selective absorption of a considerable range of organic molecules, they can for example be used to concentrate dilute

pollutants. If the zeolites are filled in TiO₂ nanotube layers or membranes, the pollutant molecules in the zeolite can be accumulated and then be photocatalytically decomposed. Thus the zeolite is regenerated and a significantly enhanced photocatalytic activity be achieved. It is crucial that the lifetime of a photocatalytically generated OH[•] radical is on the order of 10 μs, which corresponds to a penetration range of several hundred nanometers to several micrometers from the generated surface into the electrolyte; this length scale fits extremely well to inner dimensions of TiO₂ nanotubes.

In view of biomedical uses (drug delivery, fighting cancer), X-ray-induced photocatalysis was used to liberate drugs from the surfaces of TiO₂ nanotubes^[344] or to directly kill cancer cells.^[395] X-ray catalysis is crucial for any in vivo application as X-ray-induced reactions would allow intervention-free therapy (stimulation can take place directly through the human body; the energy of the X-rays then determines the penetration depth of the activating irradiation). Furthermore, it was recently demonstrated that electron-beam-induced photocatalytic reactions can occur in the vacuum of a scanning electron microscope using ionic liquids as a non-volatile solvent.^[181,396]

Regarding photocatalytic reactions, it should also be mentioned that a similar reaction (Figure 18b) can be triggered in the absence of light on anatase TiO₂ and TiO₂ nanotube surfaces if sufficiently doped.^[138] If a voltage is applied to the material that causes anodic Schottky barrier breakdown,^[397,398] that is, valence-band holes are created that react with environment in a similar manner as photogenerated holes (OH[•] radical formation, destruction of organic and organic monolayers). TiO₂ nanotubes, when annealed, have a suitable doping concentration (ca. 10¹⁸–10¹⁹ cm⁻³) and by applying voltage (> 3 V), ionization of the valence band occurs and holes are generated that leave the TiO₂ to the environment (at $E = E_v^*$). This dark photocatalysis approach may be particularly useful in environments where the use of UV light is hampered, for example in MEMS (microelectromechanical systems) devices or a lab-on-a-chip that require a photocatalytic reaction or a self-cleaning step in the dark.

6.2. Solar Cells

Another very attractive application of TiO₂ is its use in solar cells. Dye sensitization of TiO₂ was extensively investigated in about 1970. After the work of Gerischer and Tributsch in 1968,^[23] the first report on ruthenium bipyridyl sensitization on TiO₂ appeared in 1980,^[24] and in 1991, Grätzel and O'Regan^[25] used this principle to fabricate a full DSSC in which the photon-absorber layer was made of TiO₂ nanoparticles that were dye coated (Figure 19a). This assembly reached an efficiency of about 11%. The principle of DSSC^[35,399] involves a dye that absorbs light in the visible range and thereby excites electrons from the HOMO to the LUMO level, followed by a rapid injection of the excited electron into the conduction band of TiO₂. The electrons travel through the TiO₂ layer to the back contact; meanwhile, the oxidized dye on the surface is regenerated by an I⁻/I₃⁻ electrolyte. Losses by recombination may happen principally

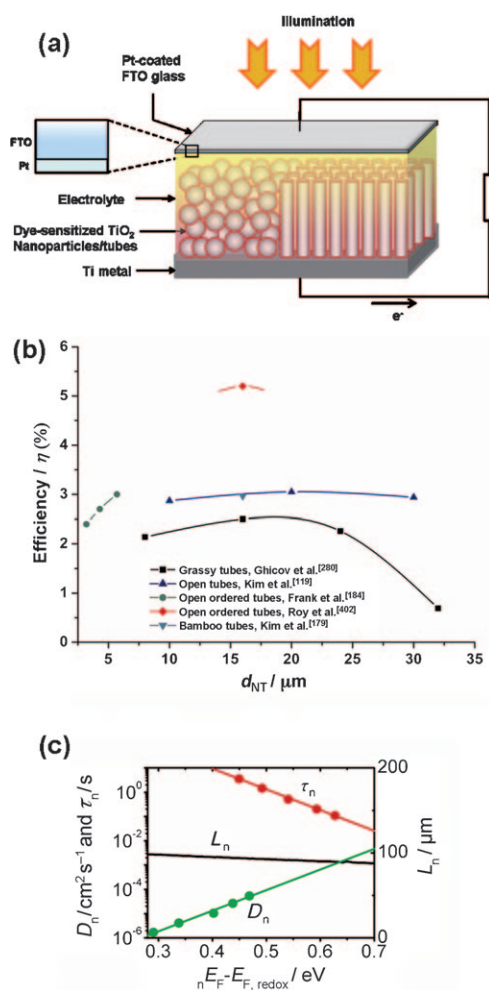


Figure 19. a) A TiO₂ nanoparticle/tube-based dye-sensitized solar cell. b) Comparison of results for solar-cell performances of TiO₂ nanotube layers used in DSSCs (non-modified by TiCl₄).^[322] d) Estimation of electron-diffusion length (L_n) TiO₂ nanotubes from the experimental values of D_n and τ_n by taking the quasi Fermi level (QFL) into account (reproduced with permission from Ref. [403]).

in three ways: 1) After electron excitation from the HOMO to the LUMO level of the dye, de-excitation of the electron occurs in a radiative or non-radiative path; 2) after injection of the electron in the conduction band of TiO₂, it may recombine with the oxidized dye; and 3) the electron may recombine with the I₃⁻ ion in the electrolyte.

In general, the rate-limiting factor is the dynamic competition between the electron transport through the TiO₂ and the interfacial recombination of electrons.^[400] An often-addressed critical issue for losses in nanoparticulate DSSCs is carrier recombination at grain boundaries (owing to the presence of trapping states) and long carrier diffusion paths (random walk) through the TiO₂ network. Therefore, replacing the TiO₂ nanoparticulate photoanode with a TiO₂ nanotubular layer in particular reduces recombination probabilities and provides a directed (ideally one-dimensional) electron traveling path.^[35] Since the first efforts to dye-sensitize TiO₂ nanotube arrays,^[401] where efficiencies of only

0.036% were reached, approximately 5% solar cell conversion efficiency has meanwhile been achieved for tubular-based systems.^[402] However, it must be clearly distinguished between cases where pure TiO₂ nanotubes are used^[119,179,280,403] and cases where the nanotubes were additionally treated with TiCl₄ (decoration with TiO₂ nanoparticles) or mixed with TiO₂ nanoparticles.^[322,404,405] Of course, the observed effects (efficiency, dye loading, transport times, reaction kinetics) can only be unambiguously ascribed to the nanotubes in cases where plain TiO₂ nanotubes were used; in mixed cases, effects may even be dominated by the added TiO₂ nanoparticles. For pure TiO₂ nanotube layers, the record efficiency stands at 5.2%,^[402] for mixtures with nanoparticles at 7%.^[404] Some critical factors were recently discussed and reviewed.^[35,280]

A very interesting study has shown that a much higher electron diffusion length can be achieved in nanotubes than in nanoparticles,^[403] in fact, from combined electron lifetime/diffusion measurements, it was deduced that electron diffusion lengths of 100 μm (Figure 19c) should be achievable. However experimentally, 15–20 μm long nanotubes show the maximum solar cell efficiency (see also Figure 19b), which is mainly ascribed to a loss of surface adhesion for longer tube layers or disordered tube tops that increasingly appear with longer anodization times (see Section 2.7).^[402]

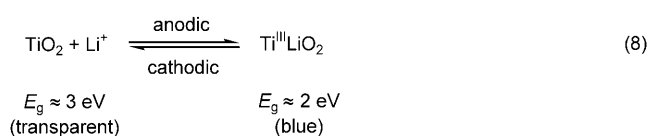
Nanotube layers annealed between 350 and 450 °C in air form anatase tubes, which proved to be more efficient than the rutile phase, as the electron transport is faster in anatase TiO₂ than in rutile.^[227,280] A temperature of 450 °C and complete anatase conversion is reported to be the optimum annealing condition to achieve high-efficiency solar cells.^[35,280]

As discussed in several works,^[179,280,322,403] the overall efficiency-limiting factor in TiO₂ nanotube-based solar cells is specific dye loading; that is, the specific surface area of the tubes (BET ≈ 30 m² g⁻¹) is considerably smaller than comparable nanoparticulate layers (BET ≈ 80–100 m² g⁻¹). Several strategies to increase the specific surface area in tube systems have been explored, such as the above-mentioned TiCl₄ treatment^[322,404–406] or modifying the tube walls by creating bamboo-type structures or double-walled nanotubes.^[179,280] The geometry of the tube tops is very crucial (see for example Ref. [402]), and several approaches have been reported for removing inhomogeneity (surface nanograss) from the tube tops.^[119,184,402] To further increase the efficiency, Tsuchiya et al.^[327] introduced a new concept by showing that using silver-decorated TiO₂ nanotubes, an enhancement of the conversion efficiency for DSSCs can be obtained. This effect may either be due to plasmon enhancement or junction formation. Some variations in TiO₂ nanotubes, such as that formed by rapid-breakdown anodization (RBA), show promising improvement regarding the photoconversion efficiency.^[75,79] Recently, an anodic self-organized TiO₂ meso-sponge/nanochannel layer was reported that has a significantly higher specific surface area than tubular layers, and it seems to be capable of outperforming nanotube layers in the field of TiO₂-based solar cells and other applications.^[80–82]

6.3. Electrochromic Devices

Various transition-metal oxides, such as MnO₂, WO₃, Nb₂O₅, MoO₃, and TiO₂, provide an excellent host lattice for ion intercalation devices, for example, lithium ion batteries or electrochromic devices.^[29,65,407,408] These devices rely on a reversible uptake of small ions such as H⁺ and Li⁺ into interstitial positions of the metal oxide upon applying and releasing an electric field.

In the case of transition metal oxides, ion uptake and release are frequently combined with a change in the redox state of the material and a resulting change in the electronic and optical properties of the material. For example, lithium ion intercalation into TiO₂, accompanied with reduction of Ti⁴⁺ at the lattice to Ti³⁺, changes the apparent bandgap of the material from the UV to the visible range (with $E_g \approx 2.2$ eV; see also Figure 15), which leads to a blue coloration of the material [Eq. (8)].^[273,409]



The currently most active electrochromic material is WO₃. As a nanoparticle layer, it shows the lowest threshold voltage for intercalation and color switching, the highest color contrast, and is cyclable over 1000 times in commercial devices with a comparably small deterioration of the effect. In aqueous environments and for pH values of 12–13, H⁺ is the dominating intercalation species, even in presence of high Li⁺ concentrations owing to the much lower radius of the solvated ion. The rate-limiting step for ion intercalation is a solid-state diffusion/migration process of the small ion into the host lattice and therefore the switching kinetics is typically comparably slow (seconds). To achieve short diffusion paths, nano-scale materials are highly desired, and most commercial devices consist of layers of compacted nanoparticles. At reasonable applied voltages (1–2 V) and moderate times (seconds), a compact layer can typically be intercalated to a depth of approximately 5–10 nm. This length scale is ideal for penetration of TiO₂ nanotube walls (with wall thicknesses in the range of 5–30 nm). Moreover, the vertical alignment makes the nanotube geometry ideal for maximizing the optical contrast (Figure 20a).

After the first report on electrochromic switching using TiO₂ nanotubes,^[410] a large body of work followed that optimized contrast, switching time, threshold voltage, and cyclability by using other oxide nanotubes/porous oxides, such as WO₃, or by using doped (mixed-oxide) TiO₂ nanotubes.^[224,308,321,355,371,378]

Mixed TiW, TiMo, and TiNb oxide nanotubes turned out to be very efficient (see Figure 20b). Of interest is the fact that for most nanotube systems, an optimized condition of the secondary element exists by which an optimum effect can be achieved. TiNb oxide nanotubes are particularly spectacular in scientific terms,^[188,308] for which it could be shown that the addition of niobium to TiO₂ leads to a widening of the anatase lattice.^[308] This not only drastically accelerates ion intercalation, lowers the threshold voltage, and makes the material much more durable in repeated switching experiments; it also allows for the reversible intercalation of much larger sodium ions, which cannot usually be intercalated into anatase under low-voltage conditions and at room temperature. Other work has shown that TiO₂ nanotube layers can be lifted off from the metallic titanium substrate and be transferred onto conducting glass^[411] or by complete anodization of titanium layers on conducting glass^[412] to construct transparent effective electrochromic devices (Figure 20a).

6.4. Cell Interaction and Biomedical Coatings

A very important application of titanium surface modification is in biomedical applications. About 40% of today's

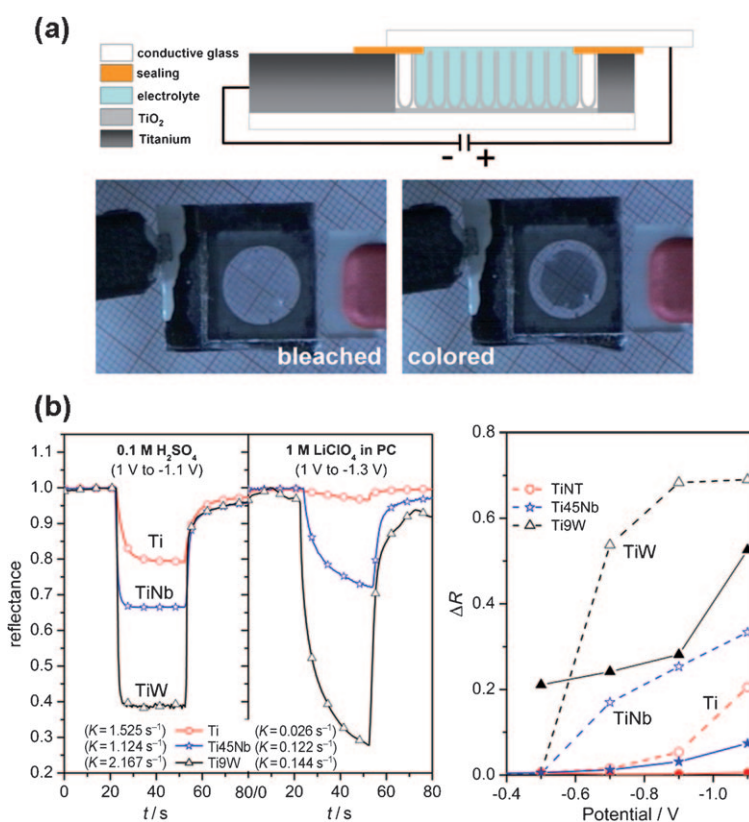


Figure 20. a) Electrochromic device based on TiO₂ nanotubes fabricated by complete anodization of sputter-deposited thin titanium film, making it transparent, on conducting glass (reproduced with permission from Ref. [405]). b) Comparison of color-switching transients for Ti, TiNb, and TiW oxide nanotubes for H⁺ and Li⁺ intercalation and voltage dependence of contrast ΔR and threshold voltage U_T for the different nanotube layers. Open symbols 0.1 M H₂SO₄, filled symbols 1 M LiClO₄ in PC (propylene carbonate).

biomedical implant materials are based on titanium or titanium alloys.^[39] TiO₂ nanotubular surfaces are ideal for studying and applying size effects with living matter or biologically relevant species. Not only can the diameter of the tube surfaces be accurately adjusted to virtually any value between 10–250 nm,^[132] but owing to the self-organizing nature, entire, even complex shaped surfaces (such as dental-implant screws or hip implants) can be coated easily with such nanotube layers.^[413]

First work on size-dependent cell interactions in 2007^[122] showed that mesenchymal stem cells react in a very pronounced way to the diameter of nanotubes. Diameters of about 15 nm strongly promote cell adhesion, proliferation, and differentiation, and tube diameters of about 100 nm were found to be detrimental, as they induced programmed cell death (apoptosis).

The work resulted in further studies^[414] with partially conflicting outcomes, and a range of questions were brought forward, such as the role of TiO₂ crystallinity, the remaining fluoride concentration, or the role of the cell type and surface pretreatment. However, subsequent work^[415–419] showed clearly that the size effect, that is, a cell-stimulating influence for tube layers with a diameter of 15 nm, is of a virtually universal nature (Figure 21). Not only mesenchymal stem cells but also hematopoietic stem cells, endothelial cells, and also osteoblasts and osteoclasts show this size-selective response. In fact, the effect of size dominates over tube crystal structure (amorphous/anatase/rutile), fluoride content, and to a large extent over the wetting properties.^[415–417,419] Even tubes made from other valve metals, such as ZrO₂, showed similar size effects.^[415] In general, the most straightforward explanation for this effect is that integrin clustering in the cell membrane leads to a focal adhesion complex with a size of about 10 nm in diameter, and this in turn leads to an excellent geometrical fit onto/into the tube openings of about 15 nm.^[122]

In view of a rapid ingrowth of biomedical implants in bone, a key factor is fast kinetics of hydroxyapatite (HAp) formation on implant surfaces from body fluid. A number of studies^[420–423] have shown that HAp formation can strongly be accelerated on TiO₂ nanotube surfaces compared with flat TiO₂ surfaces, and also in this case a strong size effect can be observed.^[420] Moreover, the 3D structure is optimal for embedding precursors for HAp formation that additionally promote HAp nucleation.^[421] In vivo experiments with adult domestic pigs showed that nanotube surfaces can indeed enhance collagen type I and BMP-2^[413] expression and that higher implant bone contacts can be established if implants are coated with a nanotube layer.^[413] However, the negative (apoptotic) effect of nanotubes may also be exploited for biomedical surfaces when cell proliferation is not desired.^[39]

6.5. Drug Delivery and the Release of Other Payloads

The geometry of the TiO₂ nanotube arrays suggests that the material may be used as a drug-delivery capsule if nanotube layers are separated (singled-out) and stabilized, or it may be used as a drug-eluting coating on biomedical

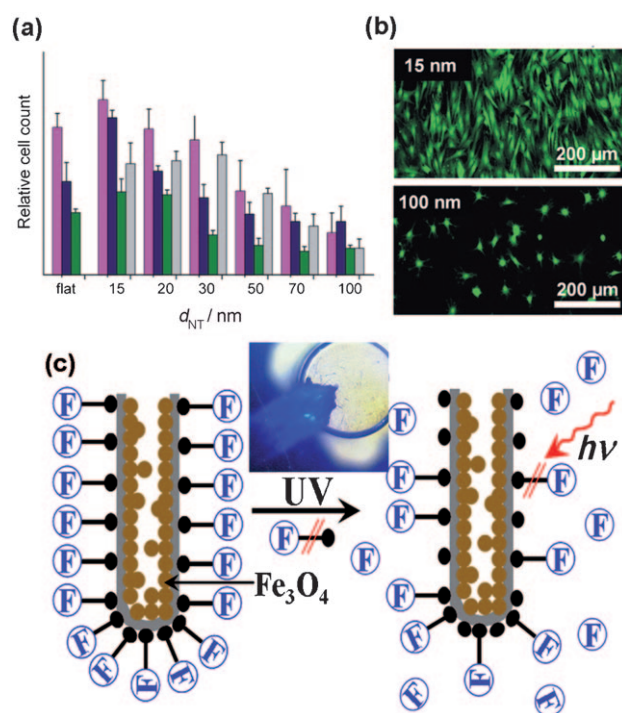


Figure 21. a, b) Influence of TiO₂ nanotube diameter on activity of cells: a) Comparison of cell activity for mesenchymal stem cells (pink), primary human osteoblasts (blue), osteoclast (green), and endothelial cells (gray) for different TiO₂ nanotube diameters; relative cell counts are shown 3 days after seeding. b) Fluorescence micrograph for GFP-labeled mesenchymal stem cells on TiO₂ nanotubular surfaces with 15 nm and 100 nm diameters, respectively (showing drastically higher population on 15 nm tube diameters). c) TiO₂ nanotube for guided drug release: Representation of magnetically loaded TiO₂ nanotubes with attached drug (F). Release is triggered by photocatalytic chain scission upon UV irradiation. Inset: an example where a blue fluorescent molecule is released from magnetically actuated nanotubes (reproduced with permission from Ref. [324]).

implant materials. A potential in vivo capsule is shown in Figure 21 c. It takes advantage of the fact that long molecules attached to a TiO₂ surface can be released photocatalytically. Shrestha et al.^[324] showed that TiO₂ nanotubes can be filled with magnetic Fe₃O₄ particles and thus be magnetically guided to desired locations. Such tubes can then be easily coated with drugs that are attached by suitable linker molecules. Drug release is not limited to UV reactions but can also be triggered electrically (voltage induced catalysis)^[138] or more importantly by X-rays,^[344] which allows in vivo treatments through living tissue. Such magnetic TiO₂ nanotubes can be used directly for photocatalytic reactions with cells or tissue, for example for the site-selective killing of cancer cells.^[324]

An even more elaborate payload filling and release mechanism was introduced by Song et al.,^[144,177] who created amphiphilic tube layers, which involves tubes that provide a hydrophobic cap (monolayer) that does not allow water (body fluid) to enter into the tubes unless opened by a photocatalytic interaction. Once the hydrophobic layer was removed, body fluids could enter and wash out hydrophilic drugs loaded within the tubes.

Conflicting reports exist regarding drug-eluting coatings. Some reports show elution times over weeks for loading with paclitaxel, sirolimus, and BSA that are seemingly based on sampling errors.^[424] Other reports could not be confirmed; in fact, when reproducing experiments of Peng et al.^[424] with identical tubes and drugs, elusion time constants of minutes^[425–427] rather than days or weeks were found. Most recent work demonstrates that to achieve slow release, capping of drug-loaded tubular or porous systems with biopolymer, such as poly(lactic acid), is required. Modified in this way, tubular or even better mesoporous anodic layers on titanium-based implants or stents may represent efficient and promising drug-release systems.^[426] For applications on stents, a considerable drawback is the somewhat limited mechanical flexibility of the nanotube layers compared to other mesoporous oxide layers.^[80,81,426] A way to increase the mechanical properties of tubular systems is their modification to more stable titanium oxycarbide nanotube layers.^[212,213]

Payload release systems are not limited to in vivo applications, but may prove extremely valuable for MEMS or specifically lab-on-a-chip applications, where release of reactants may be triggered by optical means (photocatalytic chain scission) or electrical means (voltage-induced).

6.6. Other Applications and Aspects

In terms of gas sensing, TiO₂ layers have shown to have a high sensitivity to CO, H₂, and NO_x gases, and in particular as nanoparticulated films.^[428–430] For TiO₂ nanotube layers, this sensitivity has also been demonstrated.^[283,431] In terms of in-solution sensing, it has also been shown that for gold nanoparticles supported on TiO₂ nanotube layers, a strongly enhanced reaction rate with O₂ in aqueous solution can be found,^[274] which is of great interest for oxygen sensors. Such considerable support effects were also observed for methanol oxidation reactions, not only for supporting Pt/Pd on TiO₂ nanotubes,^[275] but even more for semimetallic tubes that showed an efficiency enhancement of 700%.^[212] These findings are very promising for applications in methanol fuel cells (that is, as a substitute for carbon-based supports).

An approach that ideally takes advantage of the nanotubular geometry is as so-called nano test tubes.^[384] For example, color reactions can be carried out in the extremely small tube volume of 4×10^{-14} mL, but owing to the very high aspect ratio, an extremely high sensitivity for detection is established; that is, used as a photometric nanocuvette, a high observation length and thus high specific light-absorption path is provided. A significant advantage of using TiO₂ is its transparency for large range of light and moreover its self-cleaning properties when using static devices (MEMS or lab-on-a-chip). Fringes occurring in reflection spectra may also be used for interference applications as a gas- or liquid-based sensor, which can be optimized in performance by tailoring the roughness of the tube sidewalls.^[144] Owing to their sensitivity to H₂O₂ concentration variations, TiO₂ nanotubes decorated with coadsorbed horseradish peroxidase (HRP) and thionine chloride were also used as biosensors.^[432]

To date, the fact that considerable photochromic effects have been reported for silver-loaded TiO₂ nanotubes^[325] or that, in fact, oxide tube layers may be reduced to metallic nanostructures has remained virtually unexploited.^[172] In view of tube growth, recent studies on metallurgical aspects^[187] or the growth of nanotubes in ionic liquids are very interesting.^[111]

Novel ordered structures may be obtained by further modifying the metallic substrate. Apart from using meshes or metallic grids to improve the surface area,^[433] entirely novel concepts use for example roll-bonded substrates. Tsuchiya et al.^[187] showed strategies to achieve TiAl stripes that could be selectively porosified or by which tubes could be formed. The size limit of this approach to produce alternating tube and pore layers lies in the range of 1–100 μm. It may also be noteworthy that studies on ordered surface dimple formation^[113–115] are of course directly related to nanotube formation, as outlined in Section 2.7.4. Concepts to create nanosize oxide composition modulation in the tube walls that create for example highly defined junctions and 3D superlattices are also very spectacular.^[246]

A point that clearly should be addressed but has not yet been extensively studied is the mechanical stability of the tube layers.^[213] Although general adhesion is reported to be good, the presence of the fluoride-rich layer affects the adhesion of nanotube layers, for example when bending the substrate.^[80,81] This adhesion can be improved by carbonization of the tubes,^[213] but even better adhesion for anodic layers can be obtained using titania mesosponges^[80,81] or nanochannel layers.^[83]

While progress on nanotubes on Ti, alloys, and other valve metals is constantly advancing and new exciting findings are continuously being reported, in many aspects, an even more promising form of self-organized anodic titania has been reported, namely a mesosponge structure^[80,81] that can be grown to more than 100 μm in thickness with the main advantages that it has a much higher specific surface area than TiO₂ nanotubes and a significantly stronger adherence to the metallic substrate surface.

The authors would like to acknowledge the DFG for financial support and Prof. Dr. S. Virtanen, S. P. Albu, W. Wei, C. Das, I. Paramasivam, H. Jha, S. Bauer, H. Hilderbrand, R. Hahn, N. Shrestha, H. Tsuchiya, and K. Yasuda for their contributions.

Received: March 8, 2010

- [1] S. Iijima, *Nature* **1991**, 354, 56.
- [2] C. M. Lieber, *Solid State Commun.* **1998**, 107, 607.
- [3] C. N. R. Rao, A. Müller, A. K. Cheetham, *The Chemistry of Nanomaterials: Synthesis, Properties and Applications*, Wiley-VCH, Weinheim, Germany, **2006**.
- [4] C. Weisbuch, B. Vinter, *Quantum Semiconductor Structures: Fundamentals and Applications*, Elsevier, Amsterdam, **1991**.
- [5] C. N. R. Rao, M. Nath, *Dalton Trans.* **2003**, 1.
- [6] Y. Feldman, E. Wasserman, D. J. Srolovitz, R. Tenne, *Science* **1995**, 267, 222.
- [7] R. Tenne, L. Margulis, M. Genut, G. Hodes, *Nature* **1992**, 360, 444.

- [8] Y. Xia, P. Yang, Y. Sun, Y. Wu, B. Mayers, B. Gates, Y. Yin, F. Kim, H. Yan, *Adv. Mater.* **2003**, *15*, 353.
- [9] H. Nakamura, Matsui, *J. Am. Chem. Soc.* **1995**, *117*, 2651.
- [10] P. Hoyer, *Langmuir* **1996**, *12*, 1411.
- [11] L. Pu, X. Bao, J. Zou, D. Feng, *Angew. Chem.* **2001**, *113*, 1538; *Angew. Chem. Int. Ed.* **2001**, *40*, 1490.
- [12] M. Remškar, *Adv. Mater.* **2004**, *16*, 1497.
- [13] J. L. G. Fierro, *Metal Oxides: Chemistry and Applications*, CRC Press, Boca Raton, **2006**.
- [14] T. Kasuga, M. Hiramatsu, A. Hoson, T. Sekino, K. Niihara, *Langmuir* **1998**, *14*, 3160.
- [15] D. V. Bavykin, J. M. Friedrich, F. C. Walsh, *Adv. Mater.* **2006**, *18*, 2807.
- [16] P. Schmuki, S. Virtanen, *Electrochemistry at the Nanoscale*, Springer, New York, **2009**.
- [17] F. Krumeich, H. J. Muhr, M. Niederberger, F. Brieri, B. Schnyder, R. Nesper, *J. Am. Chem. Soc.* **1999**, *121*, 8324.
- [18] C. R. Sides, N. Li, C. J. Patrissi, B. Scrosati, C. R. Martin, *MRS Bull.* **2002**, *27*, 604.
- [19] A. Fujishima, T. N. Rao, D. A. Tryk, *J. Photochem. Photobiol. C* **2000**, *1*, 1.
- [20] A. Kudo, Y. Miseki, *Chem. Soc. Rev.* **2009**, *38*, 253.
- [21] S. K. Mohapatra, M. Misra, V. K. Mahajan, K. S. Roja, *J. Phys. Chem. C* **2007**, *111*, 8677.
- [22] A. Fujishima, K. Honda, *Nature* **1972**, *238*, 37.
- [23] H. Gerischer, H. Tributsch, *Ber. Bunsen-Ges.* **1968**, *72*, 437.
- [24] M. P. Dare-Edwards, J. B. Goodenough, A. Hamnett, K. R. Seddon, R. D. Wrigh, *Faraday Discuss. Chem. Soc.* **1980**, *70*, 285.
- [25] B. O'Regan, M. Grätzel, *Nature* **1991**, *353*, 737.
- [26] M. Grätzel, *Nature* **2001**, *414*, 338.
- [27] J. Huusko, V. Lantto, H. Torvela, *Sens. Actuators B* **1993**, *16*, 245.
- [28] A. L. Linsebigler, G. Lu, J. T. Yates, *Chem. Rev.* **1995**, *95*, 735.
- [29] S. Y. Huang, L. Kavan, I. Exnar, M. Graetzel, *J. Electrochem. Soc.* **1995**, *142*, L142.
- [30] R. Wang, K. Hashimoto, A. Fujishima, M. Chikuni, E. Kojima, A. Kitamura, M. Shimohigoshi, T. Watanabe, *Nature* **1997**, *388*, 431.
- [31] K. Satake, A. Katayama, H. Ohkoshi, T. Nakahara, T. Takeuchi, *Sens. Actuators B* **1994**, *20*, 111.
- [32] H. Gerischer, *Electrochim. Acta* **1995**, *40*, 1277.
- [33] M. Wagemaker, D. Lutzenkirchen-Hecht, A. A. van Well, R. Frahm, *J. Phys. Chem. B* **2004**, *108*, 12456.
- [34] A. R. Armstrong, G. Armstrong, J. Canales, R. Garcia, P. G. Bruce, *Adv. Mater.* **2005**, *17*, 862.
- [35] P. Roy, D. Kim, K. Lee, E. Spiecker, P. Schmuki, *Nanoscale* **2010**, *2*, 45.
- [36] A. Ghicov, P. Schmuki, *Chem. Commun.* **2009**, 2791.
- [37] J. M. Macak, H. Tsuchiya, A. Ghicov, K. Yasuda, R. Hahn, S. Bauer, P. Schmuki, *Curr. Opin. Solid State Mater. Sci.* **2007**, *11*, 3.
- [38] I. Paramasivam, H. Jha, P. Schmuki, unpublished results.
- [39] S. Bauer, P. Schmuki, J. Park, K. von der Mark, C. von Wilmsowsky, K. A. Schlegel, F. W. Neukam, unpublished results.
- [40] U. Diebold, *Surf. Sci. Rep.* **2003**, *48*, 53.
- [41] A. Hagfeldt, M. Graetzel, *Chem. Rev.* **1995**, *95*, 49.
- [42] A. Mills, S. Le Hunte, *J. Photochem. Photobiol. A* **1997**, *108*, 1.
- [43] S. Eustis, M. A. El-Sayed, *Chem. Soc. Rev.* **2006**, *35*, 209.
- [44] M. S. Sander, M. J. Cote, W. Gu, B. M. Kile, C. P. Tripp, *Adv. Mater.* **2004**, *16*, 2052.
- [45] G. L. Li, G. H. Wang, *Nanostruct. Mater.* **1999**, *11*, 663.
- [46] D. Zhang, L. Qi, J. Ma, H. Cheng, *J. Mater. Chem.* **2002**, *12*, 3677.
- [47] T. Kasuga, M. Hiramatsu, A. Hoson, T. Sekino, K. Niihara, *Adv. Mater.* **1999**, *11*, 1307.
- [48] a) G. H. Du, Q. Chen, R. C. Che, Z. Y. Yuan, L. M. Peng, *Appl. Phys. Lett.* **2001**, *79*, 3702–3704; b) Y. Suzuki, S. Yoshikawa, *J. Mater. Res.* **2004**, *19*, 982.
- [49] M. Adachi, Y. Murata, S. Yoshikawa, *Chem. Lett.* **2000**, *29*, 942.
- [50] a) M. Adachi, Y. Murata, I. Okada, S. Yoshikawa, *J. Electrochem. Soc.* **2003**, *150*, G488.
- [51] H. H. Ou, S. L. Lo, *Sep. Purif. Technol.* **2007**, *58*, 179.
- [52] B. B. Lakshmi, P. K. Dorhout, C. R. Martin, *Chem. Mater.* **1997**, *9*, 857.
- [53] H. Imai, Y. Takei, K. Shimizu, M. Matsuda, H. Hirashima, *J. Mater. Chem.* **1999**, *9*, 2971.
- [54] S. Uchida, R. Chiba, M. Tomiha, N. Masaki, M. Shirai, *Electrochemistry* **2002**, *70*, 418.
- [55] K. S. Raja, M. Misra, K. Paramguru, *Electrochim. Acta* **2005**, *51*, 154.
- [56] Y. Nakato, H. Akanuma, J. Shimizu, Y. Magori, *J. Electroanal. Chem.* **1995**, *396*, 35.
- [57] T. Sugiura, T. Yoshida, H. Minoura, *Electrochem. Solid-State Lett.* **1998**, *1*, 175.
- [58] T. Kisumi, A. Tsujiko, K. Murakoshi, Y. Nakato, *J. Electroanal. Chem.* **2003**, *545*, 99.
- [59] M. Zhang, Y. Bando, K. Wada, *J. Mater. Sci. Lett.* **2001**, *20*, 167.
- [60] H. Shin, D. K. Jeong, J. Lee, M. M. Sung, J. Kim, *Adv. Mater.* **2004**, *16*, 1197.
- [61] M. Knez, K. Nielsch, L. Niinistö, *Adv. Mater.* **2007**, *19*, 3425.
- [62] Ref. [44].
- [63] M. Leskelä, M. Ritala, *Angew. Chem.* **2003**, *115*, 5706; *Angew. Chem. Int. Ed.* **2003**, *42*, 5548.
- [64] J. Bisquert in *Synthesis Properties and Applications of Oxide Nanomaterials* (Eds.: J. A. Rodriguez, M. Fernandez-Garcia), Wiley, New York, **2007**, p. 451.
- [65] A. S. Aricò, P. Bruce, B. Scrosati, J. M. Tarascon, W. van Schalkwijk, *Nat. Mater.* **2005**, *4*, 366.
- [66] S. K. Deb, *Philos. Mag.* **1973**, *27*, 801.
- [67] M. A. B. Gomes, L. O. D. S. Bulhoses, S. C. De Castro, A. J. Damiao, *J. Electrochem. Soc.* **1990**, *137*, 3067.
- [68] S. K. Deb, *Sol. Energy Mater. Sol. Cells* **2008**, *92*, 245.
- [69] B. W. Faughnan, R. S. Crandall, P. M. Heyman, *RCA Rev.* **1975**, *36*, 177.
- [70] B. Reichman, A. J. Bard, *J. Electrochem. Soc.* **1980**, *127*, 241.
- [71] P. Jun, L. Duren, *Chem. Senses* **1998**, 565.
- [72] S. H. Lee, R. Deshpande, P. A. Parilla, K. M. Jones, B. To, A. H. Mahan, A. C. Dillon, *Adv. Mater.* **2006**, *18*, 763.
- [73] K. Nakayama et al. in *208th ECS Meeting*, California, Abstract 819 and 843, **2005**.
- [74] R. Hahn, J. M. Macak, P. Schmuki, *Electrochem. Commun.* **2007**, *9*, 947.
- [75] R. Hahn, T. Stergiopoulos, J. M. Macak, D. Tsoukleris, A. G. Kontos, S. P. Albu, D. Kim, A. Ghicov, J. Kunze, P. Falaras, P. Schmuki, *Phys. Status Solidi RRL* **2007**, *1*, 135.
- [76] H. Jha, R. Hahn, P. Schmuki, unpublished results.
- [77] H. Jha, R. Hahn, P. Schmuki, *Electrochim. Acta* **2010**, *55*, 8883.
- [78] N. F. Fahim, T. Sekino, *Chem. Mater.* **2009**, *21*, 1967.
- [79] K. I. Ishibashi, R. T. Yamaguchi, Y. Kimura, M. Niwano, *J. Electrochem. Soc.* **2008**, *155*, K10.
- [80] D. Kim, K. Lee, P. Roy, B. I. Birajdar, E. Spiecker, P. Schmuki, *Angew. Chem.* **2009**, *121*, 9490; *Angew. Chem. Int. Ed.* **2009**, *48*, 9326.
- [81] K. Lee, D. Kim, P. Roy, I. Paramasivam, B. I. Birajdar, E. Spiecker, P. Schmuki, *J. Am. Chem. Soc.* **2010**, *132*, 1478.
- [82] D. Kim, P. Roy, K. Lee, P. Schmuki, *Electrochem. Commun.* **2010**, *12*, 574.
- [83] P. Roy, T. Dey, K. Lee, D. Kim, B. Fabry, P. Schmuki, *J. Am. Chem. Soc.* **2010**, *132*, 7893.
- [84] F. Keller, M. S. Hunter, D. L. Robinson, *J. Electrochem. Soc.* **1953**, *100*, 411.

- [85] J. P. O'Sullivan, G. C. Wood, *Proc. R. Soc. London Ser. A* **1970**, 317, 511.
- [86] G. Thompson, G. C. Wood, *Anodic films on aluminum. Treatise on materials science and technology, Vol. 23*, Academic Press, New York, **1983**.
- [87] K. Uosaki, K. Okazaki, H. Kita, H. Takahashi, *Anal. Chem.* **1990**, 62, 652.
- [88] C. R. Martin, *Science* **1994**, 266, 1961.
- [89] H. Masuda, K. Fukuda, *Science* **1995**, 268, 1466.
- [90] K. Nielsch, F. Müller, A. P. Li, U. Gösele, *Adv. Mater.* **2000**, 12, 582.
- [91] M. Steinhart, J. H. Wendorff, A. Greiner, R. B. Wehrspohn, K. Nielsch, J. Schilling, J. Choi, U. Gösele, *Science* **2002**, 296, 1997.
- [92] D. AlMawlawi, N. Coombs, M. Moskovits, *J. Appl. Phys.* **1991**, 70, 4421.
- [93] M. Zhang, Y. Bando, K. Wada, *J. Mater. Res.* **2000**, 15, 387.
- [94] J. F. Vanhumbecq, J. Proost, *Electrochim. Acta* **2008**, 53, 6165.
- [95] J. P. O'Sullivan, G. C. Wood, *Proc. R. Soc. London Ser. A* **1970**, 317, 511.
- [96] O. Jessensky, F. Müller, U. Gösele, *Appl. Phys. Lett.* **1998**, 72, 1173.
- [97] S. Ono, M. Saito, H. Asoh, *Electrochem. Solid-State Lett.* **2004**, 7, B21.
- [98] S. Ono, M. Saito, M. Ishiguro, H. Asoh, *J. Electrochem. Soc.* **2004**, 151, B473.
- [99] V. Zwillig, E. Darque-Ceretti, A. Boutry-Forveille, D. David, M. Y. Perrin, M. Aucouturier, *Surf. Interface Anal.* **1999**, 27, 629.
- [100] V. Zwillig, M. Aucouturier, E. Darque-Ceretti, *Electrochim. Acta* **1999**, 45, 921.
- [101] J. J. Kelly, *Electrochim. Acta* **1979**, 24, 1273.
- [102] D. Gong, C. A. Grimes, O. K. Varghese, Z. Chen, E. C. Dickey, *J. Mater. Res.* **2001**, 16, 3331.
- [103] R. Beranek, H. Hildebrand, P. Schmuki, *Electrochem. Solid-State Lett.* **2003**, 6, B12.
- [104] J. M. Macak, K. Sirotna, P. Schmuki, *Electrochim. Acta* **2005**, 50, 3679.
- [105] J. M. Macak, H. Tsuchiya, P. Schmuki, *Angew. Chem.* **2005**, 117, 2136; *Angew. Chem. Int. Ed.* **2005**, 44, 2100.
- [106] J. M. Macak, H. Tsuchiya, L. Taveira, S. Aldabergerova, P. Schmuki, *Angew. Chem.* **2005**, 117, 7629; *Angew. Chem. Int. Ed.* **2005**, 44, 7463.
- [107] a) O. K. Varghese, M. Paulose, K. Shankar, G. K. Mor, C. A. Grimes, *J. Nanosci. Nanotechnol.* **2005**, 5, 1158; b) M. Paulose, K. Shankar, O. K. Varghese, G. K. Mor, B. Hardin, C. A. Grimes, *Nanotechnol.* **2010**, 21, 389801; c) M. Paulose, G. K. Mor, O. K. Varghese, K. Shankar, C. A. Grimes, *J. Photochem. Photobiol. A*, **2010**, 215, 229.
- [108] S. P. Albu, A. Ghicov, J. M. Macak, P. Schmuki, *Phys. Status Solidi RRL* **2007**, 1, R65.
- [109] H. Masuda, M. Satoh, *Jpn. J. Appl. Phys. Part 1* **1996**, 35, L126.
- [110] J. M. Macak, S. P. Albu, P. Schmuki, *Phys. Status Solidi RRL* **2007**, 1, 181.
- [111] I. Paramasivam, J. M. Macak, T. Selvam, P. Schmuki, *Electrochim. Acta* **2008**, 54, 643.
- [112] H. Tsuchiya, J. M. Macak, L. Taveira, E. Balaur, A. Ghicov, K. Sirotna, P. Schmuki, *Electrochem. Commun.* **2005**, 7, 576.
- [113] H. El-Sayed, S. Singh, M. T. Greiner, P. Kruse, *Nano Lett.* **2006**, 6, 2995.
- [114] a) V. Vignal, J. C. Roux, S. Flandrois, A. Fevrier, *Corros. Sci.* **2000**, 42, 1041; b) H. Tsuchiya, T. Suzumura, S. Fujimoto, 218th Meeting of the Electrochemical Society.
- [115] S. Singh, W. R. T. Barden, P. Kruse, *ACS Nano* **2008**, 2, 2453.
- [116] H. Masuda, H. Yamada, M. Satoh, H. Asoh, M. Nakao, T. Tamamura, *Appl. Phys. Lett.* **1997**, 71, 2770.
- [117] L. V. Taveira, J. M. Macak, H. Tsuchiya, L. F. P. Dick, P. Schmuki, *J. Electrochem. Soc.* **2005**, 152, B405.
- [118] S. P. Albu, A. Ghicov, S. Aldabergerova, P. Drechsel, D. LeClere, G. E. Thompson, J. M. Macak, P. Schmuki, *Adv. Mater.* **2008**, 20, 4135.
- [119] D. Kim, A. Ghicov, P. Schmuki, *Electrochem. Commun.* **2008**, 10, 1835.
- [120] Y. Y. Song, R. Lynch, D. Kim, P. Roy, P. Schmuki, *Electrochem. Solid-State Lett.* **2009**, 12, C17.
- [121] S. P. Albu, P. Schmuki, *Phys. Status Solidi RRL* **2010**, 4, 151.
- [122] J. Park, S. Bauer, K. Von Der Mark, P. Schmuki, *Nano Lett.* **2007**, 7, 1686.
- [123] S. P. Albu, A. Ghicov, J. M. Macak, R. Hahn, P. Schmuki, *Nano Lett.* **2007**, 7, 1286.
- [124] K. Yasuda, P. Schmuki, *Electrochim. Acta* **2007**, 52, 4053.
- [125] D. Kim, F. Schmidt-Stein, R. Hahn, P. Schmuki, *Electrochem. Commun.* **2008**, 10, 1082.
- [126] K. Yasuda, J. M. Macak, S. Berger, A. Ghicov, P. Schmuki, *J. Electrochem. Soc.* **2007**, 154, C472.
- [127] S. Berger, J. Kunze, P. Schmuki, D. LeClere, A. Valota, P. Skeldon, G. E. Thompson, *Electrochim. Acta* **2009**, 54, 5942.
- [128] Y. V. Bhargava, Q. A. S. Nguyen, T. M. Devine, *J. Electrochem. Soc.* **2009**, 156, E62.
- [129] J. M. Macak, H. Hildebrand, U. Marten-Jahns, P. Schmuki, *J. Electroanal. Chem.* **2008**, 621, 254.
- [130] S. P. Albu, A. Ghicov, P. Schmuki, unpublished results.
- [131] J. M. Macak, S. Aldabergerova, A. Ghicov, P. Schmuki, *Phys. Status Solidi A* **2006**, 203, R67.
- [132] S. Bauer, S. Kleber, P. Schmuki, *Electrochem. Commun.* **2006**, 8, 1321.
- [133] D. J. LeClere, A. Valota, P. Skeldon, G. E. Thompson, S. Berger, J. Kunze, P. Schmuki, H. Habazaki, S. Nagata, *J. Electrochem. Soc.* **2008**, 155, C487.
- [134] K. Lee, J. Lee, H. Kim, Y. Lee, D. Kim, P. Schmuki, Y. Tak, *J. Korean Phys. Soc.* **2009**, 54, 1027.
- [135] A. Valota, D. J. LeClere, T. Hashimoto, P. Skeldon, G. E. Thompson, S. Berger, J. Kunze, P. Schmuki, *Nanotechnology* **2008**, 19, 355701.
- [136] J. M. Macak, P. Schmuki, *Electrochim. Acta* **2006**, 52, 1258.
- [137] S. P. Albu, P. Schmuki, *Phys. Status Solidi RRL* **2010**, 4, 215.
- [138] Y. Y. Song, P. Roy, I. Paramasivam, P. Schmuki, *Angew. Chem.* **2010**, 122, 361; *Angew. Chem. Int. Ed.* **2010**, 49, 351.
- [139] S. P. Albu, P. Schmuki, unpublished results.
- [140] J. Kunze, A. Ghicov, H. Hildebrand, J. M. Macak, L. Taveira, P. Schmuki, *Z. Phys. Chem.* **2005**, 219, 1561.
- [141] J. Lausmaa, *J. Electron Spectrosc. Relat. Phenom.* **1996**, 81, 343.
- [142] F. Thébault, B. Vuillemin, R. Oltra, J. Kunze, A. Seyeux, P. Schmuki, *Electrochem. Solid-State Lett.* **2009**, 12, C5.
- [143] K. Von Der Mark, J. Park, S. Bauer, P. Schmuki, *Cell Tissue Res.* **2010**, 339, 131.
- [144] Y. Y. Song, P. Schmuki, *Electrochem. Commun.* **2010**, 12, 579.
- [145] S. Berger, J. Kunze, P. Schmuki, A. T. Valota, D. J. LeClere, P. Skeldon, G. E. Thompson, *J. Electrochem. Soc.* **2010**, 157, C18.
- [146] L. V. Taveira, J. M. Macak, K. Sirotna, L. F. P. Dick, P. Schmuki, *J. Electrochem. Soc.* **2006**, 153, B137.
- [147] W. Chanmanee, A. Watcharenwong, C. R. Chenthamarakshan, P. Kajitvichyanukul, N. R. de Tacconi, K. Rajeshwar, *J. Am. Chem. Soc.* **2008**, 130, 965.
- [148] S. Banerjee, S. K. Mohapatra, M. Misra, I. B. Mishra, *Nanotechnology* **2009**, 20, 075502.
- [149] N. B. Pilling, R. E. Bedworth, *J. Inst. Met.* **1923**, 29, 529.
- [150] H. Habazaki, M. Uozumi, H. Konno, K. Shimizu, S. Nagata, K. Takayama, Y. Oda, P. Skeldon, G. E. Thompson, *J. Electrochem. Soc.* **2005**, 152, B263.
- [151] P. Skeldon, G. E. Thompson, S. J. Garcia-Vergara, L. Iglesias-Rubianes, C. E. Blanco-Pinzon, *Electrochem. Solid-State Lett.* **2006**, 9, B47.
- [152] S. J. Garcia-Vergara, P. Skeldon, G. E. Thompson, H. Habazaki, *Electrochim. Acta* **2006**, 52, 681.

- [153] K. R. Hebert, J. E. Houser, *J. Electrochem. Soc.* **2009**, *156*, C275.
- [154] J. E. Houser, K. R. Hebert, *Nat. Mater.* **2009**, *8*, 415.
- [155] S. Berger, J. M. Macak, J. Kunze, P. Schmuki, *Electrochem. Solid-State Lett.* **2008**, *11*, C37.
- [156] Q. A. S. Nguyen, Y. V. Bhargava, V. R. Radmilovic, T. M. Devine, *Electrochim. Acta* **2009**, *54*, 4340.
- [157] A. Valota, D. J. LeClere, P. Skeldon, M. Curioni, T. Hashimoto, S. Berger, J. Kunze, P. Schmuki, G. E. Thompson, *Electrochim. Acta* **2009**, *54*, 4321.
- [158] H. Tsuchiya, S. Berger, J. M. Macak, A. Ghicov, P. Schmuki, *Electrochem. Commun.* **2007**, *9*, 2397.
- [159] S. Berger, H. Tsuchiya, P. Schmuki, *Chem. Mater.* **2008**, *20*, 3245.
- [160] R. Blachnik, J. D'Ans, E. Lax, C. Synowietz, *Taschenbuch für Chemiker und Physiker*, Volume 3, Springer, Berlin, **1998**.
- [161] W. Wei, S. Berger, N. Shrestha, P. Schmuki, unpublished results.
- [162] S. P. Albu, P. Schmuki, unpublished results.
- [163] S. Berger, F. Jakubka, P. Schmuki, *Electrochem. Solid-State Lett.* **2009**, *12*, K45.
- [164] S. Berger, F. Jakubka, P. Schmuki, *Electrochem. Commun.* **2008**, *10*, 1916.
- [165] H. Tsuchiya, J. M. Macak, A. Ghicov, L. Taveira, P. Schmuki, *Corros. Sci.* **2005**, *47*, 3324.
- [166] H. Tsuchiya, P. Schmuki, *Electrochem. Commun.* **2005**, *7*, 49.
- [167] Motoo Kawasaki, Hidemi Nawafune, *Farthest Advances in Surface Finishing of Aluminum Visualized by Electron Microscopy Observation*, The Surface Finishing Society of Japan, Tokyo, **2000**, pp. 99–100 (in Japanese).
- [168] D. J. Arrowsmith, A. W. Clifford, D. A. Moth, *J. Mater. Sci. Lett.* **1986**, *5*, 921.
- [169] S. Ono, K. Takeda, N. Masuko, 2nd International Symposium on Aluminium Surface Science and Technology, ASST **2000**, UMIST, Manchester, UK.
- [170] S.-Z. Chu, K. Wada, S. Inoue, M. Isogai, A. Yasumori, *Adv. Mater.* **2007**, *19*, 2115.
- [171] W. Wei, S. Berger, C. Hauser, K. Mayer, M. Yang, P. Schmuki, *Electrochem. Commun.* **2010**, *12*, 1184.
- [172] K. Yasuda, P. Schmuki, *Electrochem. Commun.* **2007**, *9*, 615.
- [173] a) J. J. Urban, W. S. Yun, Q. Gu, H. Park, *J. Am. Chem. Soc.* **2002**, *124*, 1186; b) B. A. Hernandez, K. S. Chang, E. R. Fisher, P. K. Dorhout, *Chem. Mater.* **2002**, *14*, 480.
- [174] a) K. G. Singh, A. A. Golovin, I. S. Aranson, *Phys. Rev. B* **2006**, *73*, 205422; b) L. G. Stanton, A. A. Golovin, *Phys. Rev. B* **2009**, *79*, 035414.
- [175] S. Ono, M. Saito, H. Asoh, *Electrochim. Acta* **2005**, *51*, 827.
- [176] Q. Van Overmeere, F. Blaffart, J. Proost, *Electrochem. Commun.* **2010**, *12*, 1174.
- [177] Y. Y. Song, F. Schmidt-Stein, S. Bauer, P. Schmuki, *J. Am. Chem. Soc.* **2009**, *131*, 4230.
- [178] S. P. Albu, D. Kim, P. Schmuki, *Angew. Chem.* **2008**, *120*, 1942; *Angew. Chem. Int. Ed.* **2008**, *47*, 1916.
- [179] D. Kim, A. Ghicov, S. P. Albu, P. Schmuki, *J. Am. Chem. Soc.* **2008**, *130*, 16454.
- [180] J. Kunze, A. Seyeux, P. Schmuki, *Electrochem. Solid-State Lett.* **2008**, *11*, K11.
- [181] P. Roy, T. Dey, P. Schmuki, *Electrochem. Solid-State Lett.* **2010**, *13*, E11.
- [182] H. Asoh, S. Ono in *Electrocrystallization in Nanotechnology* (Ed.: G. T. Staikov), Wiley-VCH, Weinheim, **2007**, p. 138.
- [183] Y.-C. Nah, N. K. Shrestha, D. Kim, S. P. Albu, I. Paramasivam, P. Schmuki, *Electrochem. Solid-State Lett.* **2010**, *13*, K73.
- [184] K. Zhu, T. B. Vinzant, N. R. Neale, A. J. Frank, *Nano Lett.* **2007**, *7*, 3739.
- [185] J. H. Lim, J. Choi, *Small* **2007**, *3*, 1504.
- [186] H. Tsuchiya, J. M. Macak, A. Ghicov, P. Schmuki, *Small* **2006**, *2*, 888.
- [187] H. Tsuchiya, T. Akaki, D. Terada, N. Tsuji, Y. Minamino, P. Schmuki, S. Fujimoto, *Electrochim. Acta* **2009**, *54*, 5155.
- [188] A. Ghicov, S. Aldabergenova, H. Tsuchiya, P. Schmuki, *Angew. Chem.* **2006**, *118*, 7150–7153; *Angew. Chem. Int. Ed.* **2006**, *45*, 6993.
- [189] K. Yasuda, P. Schmuki, *Adv. Mater.* **2007**, *19*, 1757.
- [190] H. Tsuchiya, T. Akaki, J. Nakata, D. Terada, N. Tsuji, Y. Koizumi, Y. Minamino, P. Schmuki, S. Fujimoto, *Corros. Sci.* **2009**, *51*, 1528.
- [191] X. J. Feng, J. M. Macak, S. P. Albu, P. Schmuki, *Acta Biomater.* **2008**, *4*, 318.
- [192] J. M. Macak, H. Tsuchiya, L. Taveira, A. Ghicov, P. Schmuki, *J. Biomed. Mater. Res. Part A* **2005**, *75*, 928.
- [193] S. P. Albu, A. Ghicov, S. Berger, H. Jha, P. Schmuki, *Electrochem. Commun.* **2010**, *12*, 1352.
- [194] C. J. Lin, W. Y. Yu, Y. T. Lu, S. H. Chien, *Chem. Commun.* **2008**, 6031.
- [195] K. Kant, D. Losic, *Phys. Status Solidi RRL* **2009**, *3*, 139.
- [196] J. Wang, Z. Lin, *Chem. Mater.* **2008**, *20*, 1257.
- [197] T. L. Thompson, J. T. Yates, Jr., *Chem. Rev.* **2006**, *106*, 4428.
- [198] M. R. Hoffmann, S. T. Martin, W. Choi, D. W. Bahneman, *Chem. Rev.* **1995**, *95*, 69.
- [199] R. Marchand, L. Broham, M. Tournoux, *Mater. Res. Bull.* **1980**, *15*, 1129.
- [200] J. Muscat, V. Swamy, N. M. Harrison, *Phys. Rev. B* **2002**, *65*, 224112.
- [201] S. Bauer, H. Tsuchiya, A. Pittrof, P. Schmuki, unpublished results.
- [202] M. Lazzeri, A. Vittadini, A. Selloni, *Phys. Rev. B* **2001**, *63*, 155409.
- [203] W. Huang, X. Tang, Y. Wang, Y. Kolypin, A. Gedanken, *Chem. Commun.* **2000**, 1415.
- [204] H. Yin, Y. Wada, T. Kitamura, S. Kambe, A. Murasawa, H. Mori, T. Sakata, S. Yangida, *J. Mater. Chem.* **2001**, *11*, 1694.
- [205] S. T. Aruna, S. Tirosh, A. Zaban, *J. Mater. Chem.* **2000**, *10*, 2388.
- [206] T. Ohtsuka, J. Guo, N. Sato, *J. Electrochem. Soc.* **1986**, *133*, 2473.
- [207] A. Aladjem, D. Brandon, J. Yahalom, J. Zahavi, *Electrochim. Acta* **1970**, *15*, 663.
- [208] T. Ohtsuka, T. Otsuki, *Corros. Sci.* **2003**, *45*, 1793.
- [209] S. Yamaguchi, *J. Electrochem. Soc.* **1961**, *108*, 302.
- [210] J. R. Smith, F. C. Walsh, R. L. Clarke, *J. Appl. Electrochem.* **1998**, *28*, 1021.
- [211] M. Zweynert, H. Doring, J. Garche, K. Enghardt, K. Wiesener, *Chem. Ing. Tech.* **1998**, *7*, 827.
- [212] R. Hahn, F. Schmidt-Stein, J. Salonen, S. Thiemann, Y. Y. Song, J. Kunze, V. P. Lehto, P. Schmuki, *Angew. Chem.* **2009**, *121*, 7372; *Angew. Chem. Int. Ed.* **2009**, *48*, 7236.
- [213] F. Schmidt-Stein, S. Thiemann, S. Berger, R. Hahn, P. Schmuki, *Acta Mater.* **2010**, *58*, 6317.
- [214] S. P. Albu, H. Tsuchiya, S. Fujimoto, P. Schmuki, *Europ. J. Inorg. Chem.* **2010**, *27*, 4351.
- [215] J. C. Marchenoir, J. P. Loup, J. Masson, *Thin Solid Films* **1980**, *66*, 357.
- [216] J.-L. Delplancke, A. Garnier, Y. Massiani, R. Winand, *Electrochim. Acta* **1994**, *39*, 1281.
- [217] J. C. Marchenoir, J. Gautron, J. P. L. Metaux, *Corrosion-Industrie* **1977**, 83.
- [218] J. Arbiol, J. Cerda, G. Dezaneeu, A. Cicera, F. Peiro, A. Cornet, J. R. Morante, *J. Appl. Phys.* **2002**, *92*, 853.
- [219] V. Guidi, M. C. Carotta, M. Ferroni, G. Martinelli, M. Sacerdoti, *J. Phys. Chem. B* **2003**, *107*, 120.
- [220] L. E. Depero, L. Sangaletti, B. Allieri, E. Bontempi, A. Marino, M. Zocchi, *J. Cryst. Growth* **1999**, *198*, 516.
- [221] L. E. Depero, A. Marino, B. Allieri, E. Bontempi, L. Sangaletti, C. Casale, M. Notaro, *J. Mater. Res.* **2000**, *15*, 2080.

- [222] V. Likodimos, T. Stergiopoulos, P. Falaras, J. Kunze, P. Schmuki, *J. Phys. Chem. C* **2008**, *112*, 12687.
- [223] S. B. Aldabergenova, A. Ghicov, S. Albu, J. M. Macak, P. Schmuki, *J. Non-Cryst. Solids* **2008**, *354*, 2190–2194.
- [224] Y. C. Nah, A. Ghicov, D. Kim, S. Berger, P. Schmuki, *J. Am. Chem. Soc.* **2008**, *130*, 16154.
- [225] R. Asahi, Y. Taga, W. Mannstadt, A. J. Freeman, *Phys. Rev. B* **2000**, *61*, 7459.
- [226] Z. Y. Wu, G. Ouvrared, P. Gressier, C. R. Natoli, *Phys. Rev. B* **1997**, *55*, 10382.
- [227] H. Tang, K. Prasad, R. Sanjinbs, P. E. Schmid, F. Levy, *J. Appl. Phys.* **1994**, *75*, 2042.
- [228] J. Pascual, J. Camassel, H. Mathieu, *Phys. Rev. B* **1978**, *18*, 5606.
- [229] K. Eufinger, D. Poelman, H. Poelman, R. De Gryse, G. B. Marin, *Appl. Surf. Sci.* **2007**, *254*, 148.
- [230] V. M. Naik, D. Haddad, R. Naik, J. Benci, G. W. Auner, *Mater. Res. Soc. Symp. Proc.* **2002**, *755*, 413.
- [231] A. K. Ghosh, F. G. Wakim, P. R. Addiss, *Phys. Rev. Lett.* **1969**, *22–23*, 979.
- [232] L. Forro, O. Chauvet, D. Emin, L. Zuppiroli, H. Berger, F. Levy, *J. Appl. Phys.* **1994**, *75*, 633.
- [233] R. Beranek, H. Tsuchiya, T. Sugishima, J. M. Macak, L. Taveira, S. Fujimoto, H. Kisch, P. Schmuki, *Appl. Phys. Lett.* **2005**, *87*, 243114.
- [234] A. G. Munoz, Q. Chen, P. Schmuki, *J. Solid State Electrochem.* **2007**, *11*, 1077.
- [235] R. P. Lynch, A. Ghicov, P. Schmuki, *J. Electrochem. Soc.* **2010**, *157*, G76.
- [236] S. R. Morrison, *Electrochemistry at Semiconductor and Oxidized Metal Electrodes*, Plenum Press, New York, **1980**, p. 401.
- [237] H. Tsuchiya, J. M. Macak, A. Ghicov, A. S. Räder, L. Taveira, P. Schmuki, *Corros. Sci.* **2007**, *49*, 203.
- [238] L. V. Taveira, A. A. Sagués, J. M. Macak, P. Schmuki, *J. Electrochem. Soc.* **2008**, *155*, C293.
- [239] W. W. Gartner, *Phys. Rev.* **1959**, *116*, 84.
- [240] U. Diebold, T. E. Madey, *J. Vac. Sci. Technol. A* **1992**, *10*, 2327.
- [241] D. R. Lide, *Handbook of Chemistry and Physics*, 84th ed., CRC press LLC, Florida, **2003**.
- [242] V. V. Sergentu, I. M. Tiginyanu, V. V. Ursaki, M. Enachi, S. P. Albu, P. Schmuki, *Phys. Status Solidi RRL* **2008**, *2*, 242.
- [243] B. J. Aronson, C. F. Blanford, A. Stein, *Chem. Mater.* **1997**, *9*, 2842.
- [244] W. Dong, H. Bongard, B. Tesche, F. Marlow, *Adv. Mater.* **2002**, *14*, 1457.
- [245] B. T. Holland, C. Blanford, A. Stein, *Science* **1998**, *281*, 538.
- [246] W. Wei, H. Jha, G. Yang, R. Hahn, I. Paramasivam, S. Berger, E. Spiecker, P. Schmuki, *Adv. Mater.* **2010**, *22*, 4770.
- [247] A. Tighineanu, T. Ruff, S. P. Albu, R. Hahn, P. Schmuki, *Chem. Phys. Lett.* **2010**, *494*, 260.
- [248] M. Kunat, U. Burghaus, *Surf. Sci.* **2003**, *544*, 170.
- [249] S. Funk, U. Burghaus, *Catal. Lett.* **2007**, *118*, 118.
- [250] V. I. Pârulescu, P. Grange, B. Delmon, *Catal. Today* **1998**, *46*, 233.
- [251] S. Funk, B. Hokkanen, U. Burghaus, A. Ghicov, P. Schmuki, *Nano Lett.* **2007**, *7*, 1091.
- [252] M. Kunat, U. Burghaus, C. Woll, *Phys. Chem. Chem. Phys.* **2004**, *6*, 4203.
- [253] B. Hokkanen, S. Funk, U. Burghaus, A. Ghicov, P. Schmuki, *Surf. Sci.* **2007**, *601*, 4620.
- [254] K. E. Smith, V. E. Henrich, *Phys. Rev. B* **1986**, *32*, 5384.
- [255] K. E. Smith, J. L. Mackay, V. E. Henrich, *Phys. Rev. E* **1987**, *35*, 582.
- [256] A. Kienemann, H. Idriss, R. Kieffer, P. Chaumette, D. Durand, *Ind. Eng. Chem. Res.* **1991**, *30*, 1130.
- [257] W. Gopel, G. Rocker, R. Feierabend, *Phys. Rev. E* **1983**, *28*, 3427.
- [258] J. Robertson, P. W. Peacock, *Thin Solid Films* **2003**, *445*, 155.
- [259] P. W. Peacock, J. Robertson, *Appl. Phys. Lett.* **2003**, *83*, 2025.
- [260] H. Kobayashi, M. Yamaguchi, *Surf. Sci.* **1989**, *214*, 466.
- [261] G. Lu, A. Linsebigler, J. T., Jr. Yates, *J. Phys. Chem.* **1994**, *98*, 11733.
- [262] K. E. Smith, V. E. Henrich, *Surf. Sci.* **1989**, *217*, 445.
- [263] K. S. Kim, M. A. Barteau, W. E. Farneth, *Langmuir* **1988**, *4*, 533.
- [264] K. S. Kim, M. A. Barteau, *Surf. Sci.* **1989**, *233*, 13.
- [265] J. M. Pan, B. L. Maschhoff, U. Diebold, T. E. Madey, *J. Vac. Sci. Technol. A* **1992**, *10*, 2470.
- [266] R. L. Kurtz, R. Stockbauer, T. E. Madey, E. Roman, J. L. de Segovia, *Surf. Sci.* **1989**, *218*, 178.
- [267] A. Ghicov, H. Tsuchiya, J. M. Macak, P. Schmuki, *Phys. Status Solidi A* **2006**, *203*, R28.
- [268] J. W. Schultze, M. M. Lohrengel, *Electrochim. Acta* **2000**, *45*, 2499.
- [269] L. Kavan, M. Graetzel, S. E. Gilbert, C. Klemenz, H. J. Scheel, *J. Am. Chem. Soc.* **1996**, *118*, 6716.
- [270] J. P. Randin, *J. Electron. Mater.* **1978**, *7*, 47.
- [271] I. F. Chang, Nonemissive Electrooptic Disp. [Proc. Brown Boveri Symp.], 4th, **1976**, 155–196.
- [272] T. Oi, *Annu. Rev. Mater. Sci.* **1986**, *16*, 185.
- [273] D. C. Cronemeyer, *Phys. Rev.* **1952**, *87*, 876.
- [274] J. M. Macak, F. Schmidt-Stein, P. Schmuki, *Electrochem. Commun.* **2007**, *9*, 1783.
- [275] J. M. Macak, P. J. Barczuk, H. Tsuchiya, M. Z. Nowakowska, A. Ghicov, M. Chojak, S. Bauer, S. Virtanen, P. J. Kulesza, P. Schmuki, *Electrochem. Commun.* **2005**, *7*, 1417.
- [276] J. Qu, X. Zhang, Y. Wang, C. Xie, *Electrochim. Acta* **2005**, *50*, 3576.
- [277] M. Wang, D.-J. Guo, H.-L. Li, *J. Solid State Chem.* **2005**, *178*, 1996.
- [278] F. Hu, F. Ding, S. Song, P. K. Shen, *J. Power Sources* **2006**, *163*, 415.
- [279] I. Tanahashi, H. Iwagishi, G. Chang, *Mater. Lett.* **2008**, *62*, 2714.
- [280] A. Ghicov, S. P. Albu, R. Hahn, D. Kim, T. Stergiopoulos, J. Kunze, C.-A. Schiller, P. Falaras, P. Schmuki, *Chem. Asian J.* **2009**, *4*, 520.
- [281] Y. Y. Song, H. Hildebrand, P. Schmuki, *Surf. Sci.* **2010**, *604*, 346.
- [282] Unpublished results.
- [283] M. Anpo, *Catal. Surv. Jpn.* **1997**, *1*, 169.
- [284] S. Sato, *Chem. Phys. Lett.* **1986**, *123*, 126.
- [285] R. Asahi, T. Morikawa, T. Ohwaki, K. Aoki, Y. Taga, *Science* **2001**, *293*, 269.
- [286] T. Umebayashi, T. Yamaki, S. Tanaka, K. Asai, *Chem. Lett.* **2003**, *32*, 330.
- [287] T. Ohno, T. Mitsui, M. Matsumura, *Chem. Lett.* **2003**, *32*, 364.
- [288] J. C. Yu, W. Ho, J. Yu, H. Yip, P. K. Wong, J. Zhao, *Environ. Sci. Technol.* **2005**, *39*, 1175.
- [289] S. Sakthivel, H. Kisch, *Angew. Chem.* **2003**, *115*, 5057; *Angew. Chem. Int. Ed.* **2003**, *42*, 4908.
- [290] T. Umebayashi, T. Yamaki, H. Itoh, K. Asai, *Appl. Phys. Lett.* **2002**, *81*, 454.
- [291] A. B. Murphy, *Sol. Energy Mater. Sol. Cells* **2008**, *92*, 363.
- [292] A. K. Ghosh, H. P. Maruska, *J. Electrochem. Soc.* **1977**, *124*, 1516.
- [293] M. Anpo, *Pure Appl. Chem.* **2000**, *72*, 1787.
- [294] H. Yamashita, M. Harada, J. Misaka, M. Takeuchi, K. Ikeue, M. Anpo, *J. Photochem. Photobiol. A* **2002**, *148*, 257.
- [295] X. Chen, C. Burda, *J. Phys. Chem. B* **2004**, *108*, 15446.
- [296] S. M. Prokes, J. L. Gole, X. Chen, C. Burda, W. E. Carlos, *Adv. Funct. Mater.* **2005**, *15*, 161.
- [297] X. Qiu, C. Burda, *Chem. Phys.* **2007**, *339*, 1.
- [298] J. H. Park, S. Kim, A. J. Bard, *Nano Lett.* **2006**, *6*, 24.
- [299] R. Hahn, A. Ghicov, J. Salonen, V.-P. Lehto, P. Schmuki, *Nanotechnology* **2007**, *18*, 105604.

- [300] E. Barborini, A. M. Conti, I. Kholmanov, P. Piseri, A. Podesta, P. Milani, C. Cepek, O. Sakho, R. Macovez, M. Sancrotti, *Adv. Mater.* **2005**, *17*, 1842.
- [301] T. Morikawa, R. Asahi, T. Ohwaki, K. Aoki, Y. Taga, *Jpn. J. Appl. Phys.* **2001**, *40*, L561.
- [302] A. Ghicov, J. M. Macak, H. Tsuchiya, J. Kunze, V. Haeublein, L. Frey, P. Schmuki, *Nano Lett.* **2006**, *6*, 1080.
- [303] A. Ghicov, J. M. Macak, H. Tsuchiya, J. Kunze, V. Haeublein, S. Kleber, P. Schmuki, *Chem. Phys. Lett.* **2006**, *419*, 426.
- [304] D. Kim, S. Fujimoto, P. Schmuki, H. Tsuchiya, *Electrochem. Commun.* **2008**, *10*, 910.
- [305] A. Ghicov, B. Schmidt, J. Kunze, P. Schmuki, *Chem. Phys. Lett.* **2007**, *433*, 323.
- [306] R. P. Vitiello, J. M. Macak, A. Ghicov, H. Tsuchiya, L. F. P. Dick, P. Schmuki, *Electrochem. Commun.* **2006**, *8*, 544.
- [307] R. Beraneka, J. M. Macak, M. Gärtner, K. Meyer, P. Schmuki, *Electrochim. Acta* **2009**, *54*, 2640.
- [308] A. Ghicov, M. Yamamoto, P. Schmuki, *Angew. Chem.* **2008**, *120*, 8052–8055; *Angew. Chem. Int. Ed.* **2008**, *47*, 7934.
- [309] O. K. Varghese, M. Paulose, T. J. LaTempa, C. A. Grimes, *Nano Lett.* **2009**, *9*, 731.
- [310] F. Jona, G. Shirane, *Ferroelectric Crystals*, MacMillan, New York, **1976**.
- [311] S. Euphrasie, S. Daviero-Minaud, P. Pernod, *Mater. Sci. Eng. B* **2003**, *104*, 180.
- [312] Y. Hu, H. Gu, J. You, K. Zheng, J. Wang, *Key Eng. Mater.* **2007**, *2157*, 336.
- [313] Y. Mao, S. Banerjee, S. S. Wong, *Chem. Commun.* **2003**, 408.
- [314] N. P. Padture, X. Wei, *J. Am. Ceram. Soc.* **2003**, *86*, 2215.
- [315] X. Wei, A. L. Vasiliev, N. P. Padture, *J. Mater. Res.* **2005**, *20*, 2140.
- [316] Y. Xin, J. Jiang, K. Huo, T. Hu, P. K. Chu, *ACS Nano* **2009**, *3*, 3228.
- [317] J. M. Macak, C. Zollfrank, B. J. Rodriguez, H. Tsuchiya, M. Alexe, P. Greil, P. Schmuki, *Adv. Mater.* **2009**, *21*, 3121.
- [318] Y. Yang, X. Wang, C. Zhong, C. Sun, L. Li, *Appl. Phys. Lett.* **2008**, *92*, 122907.
- [319] Q. Chen, G. H. Du, S. Zhang, L.-M. Peng, *Acta Crystallogr. Sect. B* **2002**, *58*, 587.
- [320] J. M. Macak, B. G. Gong, M. Hueppe, P. Schmuki, *Adv. Mater.* **2007**, *19*, 3027.
- [321] A. Benoit, I. Paramasivam, Y. C. Nah, P. Roy, P. Schmuki, *Electrochem. Commun.* **2009**, *11*, 728.
- [322] P. Roy, D. Kim, I. Paramasivam, P. Schmuki, *Electrochem. Commun.* **2009**, *11*, 1001.
- [323] N. K. Shrestha, M. Yang, Y. C. Nah, I. Paramasivam, P. Schmuki, *Electrochem. Commun.* **2010**, *12*, 254.
- [324] N. K. Shrestha, J. M. Macak, F. Schmidt-Stein, R. Hahn, C. T. Mierke, B. Fabry, P. Schmuki, *Angew. Chem.* **2009**, *121*, 987; *Angew. Chem. Int. Ed.* **2009**, *48*, 969.
- [325] I. Paramasivam, J. M. Macak, A. Ghicov, P. Schmuki, *Chem. Phys. Lett.* **2007**, *445*, 233.
- [326] I. Paramasivam, J. M. Macak, P. Schmuki, *Electrochem. Commun.* **2008**, *10*, 71.
- [327] H. Tsuchiya, N. Tokuoka, S. Honda, Y. Shinkai, Y. Shimizu, S. Fujimoto, *J. Phys. Conf. Series* **2009**, *165*, 012037.
- [328] I. Paramasivam, A. Avhale, A. Inayat, A. Bosmann, P. Schmuki, W. Schwieger, *Nanotechnology* **2009**, *20*, 225607.
- [329] A. Kongkanand, K. Tvrđy, K. Takechi, M. Kuno, P. V. Kamat, *J. Am. Chem. Soc.* **2008**, *130*, 4007.
- [330] W. T. Sun, Y. Yu, H. Y. Pan, X. F. Gao, Q. Chen, L.-M. Peng, *J. Am. Chem. Soc.* **2008**, *130*, 1124.
- [331] H. Gerischer, M. Luebke, *J. Electroanal. Chem.* **1986**, *204*, 225.
- [332] R. Plass, S. Pelet, J. Krueger, M. Gratzel, U. Bach, *J. Phys. Chem. B* **2002**, *106*, 7578.
- [333] R. Helmy, A. Y. Fadeev, *Langmuir* **2002**, *18*, 8924.
- [334] B. M. Silverman, K. A. Wiegand, J. Schwartz, *Langmuir* **2005**, *21*, 225.
- [335] E. Balaur, J. M. Macak, L. Taveira, P. Schmuki, *Electrochem. Commun.* **2005**, *7*, 1066.
- [336] A. Mishra, M. K. R. Fischer, P. Bäuerle, *Angew. Chem.* **2009**, *121*, 2510; *Angew. Chem. Int. Ed.* **2009**, *48*, 2474.
- [337] W. Lu, G. Wang, Y. Jin, X. Yao, J. Hu, J. Li, *Appl. Phys. Lett.* **2006**, *89*, 263902.
- [338] A. Nanci, J. D. Wuest, L. Peru, P. Brunet, V. Sharma, S. Zalzal, M. D. McKee, *J. Biomed. Mater. Res.* **1998**, *40*, 324.
- [339] X. Liu, P. K. Chub, C. Dinga, *Mater. Sci. Eng.* **2004**, *47*, 49.
- [340] B. D. Ratner in *Biomaterials Science: An Interdisciplinary Endeavour* (Eds.: B. D. Ratner, A. S. Hoffmann, F. J. Schoen, J. E. Lemons), Academic Press, San Diego, **1996**, pp. 37–130.
- [341] M. Morra, *Cells Mater.* **2006**, *12*, 1.
- [342] J. M. White, J. Szanyi, M. A. Henderson, *J. Phys. Chem. B* **2003**, *107*, 9029.
- [343] E. Balaur, J. M. Macak, H. Tsuchiya, P. Schmuki, *J. Mater. Chem.* **2005**, *15*, 4488.
- [344] F. Schmidt-Stein, R. Hahn, J. F. Gnichwitz, Y. Y. Song, N. K. Shrestha, A. Hirsch, P. Schmuki, *Electrochem. Commun.* **2009**, *11*, 2077.
- [345] A. B. D. Cassie, S. Baxter, *Trans. Faraday Soc.* **1944**, *40*, 546.
- [346] D. Kim, J. M. Macak, F. Schmidt-Stein, P. Schmuki, *Nanotechnology* **2008**, *19*, 305710.
- [347] F. Schmidt-Stein, J. F. Gnichwitz, J. Salonen, R. Hahn, A. Hirsch, P. Schmuki, *Electrochem. Commun.* **2009**, *11*, 2000.
- [348] S. Berger, J. Faltenbacher, S. Bauer, P. Schmuki, *Phys. Status Solidi RRL* **2008**, *2*, 102.
- [349] H. Tsuchiya, P. Schmuki, *Electrochem. Commun.* **2004**, *6*, 1131.
- [350] H. Tsuchiya, J. M. Macak, L. Taveira, P. Schmuki, *Chem. Phys. Lett.* **2005**, *410*, 188.
- [351] W. J. Lee, W. H. Smyrl, *Electrochem. Solid-State Lett.* **2005**, *8*, B7.
- [352] Y. Shin, S. Lee, *Nanotechnology* **2009**, *20*, 105301.
- [353] H. Tsuchiya, J. M. Macak, I. Sieber, L. Taveira, A. Ghicov, K. Sirotna, P. Schmuki, *Electrochem. Commun.* **2005**, *7*, 295.
- [354] N. R. de Tacconi, C. R. Chenthamarakshan, G. Yogeewaran, A. Watcharenwong, R. S. de Zoysa, N. A. Basit, K. Rajeshwar, *J. Phys. Chem. B* **2006**, *110*, 25347.
- [355] M. Yang, N. K. Shrestha, P. Schmuki, *Electrochem. Commun.* **2009**, *11*, 1908.
- [356] A. Watcharenwong, W. Chanmanee, N. R. de Tacconi, C. R. Chenthamarakshan, P. Kajitvichyanukul, K. Rajeshwar, *J. Electroanal. Chem.* **2008**, *612*, 112.
- [357] I. Sieber, H. Hildebrand, A. Friedrich, P. Schmuki, *Electrochem. Commun.* **2005**, *7*, 97.
- [358] S. Ono, T. Nagasaka, H. Shimazaki, H. Asoh, *Electrochem. Soc. Interface* **2006**, *123*, 2004.
- [359] I. Sieber, B. Kannan, P. Schmuki, *Electrochem. Solid-State Lett.* **2005**, *8*, J10.
- [360] I. V. Sieber, P. Schmuki, *J. Electrochem. Soc.* **2005**, *152*, C639.
- [361] W. Wei, J. M. Macak, P. Schmuki, *Electrochem. Commun.* **2008**, *10*, 428.
- [362] W. Wei, J. M. Macak, N. K. Shrestha, P. Schmuki, *J. Electrochem. Soc.* **2009**, *156*, K104.
- [363] H. A. El-Sayed, V. I. Birss, *Nano Lett.* **2009**, *9*, 1350.
- [364] S. P. Albu, A. Ghicov, P. Schmuki, *Phys. Status Solidi RRL* **2009**, *3*, 64.
- [365] T. D. Burleigh, P. Schmuki, S. Virtanen, *J. Electrochem. Soc.* **2009**, *156*, C45.
- [366] S. K. Mohapatra, S. E. John, S. Banerjee, M. Misra, *Chem. Mater.* **2009**, *21*, 3048.
- [367] C. M. Turhan, R. Lynch, H. Jha, P. Schmuki, S. Virtanen, *Electrochem. Commun.* **2010**, *12*, 796.
- [368] S. Berger, H. Tsuchiya, A. Ghicov, P. Schmuki, *Appl. Phys. Lett.* **2006**, *88*, 203119.

- [369] H. D. Zheng, A. Z. Sadek, K. Latham, K. Kalantar-Zadeh, *Electrochem. Commun.* **2009**, *11*, 768.
- [370] A. Z. Sadek, H. D. Zheng, M. Breedon, *Langmuir* **2009**, *25*, 9545.
- [371] Y. C. Nah, A. Ghicov, D. Kim, P. Schmuki, *Electrochem. Commun.* **2008**, *10*, 1777.
- [372] S. Hotchandani, I. Bedja, R. Fessenden, P. Kamat, *Langmuir* **1994**, *10*, 17.
- [373] M. Deepa, N. Sharma, P. Varshney, S. P. Varma, S. A. Agnihostry, *J. Mater. Sci.* **2000**, *35*, 5313.
- [374] W. Lee, D. Kim, K. Lee, P. Roy, P. Schmuki, *Electrochim. Acta* **2010**, *56*, 828.
- [375] C. Santato, M. Odziemkowski, M. Ulmann, J. Augustynski, *J. Am. Chem. Soc.* **2001**, *123*, 10639.
- [376] R. Hahn, S. Berger, P. Schmuki, *J. Solid State Electrochem.* **2010**, *14*, 285.
- [377] H. Tsuchiya, J. Nakata, S. Fujimoto, S. Berger, P. Schmuki, *ECS Trans.* **2008**, *16*, 359.
- [378] N. K. Shrestha, Y. C. Nah, H. Tsuchiya, P. Schmuki, *Chem. Commun.* **2009**, *15*, 2008.
- [379] H. Tsuchiya, J. M. Macak, A. Ghicov, Y. C. Tang, S. Fujimoto, M. Niinomi, T. Noda, P. Schmuki, *Electrochim. Acta* **2006**, *52*, 94.
- [380] S. H. Jang, H. C. Choe, Y. M. Ko, *Thin Solid Films* **2009**, *517*, 5038.
- [381] P. Agarwal, I. Paramasivam, N. K. Shrestha, P. Schmuki, *Chem. Asian J.* **2010**, *5*, 66.
- [382] A. N. Kamkin, L. A. Fishgoit, A. D. Davydov, *Russ. J. Electrochem.* **2003**, *39*, 665.
- [383] Y. Song, X. Zhu, X. Wang, J. Che, Y. Du, *J. Appl. Electrochem.* **2001**, *31*, 1273.
- [384] Y.-Y. Song, F. Schmidt-Stein, S. Berger, P. Schmuki, *Small* **2010**, *6*, 1180.
- [385] A. Fujishima, X. Zhang, D. A. Tryk, *Surf. Sci. Rep.* **2008**, *63*, 515.
- [386] Y. Xie, *Electrochim. Acta* **2006**, *51*, 3399.
- [387] Y. K. Lai, L. Sun, Y. C. Chen, *J. Electrochem. Soc.* **2006**, *153*, D123.
- [388] J. M. Macak, M. Zlamal, J. Krysa, P. Schmuki, *Small* **2007**, *3*, 300.
- [389] M. Zlamal, J. M. Macak, P. Schmuki, J. Kry'sa, *Electrochem. Commun.* **2007**, *9*, 2822.
- [390] I. Paramasivam, Y.-C. Nah, C. Das, N. K. Shrestha, P. Schmuki, *Chem. Eur. J.* **2010**, *16*, 8993.
- [391] S. K. Mohapatra, M. Misra, V. K. Mahajan, K. S. Raja, *J. Catal.* **2007**, *246*, 362.
- [392] C. J. Lin, Y. T. Lu, C. H. Hsieh, *Appl. Phys. Lett.* **2009**, *94*, 113102.
- [393] S. Banerjee, S. K. Mahapatra, M. Misra, *Chem. Commun.* **2009**, 7137.
- [394] C. Aprile, A. Corma, H. Garcia, *Phys. Chem. Chem. Phys.* **2008**, *10*, 769.
- [395] M. Kalbacova, J. M. Macak, F. Schmidt-Stein, C. T. Mierke, P. Schmuki, *Phys. Status Solidi RRL* **2008**, *2*, 194.
- [396] P. Roy, R. Lynch, P. Schmuki, *Electrochem. Commun.* **2009**, *11*, 1567.
- [397] P. Schmuki, L. E. Erickson, *Phys. Rev. Lett.* **2000**, *85*, 2985.
- [398] P. Schmuki, L. E. Erickson, D. J. Lockwood, *Phys. Rev. Lett.* **1998**, *80*, 4060.
- [399] M. Grätzel, *J. Photochem. Photobiol. C* **2003**, *4*, 145.
- [400] M. Grätzel, *Inorg. Chem.* **2005**, *44*, 6841.
- [401] J. M. Macak, H. Tsuchiya, A. Ghicov, P. Schmuki, *Electrochem. Commun.* **2005**, *7*, 1133.
- [402] P. Roy, S. P. Albu, P. Schmuki, *Electrochem. Commun.* **2010**, *12*, 949.
- [403] J. R. Jennings, A. Ghicov, L. M. Peter, P. Schmuki, A. B. Walker, *J. Am. Chem. Soc.* **2008**, *130*, 13364.
- [404] J. H. Park, T.-W. Lee, M. G. Kang, *Chem. Commun.* **2008**, 2867.
- [405] G. K. Mor, K. Shankar, M. Paulose, O. K. Varghese, C. A. Grimes, *Nano Lett.* **2006**, *6*, 215.
- [406] M. K. Nazeeruddin, A. Kay, I. Rodicio, R. Humpbry-Baker, E. Müller, P. Liska, N. Vlachopoulos, M. Grätzel, *J. Am. Chem. Soc.* **1993**, *115*, 6382.
- [407] T. Ohzuku, K. Sawai, T. Hirai, *J. Power Sources* **1987**, *19*, 287.
- [408] C. R. Granqvist, *Nat. Mater.* **2006**, *5*, 89.
- [409] D. C. Cronemeyer, *Phys. Rev.* **1959**, *113*, 1222.
- [410] A. Ghicov, H. Tsuchiya, R. Hahn, J. M. Macak, A. G. Muñoz, P. Schmuki, *Electrochem. Commun.* **2006**, *8*, 528.
- [411] A. Ghicov, S. P. Albu, J. M. Macak, P. Schmuki, *Small* **2008**, *4*, 1063.
- [412] S. Berger, A. Ghicov, Y. C. Nah, P. Schmuki, *Langmuir* **2009**, *25*, 4841.
- [413] C. Von Wilmsowsky, S. Bauer, R. Lutz, M. Meisel, F. W. Neukam, T. Toyoshima, P. Schmuki, E. Nkenke, K. A. Schlegel, *J. Biomed. Mater. Res. Part B* **2009**, *89*, 165.
- [414] S. Oh, K. S. Brammer, Y. S. J. Li, D. Teng, A. J. Engler, S. Chien, S. Jin, *Proc. Natl. Acad. Sci. USA* **2009**, *106*, 2130.
- [415] S. Bauer, J. Park, J. Faltenbacher, S. Berger, K. von der Mark, P. Schmuki, *Integr. Biol.* **2009**, *1*, 525.
- [416] J. Park, S. Bauer, P. Schmuki, K. von der Mark, *Nano Lett.* **2009**, *9*, 3157.
- [417] S. Bauer, J. Park, K. von der Mark, P. Schmuki, *Acta Biomater.* **2008**, *4*, 1576.
- [418] K. von der Mark, S. Bauer, J. Park, P. Schmuki, *Proc. Natl. Acad. Sci. USA* **2009**, *106*, E60.
- [419] J. Park, S. Bauer, K. A. Schlegel, F. W. Neukam, K. von der Mark, P. Schmuki, *Small* **2009**, *5*, 666.
- [420] H. Tsuchiya, J. M. Macak, L. Müller, J. Kunze, F. Müller, P. Greil, S. Virtanen, P. Schmuki, *J. Biomed. Mater. Res. Part A* **2006**, *77*, 534.
- [421] A. Kodama, S. Bauer, A. Komatsu, H. Asoh, S. Ono, P. Schmuki, *Acta Biomater.* **2009**, *5*, 2322.
- [422] J. Kunze, L. Müller, J. M. Macak, P. Greil, P. Schmuki, F. A. Müller, *Electrochim. Acta* **2008**, *53*, 6995.
- [423] A. Kar, K. S. Raja, M. Misra, *Surf. Coat. Technol.* **2006**, *201*, 3723.
- [424] L. Peng, A. D. Mendelsohn, T. J. LaTempa, S. Yoriya, C. A. Grimes, T. A. Desai, *Nano Lett.* **2009**, *9*, 1932.
- [425] K. C. Popat, M. Eltgroth, T. J. LaTempa, C. A. Grimes, T. A. Desai, *Small* **2007**, *3*, 1878.
- [426] T. Dey, P. Roy, B. Fabry, P. Schmuki, unpublished results.
- [427] G. E. Aninwene II, C. Yao, T. J. Webster, *Int. J. Nanomed.* **2008**, *3*, 257.
- [428] I. D. Kim, A. Rothschild, B. H. Lee, D. Y. Kim, S. M. Jo, H. L. Tuller, *Nano Lett.* **2006**, *6*, 2009.
- [429] M.-H. Seo, M. Yuasa, T. Kida, J.-S. Huh, K. Shimanoe, N. Yamazoe, *Sens. Actuators B* **2009**, *137*, 513.
- [430] M.-H. Seo, M. Yuasa, T. Kida, J.-S. Huh, N. Yamazoe, K. Shimanoe, *Procedia Chem.* **2009**, *1*, 192.
- [431] O. K. Varghese, D. Gong, M. Paulose, K. G. Ong, C. A. Grimes, *Sens. Actuators B* **2003**, *93*, 338.
- [432] P. Xiao, B. B. Garcia, Q. Guo, D. Liu, G. Cao, *Electrochem. Commun.* **2007**, *9*, 2441.
- [433] K. Y. Chun, B. W. Park, Y. M. Sung, D. J. Kwak, Y. T. Hyun, M. W. Park, *Thin Solid Films* **2009**, *517*, 4196.